Technical University of Denmark

DTU

Longitudinal MRI studies of brain morphometry

Skimminge, Arnold Jesper Møller; Larsen, Rasmus; Baare, William

Link back to DTU Orbit

DTU Library
Technical Information Center of Denmark

Longitudinal MRI studies of brain morphometry

Arnold Skimminge

Summary

High resolution MR images acquired at multiple time points of the brain allow quantification of localized changes induced by external factors such as maturation, ageing or disease progression/recovery. High-dimensional warping of such MR images incorporates changes induced by external factors into the accompanying deformation field. Deformation fields from high dimensional warping founds tensor based morphometry (TBM), and provides unique opportunities to study human brain morphology and plasticity. In this thesis, specially adapted image processing streams utilizing several image registration techniques to characterize differences between brains, demonstrate the versatility and specificity of the employed voxel-wise morphometric methods.

More specifically TBM is used to study neurodegenerative changes following severe traumatic brain injuries. Such injuries progress for months, perhaps even years post-injury. Little information is known about the spatial distribution and the clinical significance of this late atrophy. TBM revealed a large coherent cluster of significant atrophy consisting of the brain stem and cerebellar peduncles extending bilaterally through the thalamus, internal and external capsules, putamen, inferior and superior longitudinal fasciculus, corpus callosum and corona radiata. This indicates that the long-term atrophy is attributable to consequences of traumatic axonal injury. Despite progressive atrophy, remarkable clinical improvement occurred in most patients.

The other study utilized TBM and voxel based morphometry (VBM) in two separate papers concerning antipsychotic-naïve first episode schizophrenia. Volume reductions of hippocampal and caudate regions were found in patients compared to controls using VBM. Six months later, TBM revealed continued volume loss in striatum and hippocampus, despite treatment with quetiapine. The mechanisms underlying these progressive brain dynamics, specific antipsychotic compounds and clinical symptoms warrant further clarification.

Resumé

MR billeder af den menneskelige hjerne som er optaget med høj rumlig opløsning og på flere tidspunkter giver mulighed for at kvantificere lokale tidslige forandringer som følge af eksterne faktorer såsom modning, aldring eller sygdomsprogression. Billedregistrering med millioner af frihedsgrader af sådanne MR billeder kvantificerer forandringerne som følge af eksterne faktorer i det tilhørende deformationsfelt. Sådanne deformationsfelter danner grundlag for tensor baseret morfometri (TBM), og giver enestående muligheder for at studere morfologi og plasticitet i menneskets hjerne. Specielt tilpassede billedbehandlingsmetoder, der benytter sig af mange forskellige teknikker til billedregistrering for at karakterisere forskelle mellem hjerner, viser alsidigheden og specificiteten af de anvendte voxel-vise morfometriske metoder i to kliniske studier .

I første studie anvendes TBM til at undersøge neurodegenerative forandringer efter alvorlige traumatiske hjerneskader. Sådanne hjerneskader udvikles over flere måneder, endsige år efter skadestidspunktet. Der eksisterer kun få studier om den rumlige fordeling og den kliniske betydning af disse sene atrofiske hjerneskader. I dette studie afslører TBM en stor sammenhængende klynge af atrofi, bestående af hjernestammen, de cerebellare pedunklers forlængelse bilateralt gennem thalamus, capsula interna og eksterna, putamen, inferior og superior longitudinal fasciculus, corpus callosum og corona radiata. De regioner som udviste størst volumentab var strukturer, der er særlig udsatte for traumatisk aksonal skade og resulterende Wallersk degeneration. Dette indikerer at den progressive atrofi betinges af konsekvenserne af aksonal skade.

Andet studie udgøres af to seperate artikler om antipsykotika-naive første-episode ski-zofrene, hvor både TBM og voxel baseret morfometri (VBM) anvendes. Her blev volumentab i striatum og hippocampus regioner afsløret hos patienter i forhold til kontrolgruppen ved baseline. Seks måneder senere, viste TBM fortsat volumentab i både striatum og hippocampus, på trods af behandling med anti-psykotika stoffet quetiapin. Mekanismerne bag disse progressive hjerne forandringer, samt de strukturelle ændringers relation til den antipsykotiske behandling og de kliniske symptomer berettiger yderligere MR undersøgelser.

Preface

This PhD project was carried out as co-operation between the DTU Informatics Graduate School ITMAN and the Danish Research Centre for Magnetic Resonance, DRCMR.

The thesis consists of a summary report and a collection of 3 research papers written during the period 2006–2010.

Supervisors

Rasmus Larsen, Professor, PhD, DTU Informatics, Technical University of Denmark, Lyngby, Denmark

William Baaré, Senior researcher, PhD, Danish Research Centre for Magnetic Resonance, DRCMR, MR-department, Copenhagen University Hospital Hvidovre, Hvidovre, Denmark and Center for Integrated Molecular Brain Imaging, CIMBI, Copenhagen, Denmark

Lyngby, June 2010

Arnold Skimminge

Scientific contributions

This thesis is based on three papers [27, 28, 102] concerning longitudinal studies of brain morphometry. Below is a full list including abstract of all peer-reviewed scientific contributions made in the years 2006–2010 in order of publication; 9 Journal papers, and 17 conference proceedings.

Conference proceedings [48–51, 105] are all derivatives of [47] concerning the development of a gradient insensitive, generic technique for recording of non-MR signals by use of surplus scanner bandwidth. However, due to my many other engagements the project never really gained momentum, and my focus was redirected towards statistics and image analysis. My scientific contributions to these publications was the development and testing of methods to extract the recorded non-MR signals from the MR signal.

Design of image processing methods, statistical design and analysis of functional MRI (fMRI), was my scientific contribution to papers [68, 92] and conference proceedings [77, 79, 89, 90, 93]. These papers address widely different neuroscientific questions, such as recovery from acute optic neuritis, healthy aging, MDMA abuse and modulation of the serotonin system.

Diffusion tensor imaging (DTI) and related image processing techniques, including image distortion correction, were the focus of my involvement in the papers [78, 120] and conference proceedings [46, 80]. Both papers revolve around the HUBU ("Hjernens Udvikling hos Børn og Unge") project, addressing brain maturation of typically developing children and adolescents.

The papers [27, 28, 102, 134] concern studies on brain morphometry, and related conference proceeding [106] constitutes the scientific work of the latter part of my PhD project. My scientific contributions to these publications were design, development and implementation of complex image processing streams, statistical design and analysis, as well as supervision.

The toolbox for correction of image distortions due to non-linearities in the scanner gradient system (see section 2.1) was used in [27, 28, 75, 78, 120] and conference proceedings [46, 80, 103, 104], and development and testing of the toolbox was part of my scientific contributions to these.

Journal papers

[68] Korsholm, K., Madsen, K. H., Frederiksen, J. L. , Skimminge, A. and Lund, T. E.; Recovery from optic neuritis: an ROI-based analysis of LGN and visual cortical areas *Brain. 2007 May;130(Pt 5):1244-53.*

Optic neuritis (ON) is the first clinical manifestation in approximately 20% of patients with multiple sclerosis (MS). The inflammation and demyelination of the optic nerve are characterized by symptomatic visual impairment and retrobulbar pain, and associated with decreased visual acuity, decreased colour and contrast sensitivity, delayed visual evoked potentials and visual field defects. Spontaneous recovery of vision typically occurs within weeks or months after onset, depending on the resolution of inflammation, remyelination, restoration of conduction in axons which persist demyelinated and neuronal plasticity in the cortical and subcortical visual pathways. To assess where recovery takes place along the visual pathway, visual activation was studied in the lateral geniculate nucleus (LGN), the main thalamic relay nucleus in the visual pathway and in three areas of the visual cortex: the lateral occipital complexes (LOC), V1 and V2. We conducted a longitudinal functional magnetic resonance imaging (fMRI) study of regions of interest (ROI) of activation in LGN and visual cortex in 19 patients with acute ON at onset, 3 and 6 months from presentation. With fMRI we measured the activation in the ROIs and compared activation during monocular stimulation of the affected and unaffected eye. In the acute phase the activation of LGN during visual stimulation of the affected eye was significantly reduced (P ¡ 0.01) compared to the unaffected eye. This difference in LGN activation between the affected and unaffected eye diminished during recovery, and after 180 days the difference was no longer significant (P = 0.59). The decreased difference during recovery was mainly due to an increase in the fMRI signal when stimulating the affected eye, but included a component of a decreasing fMRI signal from LGN when stimulating the unaffected eye. In LOC, V1 and V2 activation during visual stimulation of the affected eye in the acute phase was significantly reduced (p < 0.01) compared to the unaffected eye, and during recovery the difference diminished with no significant differences left after 180 days. As the pattern of activation in LOC, V1 and V2 resembled the development in LGN we found no evidence of additional cortical adaptive changes. The reduced activation of the LGN to stimulation of the unaffected eye is interpreted as a shift away from early

compensatory changes established in the acute phase in LGN and may indicate very early plasticity of the visual pathways.

[102] Sidaros, A., Skimminge, A., Liptrot, M.G., Sidaros, K., Engberg, A.W., Herning, M., Paulson, O.B., Jernigan, T.L. and Rostrup, E.; Long-term global and regional brain volume changes following severe traumatic brain injury: a longitudinal study with clinical correlates *Neuroimage. 2009 Jan 1;44(1):1-8.*

Traumatic brain injury (TBI) results in neurodegenerative changes that progress for months, perhaps even years post-injury. However, there is little information on the spatial distribution and the clinical significance of this late atrophy. In 24 patients who had sustained severe TBI we acquired 3D T1- weighted MRIs about 8 weeks and 12 months post-injury. For comparison, 14 healthy controls with similar distribution of age, gender and education were scanned with a similar time interval. For each subject, longitudinal atrophy was estimated using SIENA, and atrophy occurring before the first scan time point using SIENAX. Regional distribution of atrophy was evaluated using tensor-based morphometry (TBM). At the first scan time point, brain parenchymal volume was reduced by mean 8.4% in patients as compared to controls. During the scan interval, patients exhibited continued atrophy with percent brain volume change (%BVC) ranging between -0.6% and -9.4% (mean -4.0%). %BVC correlated significantly with injury severity, functional status at both scans, and with 1-year outcome. Moreover, %BVC improved prediction of long-term functional status over and above what could be predicted using functional status at approximately 8 weeks. In patients as compared to controls, TBM (permutation test, FDR 0.05) revealed a large coherent cluster of significant atrophy in the brain stem and cerebellar peduncles extending bilaterally through the thalamus, internal and external capsules, putamen, inferior and superior longitudinal fasciculus, corpus callosum and corona radiata. This indicates that the long-term atrophy is attributable to consequences of traumatic axonal injury. Despite progressive atrophy, remarkable clinical improvement occurred in most patients.

[78] Madsen, K. S., Baaré, W. F., Vestergaard, M., Skimminge, A., Ejersbo, L.R., Ramsøy, T. Z., Gerlach, C., Åkeson, P., Paulson, O.B. and Jernigan, T.L.; Response inhibition is associated with white matter microstructure in children, Accepted in *Neuropsychologia*, available as E-publication

Cognitive control of thoughts, actions and emotions is important for normal behaviour and the development of such control continues throughout childhood and adolescence. Several lines of evidence suggest that response inhibition is primarily mediated by a right-lateralized network involving inferior frontal gyrus (IFG), presupplementary motor cortex (preSMA), and subthalamic nucleus. Though the brain's fibre tracts are known to develop during childhood, little is known about how fibre tract development within this network relates to developing behavioural control. Here we examined the relationship between response inhibition, as measured with the stop-signal task, and indices of regional white matter microstructure in typically-developing children. We hypothesized that better response inhibition performance would be associated with higher fractional anisotropy (FA) in fibre tracts within right IFG and preSMA after controlling for age. Mean FA and diffusivity values were extracted from right and left IFG and preSMA. As hypothesized, faster response inhibition was significantly associated with higher FA and lower perpendicular diffusivity in both the right IFG and the right preSMA, possibly reflecting faster speed of neural conduction within more densely

packed or better myelinated fibre tracts. Moreover, both of these effects remained significant after controlling for age and whole brain estimates of these DTI parameters. Interestingly, right IFG and preSMA FA contributed additively to the prediction of performance variability. Observed associations may be related to variation in phase of maturation, to activity-dependent alterations in the network subserving response inhibition, or to stable individual differences in underlying neural system connectivity.

[92] Ramsøy, T.Z., Liptrot, M.G., Skimminge, A., Lund, T.E., Sidaros, K., Christensen, M. S., Baaré, W., Paulson, O. B. and Jernigan, T. L.; Regional activation of the human medial temporal lobe during intentional encoding of objects and positions, *Neuroimage. 2009 Oct 1;47(4):1863-72.*

> The medial temporal lobe (MTL) consists of several regions thought to be involved in learning and memory. However, the degree of functional specialization among these regions remains unclear. Previous studies have demonstrated effects of both content and processing stage, but findings have been inconsistent. In particular, studies have suggested that the perirhinal cortex is more involved in object processing than spatial processing, while other regions such as the parahippocampal cortex have been implicated in spatial processing. In this study, functional magnetic resonance imaging (fMRI) optimized for the MTL region was used to probe MTL activation during intentional encoding of object identities or positions. A region of interest analysis showed that object encoding evoked stronger activation than position encoding in bilateral perirhinal cortex, temporopolar cortex, parahippocampal cortex, hippocampus and amygdala. Results also indicate an unexpected significant correlation in activation level between anterior and posterior portions in both the left parahippocampal cortex and left hippocampus. Exploratory analysis did not show any regional content effects during preparation and rehearsal stages. These results provide additional evidence for functional specialization within the MTL, but were less clear regarding the specific nature of content specificity in these regions.

[27] Bjørn H. Ebdrup, Birte Glenthøj, Hans Rasmussen, Bodil Aggernaes, Annika R. Langkilde, Olaf B. Paulson, Henrik Lublin, Arnold Skimminge, William Baaré; Hippocampal and Caudate Volume Reductions in Antipsychotic-Naïve First Episode Schizophrenia, *Journal of Psychiatry and Neuroscience. 2010;35(2):95-104*

> Enlarged ventricles and reduced hippocampal volumes are consistently found in first episode schizophrenia Studies investigating brain structure in antipsychotic-naïve patients generally focused on the striatum. Here we examined whether ventricular enlargement, hippocampal and caudate volume reductions are morphological traits in antipsychotic-naïve first episode schizophrenia.
>
> High-resolution 3D T1-weighted magnetic resonance imaging scans were obtained in 38 antipsychotic-naïve first episode schizophrenia patients and 43 matched healthy control subjects on a 3 Tesla scanner. Brain images were warped to each other using a high-dimensional inter-subject registration algorithm. Voxel-wise group comparisons were performed with permutation tests. Small volume correction was performed for the hippocampus, the caudate and the ventricles, using a FDR-correction ($p<0.05$) to control for multiple comparisons. Brain structure volumes estimates were derived and analyzed. Patients were divided into those with (N=9) or without (N=29) any lifetime substance abuse diagnosis to examine the possible effects of abuse.

As hypothesized, hippocampal and caudate volumes were decreased in patients. Ventricular enlargement was absent. No differences in global volumes were found and no significant associations between tissue volumes and duration of untreated illness and psychopathology, respectively, were observed. The hippocampal reductions appeared influenced by a history of substance abuse. Exploratory analyses indicated reduced nucleus accumbens volumes in the patients.

This study was not designed to test for differences a priori between schizophrenia patients with or without lifetime substance abuse and the sub-group comprising abusing patients was small.

Hippocampal and caudate volume reductions may constitute a morphological trait in antipsychotic-naïve first episode schizophrenia patients. However, the clinical implications of these findings are still unclear. Moreover, past substance abuse may accentuate hippocampal volume reductions. MRI studies explicitly addressing the potential effects of substance abuse in antipsychotic-naïve first episode schizophrenia patients are warranted.

[28] Bjørn H. Ebdrup, Arnold Skimminge, Hans Rasmussen, Bodil Aggernaes, Bob Oranje, Henrik Lublin, William Baaré, Birte Glenthøj; Regional brain changes in antipsychotic-naïve first-episode schizophrenia patients treated with quetiapine: Relation to dose and psychopathology Published in *The international journal of neuropsychopharmacology, August 2010.*

MRI studies have shown progressive brain alterations in the course of schizophrenia. Whereas first- generation antipsychotics have been associated with striatal volume increases, the effects of second- generation antipsychotics (SGA) on striatal volumes are unclear. Neuroprotective effects of SGA's have been suggested on hippocampal volumes, whereas ventricular enlargement may be associated with clinical outcome. Dose-dependent volumetric effects of individual SGA's have been scarcely investigated. Here we examined structural brain changes in initially antipsychotic-naÃ¯ve first-episode schizophrenia patients after six months treatment with quetiapine.

High-resolution 3D T1-weighted magnetic resonance imaging scans were obtained on a 3 Tesla scanner at baseline and after six months in 22 antipsychotic-naïve first-episode schizophrenia patients and 28 matched healthy control subjects. Baseline and follow-up brain images were analyzed using tensor based morphometry (TBM). Voxel-wise group comparisons were performed with SPM5. Small volume correction was performed for striatum, hippocampus and the ventricles, using a FDR-correction (p¡0.05) to control for multiple comparisons. Additionally, volumetric estimates were derived and analyzed. Effects of medication, including dose-dependent effects, and associations with psychopathology (PANSS-scores) were assessed.

Patients had significant striatal and hippocampal volume loss over the six months treatment period. The striatal volume loss was most pronounced in low quetiapine doses and less apparent in high doses. Conversely, hippocampal volume loss appeared more pronounced in high quetiapine doses than in than low doses. Clinically, higher baseline positive symptoms were associated with more striatal and hippocampal volume loss over time. Although patients' ventricles did not change significantly, ventricular increases correlated with less improvement on negative symptoms.

Progressive regional volume loss in quetiapine-treated first-episode schizophrenia patients may be dose-dependent and clinically relevant. The mechanisms underlying progressive brain changes, specific antipsychotic compounds and clinical symptoms warrant further clarification.

[75] H. Lundell, D. Barthelemy, A. Skimminge, T.B. Dyrby, F. Biering-Sørensen, J.B. Nielsen; Independent spinal cord atrophy measures correlate to motor and sensory deficits in individuals with spinal cord injury accepted for publication *Spinal Cord*

The aim of this study was to present anatomically consistent and independent spinal cord atrophy measures based on standard MRI material and analyze their specific relations to sensory and motor outcome in individuals with chronic incomplete spinal cord injury (SCI).

We included 19 individuals with chronic incomplete SCI and 16 healthy controls. Participants underwent MRI and a neurological examination including sensory testing for light touch and pinprick, and muscle strength. Antero-posterior width (APW), left-right width (LRW) and cross- sectional spinal cord area (SCA) were extracted from MRI at the spinal level of C2. The angular variation of the spinal cord radius over the full circle was also extracted and compared with the clinical scores.

The motor score was correlated to LRW and the sensory scores were correlated to APW. The scores correlated also well with decreases in spinal cord radius in oblique angles in coherent and non-overlapping sectors for the sensory and motor qualities respectively.

APW and LRW can independently be used to assess sensory and motor function independently. The finding is corresponding well with the respective locations of the main sensory and motor pathways.

[120] Martin Vestergaard, Kathrine Skak Madsen, William F.C. Baaré, Arnold Skimminge, Lisser Rye Ejersbo, Thomas Z. Ramsøy, Christian Gerlach, Per Åkeson, Olaf B. Paulson, Terry L. Jernigan; White matter microstructure in superior longitudinal fasciculus associated with spatial working memory performance in children submitted to *Jounal of Cognitive Neuroscience*

During childhood and adolescence ongoing white matter maturation in the fronto-parietal cortices and connecting fiber tracts is measurable with diffusion weighted imaging. Important questions remain, however, about the links between these changes and developing cognitive functions. Spatial working memory (SWM) performance improves significantly throughout the childhood years and several lines of evidence implicate the left fronto-parietal cortices and connecting fiber tracts in SWM processing. Here we report results from a study of 76 typically developing children, 7 to 13 years of age. We hypothesized that better SWM performance would be associated with increased fractional anisotropy (FA) in a left fronto-parietal network comprised of the superior longitudinal fasciculus (SLF) and regional white matter underlying the dorsolateral prefrontal cortex (DLPFC), and posterior parietal cortex (PPC). As hypothesized, we observed a significant association between higher FA in the left fronto-parietal network and better SWM skills, and the effect was independent of age. This association was mainly accounted for by variability in left SLF FA and remained significant when FA measures from global fiber tracts or right SLF were included in the model. Further, the effect of FA in left SLF appeared to be mediated primarily by decreasing perpendicular diffusivity. Such associations could be related to individual differences among children in the architecture of fronto-parietal connections and/or to differences in the pace of fiber tract development. Further studies are needed to determine the contributions of intrinsic and experiential factors to the development of functionally significant individual differences in fiber tract structure.

[134] Xingchen Wu, Lars G. Hanson, Arnold Skimminge, Per Soelberg Sørensen, Olaf B. Paulson, Morten Blinkenberg, Henrik Kahr Mathiesen Cortical N-acetyl aspartate is a predictor of long-term clinical disability in newly diagnosed relapsing-remitting multiple sclerosis submitted to *Multiple Sclerosis*

> Sixteen patients with newly diagnosed RRMS were studied by serial MRI and MR spectroscopic imaging (MRSI) once every 6 months for 24 months. Clinical examinations, including the Expanded Disability Status Scale (EDSS), were performed at baseline, month 24, and year 7.
>
> Baseline cortical NAA/Cr correlated inversely with EDSS at month 24 ($r = -0.61$, $p < 0.05$), and follow-up at month 24 showed that patients with EDSS ≥ 4 had a lower baseline cortical NAA/Cr compared to those with EDSS less than 4 ($p < 0.05$). Baseline cortical NAA/Cr also correlated inversely with EDSS at year 7 ($r = -0.60$, $p < 0.05$), and follow-up at year 7 revealed that patients with EDSS ≥ 4 had a lower baseline cortical NAA/Cr compared to those with EDSS less than 4 ($p < 0.05$). Baseline brain parenchymal fraction (BPF) correlated inversely with EDSS at month 24 ($r = -0.62$, $p < 0.05$), but not with EDSS at year 7.
>
> Cortical NAA/Cr in early RRMS correlated with clinical disability in 2 and 7 years and may be used as a predictor of long-term disease outcome.

Conference proceedings – peer reviewed

2006

[51] Lars G Hanson, Arnold Skimminge, Torben E Lund and Christian G Hanson, Encoding of EEG in MR images in *Proceedings of the 12th Annual Meeting of the Organization for Human Brain Mapping, Florence, 2006*

> It was previously shown in that electrophysiology and other non-MR signals can be measured by MR equipment after modulation to frequencies close to those of the MR-signals. The signals are encoded in the oversampled region of the field-of-view normally discarded by the image reconstruction. Using surplus sampling and storage capacity of the scanner, non-MR signals can thereby be recorded without affecting the acquired images. In addition, imaging-induced distortions are largely avoided, and residuals are simple to filter away due to intrinsic perfect synchronization of MR- and non-MR recordings. Here we present the first EEG recordings made with the new technique.

[105] A. Skimminge, C.G. Hansonand L.G. Hanson, A simple approach to electro-physiological recording during fMRI in *Proceedings of the 12th Annual Meeting of the Organization for Human Brain Mapping, Florence, 2006*

> A simple technique involving only an MR-scanner and a standard signal generator demonstrates how any non-MR signal can be embedded in an MR-image using similar principles as soundtrack encoding in movies. The presented method largely avoids gradient artifacts normally compromising EEG/fMRI. The method uses off-the-shelf

hardware but requires specialised software to extract the embedded signals. However it may be attrative to implement if only a few channels are needed.

[89] K. Nielsen, K. H. Madsen, J. L. Fredriksen, A. Tsakiri, A. Skimminge and T. E. Lund, LGN activation in patients recovering from acute optic neuritis, in *Proceedings of the 12th Annual Meeting of the Organization for Human Brain Mapping, Florence, 2006*

Optic neuritis (ON) is a disease characterized by decreased visual acuity, visual field defects and abnormal VEP (visual evoked potentials). Inflammation and demyelination of the optic nerve are the major causes of the symptoms in ON. To further elucidate the mechanisms behind the recovery process in ON, we conducted a longitudinal fMRI study of LGN (lateral geniculate nucleus) activation in patients recovering from acute ON. There is a clear tendency towards smaller differences in LGN activation between the affected and the unaffected eyes over time.

[48] Hanson, Lars G. and Skimminge, Arnold and Hanson, Christian G., Strategies for Avoiding Image Artefacts When Scanner is Used for Recording of Non-MR Signals, in *Proceedings 14th Scientific Meeting, International Society for Magnetic Resonance in Medicine, Seattle, 2006*

Surplus sampling capacity of MR scanners can be used to record non-MR signals as has been demonstrated previously. If the non-MR signals are encoded in the oversampled frequency range of the scanner, i.e. outside the field of view, such signals are invisible in the images but can be extracted from the imaging raw data, a technique resembling "mag stripe" encoding of soundtracks in movies. Even though the non-MR-signals are encoded at frequencies corresponding to positions outside the field of view, there may be ringing artefacts appearing in the MR images. Two strategies for eliminating such artefacts are presented.

[90] Nielsen, Kirsten and Madsen, Kristoffer Hougaard and Frederiksen, Jette Lautrup and Tsakiri, Anna and Skimminge, Arnold and Lund, Torben Ellegaard, Investigations of LGN Activation During Recovery from Acute Optic Neuritis, in *Proceedings 14th Scientific Meeting, International Society for Magnetic Resonance in Medicine, Seattle, 2006*

To further elucidate the mechanisms of recovery of vision in acute optic neuritis (ON), we conducted a longitudinal fMRI-study at 3T of activation of the lateral geniculate nucleus (LGN) during visual stimulation of patients with ON. Sixteen patients were examined acutely, and two weeks, three and six months later.At each time-point we calculated the average BOLD signal change in LGN during stimulation of affected and unaffected eyes. We found a clear tendency towards smaller differences in LGN activation between affected and unaffected eyes over time, indicating that the amount of signals reaching LGN from affected eyes increases during recovery.

2007

[107] Skimminge, Arnold and Sidaros, Karam and Liptrot, Matthew and Sidaros, An-nette, Partial Volume Effects in DTI, in *Proceedings 15th Scientific Meeting, International Society for Magnetic Resonance in Medicine, Berlin, 2007*

> We present a method for analysing and correcting for partial volume effects in DTI acquired with large voxels, using a high resolution MPRAGE and its corresponding SPM2 tissue segmentation. The analysis shows that voxels with mixed tissue types contributes to a broadened profile of ADC and FA values within an ROI of the sple-nium. Furthermore a correction scheme is devised which is robust with respect to mixed tissue voxels.

[49] Hanson, Lars G. and Skimminge, Arnold and Hanson, Christian G., Encoding of EEG in MR Images, in *Proceedings 15th Scientific Meeting, International Society for Magnetic Resonance in Medicine, Berlin, 2007*

> It was shown earlier that electrophysiology and other non-MR signals can be measured by MR equipment after modulation to frequencies close to those of the MR-signals. After wireless transmission to the scanner, MR and and non-MR signals were recorded together. The technique is somewhat similar to the "mag stripe" technique used for encoding soundtracks in movies: The signals are encoded in the oversampled region just outside the field-of-view. Here we demonstrate 6 channel simultaneous ECG, EOG and alpha-EEG, all recorded by the scanner during fast echo planar imaging at 3 tesla

2008

[86] Mikkelsen, I. and Ziegelitz, D. and Kjølby, B. and Starck, G. and Skimminge, A. and Widmark, M. and Tullberg, M. and Holtås, S. and Wikkelsø, C. DSC-MRI perfusion imaging: which input function? – A comparison to CT perfusion imag-ing in *Proceedings 16th Scientific Meeting, International Society for Magnetic Resonance in Medicine, Toronto, 2008*

> The choice of artery for input function (AIF) measurement in dynamic susceptibility contrast imaging (DSC-MRI) influences the cerebral blood flow estimates (CBF). The DSC-MRI has no simple correction scheme for partial volume effects, whereas this is easily corrected for with CT. This study investigates the correlation between DSC-MRI and CT perfusion values for a typical CT and MR input functions. It is demonstrated that the correlation between DSC-MRI and CT are moderate for absolute perfusion values whereas the correlation of the GM/WM CBF ratio between modalities follows the identity line.

[50] Hanson, L. and Skimminge, A. and Hanson, C., Minimalist EEG-recording for improving fMRI: Simple encoding of noise variables in MRI data, in *Proceed-ings 16th Scientific Meeting, International Society for Magnetic Resonance in Medicine, Toronto, 2008*

Most fMRI studies can benefit from simultaneous recording of EEG and other electrophysiological signals, even when EEG is not of interest in itself. It is demonstrated that simple hardware and few, easily positioned electrodes can provide measures of eye-blinks, alpha-activity and pulse that increases fMRI sensitivity and reliability. The analysis is facilitated by EEG and MRI being measured and stored together by the scanner.

2009

[46] M.V. Hansen, Madsen, K.S., Baaré, W., Skimminge, A., Ejersbo, L.R., Gerlach, C., Åkeson, P., Paulson, O.B. and Jernigan, T.L., Verbal fluency performance is associated with white matter microstructure in a left hemisphere network in children in *Proceedings 15th Annual Meeting of the Organization for Human Brain Mapping, San Francisco, 2009*

> During childhood, ongoing maturation in fiber tracts is measurable with DT1, and different tracts exhibit distinct developmental trajectories. Verbal fluency (VF) is the efficiency of lexical retrieval processes, and performance on VF tasks improves significantly from 7-13 years of age. Here we report results from baseline assessments of a longitudinal study of typically developing children. The results support a significant association between variability in white matter microstructure in left hemisphere language processing network and VF performance in children.

[93] Ramsøy, TZ, Madsen, KH, Wegener, JS, Gelskov, SAV, Erritzøe, D, Knudsen, GM and Skimminge, A, From ecstasy to agony: chronic effects of MDMA use on emotional processing, in *Proceedings 15th Annual Meeting of the Organization for Human Brain Mapping, San Francisco, 2009*

> Chronic use of 3,4-Methylenedioxymethamphetamine (MDMA, or ecstasy) results in depletion of the neurotransmitter serotonin, and problems in cognitive and affective functioning. Our result suggests that chronic serotonin depletion following current use of MDMA leads to emotional dysfunctions governed by the serotonin system. In addition, our results may suggest a further impaired function of the medial temporal lobe functions in the processing of facial expression.

[103] Skimminge, A, Baare, WFC, Macoveanu, J and Christensen, MS Gradient non-linearity correction relocates normalized group activation hotspot in *Proceedings 15th Annual Meeting of the Organization for Human Brain Mapping, San Francisco, 2009*

> Gradient coils in MR scanners are assumed to produce linear magnetic field gradients, however high- speed gradients exhibit non-linearities [61]. The latter causes spatial deformations in MR images after reconstruction, as the gradients are assumed to be linear. Here we show that correcting for gradient field distortions give rise to significant differences in the localization of activations, even in situations supposed to be unaffected by these distortions, e.g. in group comparisons where EPI-times series typically are realigned, spatial normalized and smoothed before inferences are made.

[80] Madsen, KS and Jernigan, TL and Skimminge, A and Mortensen, EL and Knudsen, GM and Baaré, WFC, Inferior Cingulum Bundle Asymmetry Predicts Extroversion: A DTI study in *Proceedings 15th Annual Meeting of the Organization for Human Brain Mapping, San Francisco, 2009*

> Extroversion relates to the social dimensions of personality and has been positively associated with positive emotionality, and negatively with psychiatric disorders, e.g. anxiety disorders. The results suggest that higher FA in the left relative to the right inferior cingulum is associated with higher extroversion scores.

[106] Skimminge, A, Sidaros, K, Liptrot, M, Engberg, AW, Herning, M, Paulson, O, Jernigan, TL, Rostrup, E and Sidaros, A, Long-term regional atrophy and association with clinical outcome following severe traumatic brain injury: A tensor based morphometry study, in *Proceedings 15th Annual Meeting of the Organization for Human Brain Mapping, San Francisco, 2009*

> Here we present additional analysis of the TBM results from [102] was made in order to investigate whether a different pattern of late atrophy would be found in patients with unfavourable outcome versus favourable outcome, according to the Extended Glasgow Outcome Scale (GOS-E = 1-4 and GOS-E = 5-8, respectively). We found late atrophy to be significantly more pronounced in TBI patients with unfavourable outcome as compared to those with favourable outcome, particularly in the brain stem.

[77] Macoveanu, J., Wegener, J., Skimminge, A., Hornbøll, B., Elliott, R., Siebner, H., Paulson, O. and Rowe, J., Separate neural systems for evaluating risks and reward in decision making, in *Proceedings 17th Scientific Meeting, International Society for Magnetic Resonance in Medicine, Honolulu, 2009*

> When making a decision, the risk can be expressed as the probability of wining vs. losing, or the outcome winnings vs. losses. We used a novel gambling task with 30 subjects in fMRI to study the different roles of fronto-striatal systems in the integration of probability vs. outcome. The probability of winning correlated with activity in the rostral Ventral Striatum (VS), dorsal anterior-cingulate (ACC) and orbitofrontal cortex. The magnitude of winnings correlated with caudal-VS and subgenual-ACC activity. Conclusion: separate regions of VS and ACC are sensitive to different aspects of risk, even when the expected utility of choices is equated.

[79] Madsen, K., Jernigan, T., Skimminge, A., Mortensen, E., Knudsen, G. and Baaré, W., Cingulum bundle asymmetry predicts trait neuroticism: A DTI study in *Proceedings 17th Scientific Meeting, International Society for Magnetic Resonance in Medicine, Honolulu, 2009*

> Amygdala and subgenual cingulate are linked to anxiety and mood disorders, for which the trait neuroticism is a risk factor. Left and right subgenual cingulate functional imbalances may contribute to behavioural and physical symptoms observed in depression. We investigated associations between neuroticism and cingulum FA in 45 healthy adults. DWI images were processed with TBSS to align main fibre tracts and ROIs were drawn in right and left cingulum. As hypothesized, cingulum FA laterality index (asymmetry) significantly predicted neuroticism. It is unclear whether cingulum FA asymmetry is a possible marker of increased risk of developing anxiety and mood disorders.

[104] Skimminge, A. and Christensen, M., Gradient non-linearity correction relocates normalised group activation hotspot, in *Proceedings 17th Scientific Meeting, International Society for Magnetic Resonance in Medicine, Honolulu, 2009*

High-speed MRI gradients tend to be nonlinear outside the center of the magnetic field. This introduces structural deformations which may influence not only the shape of structural images but also the location of activation in fMRI studies. In worst case scenarios it could have serious impact for presurgical planning fMRI studies if activation gets mislocalised. Here we show that even in a best case scenario where functional images are normalised, smoothed and group activation maps created, there is still a significant difference in activation localisation with and with a correction for the gradient nonlinearities.

Acknowledgements

I thank my supervisor, Rasmus Larsen, for guidance and inspiration. In addition I also owe many thanks to my co-supervisor, William F.C. Baaré, for great inspiration, for always being willing to discuss various research topics and not least for his enjoyable company and friendship during the Ph.D. I wish also to thank Olaf Paulson who on behalf of DRCMR provided the possibility of using the MR scanner when needed, and a warm welcome DRCMR at including academic and financial support. I would also like to thank co-workers at both the image group at IMM and DRCMR at Hvidovre Hospital for their encouragement and company during the last three years.

In particular I wish to thank Annette Sidaros and Bjørn Ebdrup, without whom this Ph.D. would not have been possible in its current form and for letting me introduce them to the exciting topic of tensor based morphometry. I have really enjoyed our friendship and many fruitful discussions on almost every topic covered in this thesis.

I also wish to thank other people with whom I have had the pleasure to work with during the Ph.D., in particular this includes Lars G. Hanson, Kristoffer Madsen, Mark Schram Christensen, Julian Macoveanu and Hartwig Siebner for their expertise and pleasant company. In addition I wish to thank Kathrine Skak Madsen, Karam Sidaros, Henrik Lundell, Tim Dyrby, Martin Vestergaard, Kirsten Korsholm, Thomas Ramsøy and Xingchen Wu for working together with me on various interesting topics unfortunately not covered in this thesis. Special thanks are directed to friends, co-workers and family for help and guidance throughout the project period, in particular I thank my family, Heidi, Emilie and Johan, for their love and support.

Contents

List of Figures

CHAPTER 1

Computational
neuroanatomy

Neuroanatomical structures show extraordinary morphological variability, and specific neuroanatomical features, such as volume, cortical shape and area, and gyrification patterns often need to be compared within and between groups of individuals. Computational neuroanatomy harnesses the vastly growing computational power of modern large-scale computer systems to characterize differences between brains, using sophisticated mathematical models sensitive to subtle changes in the size, position, shape, and tissue characteristics of brain structures. Advanced statistical methods are then employed to make inferences about the structural characteristics of health and disease while taking into account factors such as age, sex, genetic background, and disease state of individual subjects.

Magnetic resonance imaging non-invasively provides highly detailed images of brain anatomy. 3D high-resolution ($\sim 1\,\mathrm{mm}^3$ voxels) scans of the entire brain can be obtained in less than 10 minutes. This type of rapidly acquired high-resolution images is described in detail in chapter 2. Furthermore techniques for correcting scanner specific artifacts are demonstrated.

Acquired brain scans are generally placed in a common coordinate system such as Talairach[113] and MNI (Montreal Neurological Institute)[29, 30], to allow comparison

of neuroanatomical characteristics within and between individuals. To this end many different registration techniques, with varying levels of complexity, are employed. Linear techniques are generally used to correct for rotation and translation (i.e. 6 parameter rigid body registration) and global size differences between subjects (i.e. 9 or 12 parameter affine registration entailing scaling and scaling plus shears, respectively). Non-linear techniques are used to compensate for local neuroanatomical differences within or between subjects and differ in the amount of degrees of freedom [66]. Non-linear techniques with millions degrees of freedom allow discerning neuroanatomical dynamics not only within single subjects but also between different subjects. The different registration techniques that are employed in this thesis are described in chapter 3.

Two morphometric methods are used in this thesis, voxel- and tensor based morphometry. Voxel based morphometry (VBM) allows assessing voxel-wise anatomical differences throughout the brain and generally compares gray matter concentrations or volumes. Tensor based morphometry (TBM) uses the gradients of deformations fields obtained from high-dimensional non-linear registration techniques to identify local neuroanatomical differences(e.g shape, volume) in neuroanatomy. Both methods have been passionately discussed in the literature, especially regarding anatomical specificity as well as interpretation of results. Both methods are introduced and discussed in chapter 4.

The statistical methods employed in this thesis are general linear models, with the added complexity of the multiple comparisons problem as well as non-normality of the underlying probability distributions. The general linear model is discussed in chapter 5.

The papers [27, 28, 102] concerning studies of brain morphometry, and related conference proceeding [106] are discussed in chapters 6 and 7.

Final remarks are given in chapter 8.

Magnetic resonance imaging

Computational neuroanatomy relies heavily on good quality high-resolution MR images, generally obtained using a fast T1-weighted imaging technique. An example is the Magnetization Prepared Rapid Gradient Echo (MPRAGE) sequence, a fast 3D gradient echo pulse sequence using a magnetization preparation pulse for contrast enhancement. MPRAGE is designed for rapid acquisition with T1 weighted dominance in the image contrast, thus providing good contrast between different tissue types in the brain. Fast gradient echoes are characterized by their rapid sampling time, high signal intensity and good image contrast. The rapid speed of the acquisition makes it an invaluable sequence in every MR research protocol for anatomical reference. A typical MPRAGE image of a normal subject is shown in figure 2.1 with 3 axial slices, 3 sagittal slices and 3 coronal slices.

The pulse sequence timing diagram for the MPRAGE sequence is shown in figure 2.2. The diagram illustrates the steps of basic hardware activity that are played out during image acquisition. Time during pulse sequence execution is indicated along the horizontal axes. Important timing parameters are

TE Echo time represents the time between the application of the excitation RF pulse and the peak of the MR signal during readout.
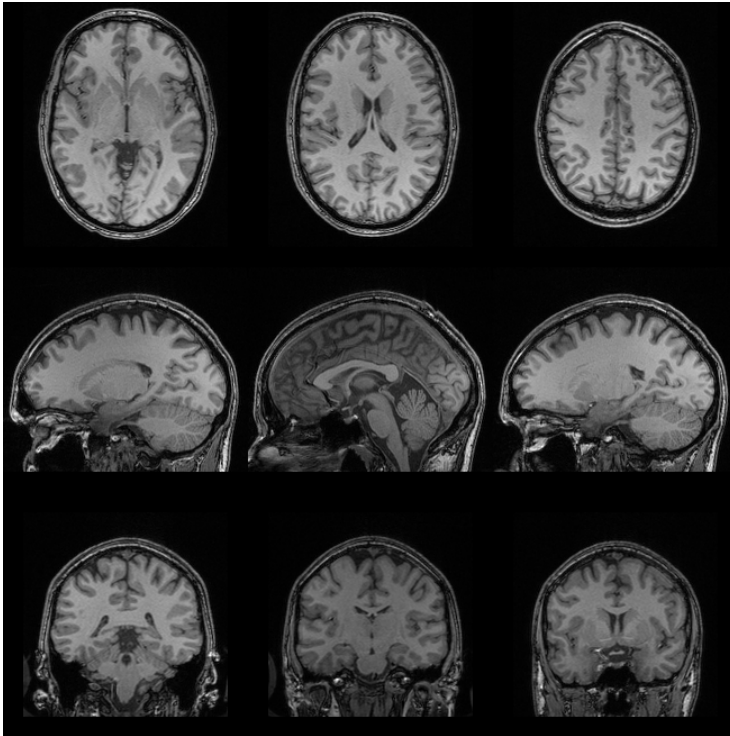
Figure 2.1: A typical conventional 3D high resolution T1 weighted image of a normal subject. Here shown with 3 axial slices, 3 sagittal slices and 3 coronal slices.

TR Repetition time represents the time between successive RF pulses sequences applied to the same slice.

TI Inversion time represents the time period between the inversion pulse and the excitation pulse.

TD Delay time: After the acquisition, for all rows a delay time is used to prevent saturation effects.

Typical scanning parameters are: Echo time (TE) 3.04 ms, repetition time (TR) 1550 ms, inversion time (TI) 800 ms, flip angle 9°, field of view 256 mm, matrix 256 x 256, 1 x 1 x 1 mm voxels, 192 slices with a total acquisition time of ∼6.38 minutes.[45]
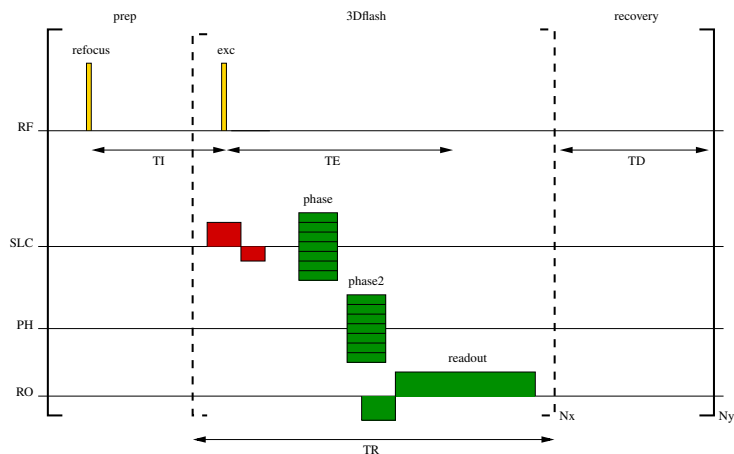
Figure 2.2: MPRAGE pulse sequence timing diagram. The diagram illustrates the steps of basic hardware activity that are played out during image acquisition. Time during pulse sequence execution is indicated along the horizontal axes. Each line represents a different hardware component, thus one line is needed for the radio frequency transmitter and one for each imaging gradient (SLC = slice selection gradient (x), PH = phase encoding gradient (y), RO = frequency encoding gradient (z), also called readout gradient). The MR signal is sampled during the positive RO gradient. Brackets indicate repetition.

2.1 Imaging artifacts

MRI images exhibit intensity and geometric distortion artifacts affecting various morphometric measures, depending on the sequence, vendor-specific gradient design geometry and patient anatomy.

An artifact often seen in MRI images is a smooth variation of the signal intensity across images. This artifact is variously referred to as RF inhomogeneity, shading artifact, bias field, or B_1 intensity non-uniformity. The artifact is usually attributed to several factors, such as poor radio frequency (RF) field uniformity, eddy currents driven by the switching of field gradients, and patient anatomy both inside and outside the field of view. There are several approaches to correct for intensity non-uniformity in MRI data that achieves high performance without requiring supervision. Correction of intensity non-uniformity in MRI data for has been shown to substantially improve the accuracy of anatomical analysis techniques such as tissue classification, registration and cortical surface extraction.[13, 108]

Before engaging in longitudinal analyzes it is important to correct for scanner-specific image distortions thereby allowing a more accurate comparison of quantitative morphometry results. Multi-modal and multi-site studies also requires correction of image distortions, as well as studies of populations where image distortions are likely to be systematic between groups, e.g. head size of children induces systematic image distortions which will covary with age. Although, cross-sectional studies also suffer from such distortions, the distortions can be considered stochastic and just add to the variance of the measurements. Image distortions can potentially affect the accuracy of quantitative morphometric measures such as volume [33], shape [87] and boundaries of sub-cortical structures[14].

A prominent source of distortions in structural MRI arises from imaging gradient non-linearities, which degrades both geometry and image intensities. The distortions arise because spatial localization is usually achieved using Fourier encoding. The encoding is realized by applying a magnetic field gradient along the dimension of interest, which is assumed to create a linear correspondence between the resonance frequency and spatial location following the Larmor equation. Any non-linearities in the magnetic field gradient will result in distorted images.[45] The distortion field specific to the Siemens sonata gradient coil is visualized in figure 2.3.

Figure 2.4 shows examples of the effect of gradient non-linearity distortions on one subject scanned several times at different positions within the scanner. It is worth noting that most of the intensity differences with low spatial frequencies are due to differences in radio wave inhomogeneities. The effect of the gradient non-linearities is the geometric distortions, which are apparent near the rim of features. The top images show the first scan from the scanning session, and the four subsequent images show the scaled absolute differences between the first scan and the subsequently acquired scans. All the scans have been coregistered using rigid body transformations to account for the different positions(see section 3.2).
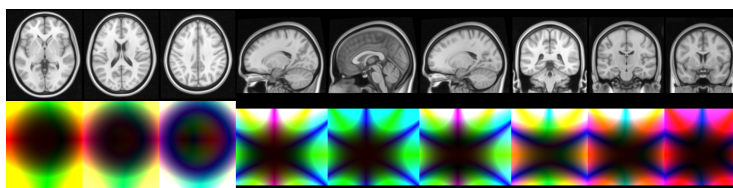
Figure 2.3: Geometric distortion field due to gradient non-linearities specific to the Siemens sonata gradient coils. Color indicate direction with red, green and blue color components corresponding to *x*, *y* and *z* directions respectively. The largest distortions within the image shown is about 6mm, and these are located furthest away from the centre of the bore. The top image shows the MNI template image.

Two main 3D correction methods have been developed. a) direct 3D measurements of the geometric distortions using specially designed imaging phantoms[69, 121, 122]. b) 3D calculations of the geometric displacements from the spherical harmonic expansion for the representation of the magnetic fields generated by the gradient coils[57, 61, 99]. The methods described in [61], have been extended reimplemented in a SPM toolbox. The new implementation relies on the same principles and algorithms, but has more flexible output, such as retaining the original voxel sizes in the images, and can be combined with other geometric distortion corrections. Images corrected using the toolbox are shown in figure 2.5. All the scans have been coregistered after correction using rigid body transformations to account for the different positions.

Gradient non-linearity correction was found crucial in the paper about spinal cord atrophy measures[75], for reducing the effect of subject positioning and vendor-specific gradient design geometry. Specifically, as a consequence of the gradient non-linearity correction, the coefficient of variance was reduced from 8.05 to 1.01% for the spinal cord area, 4.33 to 0.95% for the left-right widths and 4.03 to 0.93% for the anterior-posterior widths.

Homogeneity of the main magnetic field, B_0 is another important prerequisite for accurate spatial localization in magnetic resonance imaging. In the presence of B_0 inhomogeneities along any dimension, the linear mapping prescribed by the Larmor equation does not hold and spatial distortions arise in the acquired images. B_0 inhomogeneities are particularly pronounced at borders between low and high magnetic susceptibility, e.g. the interface of tissue and air. Spatial distortions at such interfaces increase with field strength, and will affect the accuracy of morphometric measures locally.
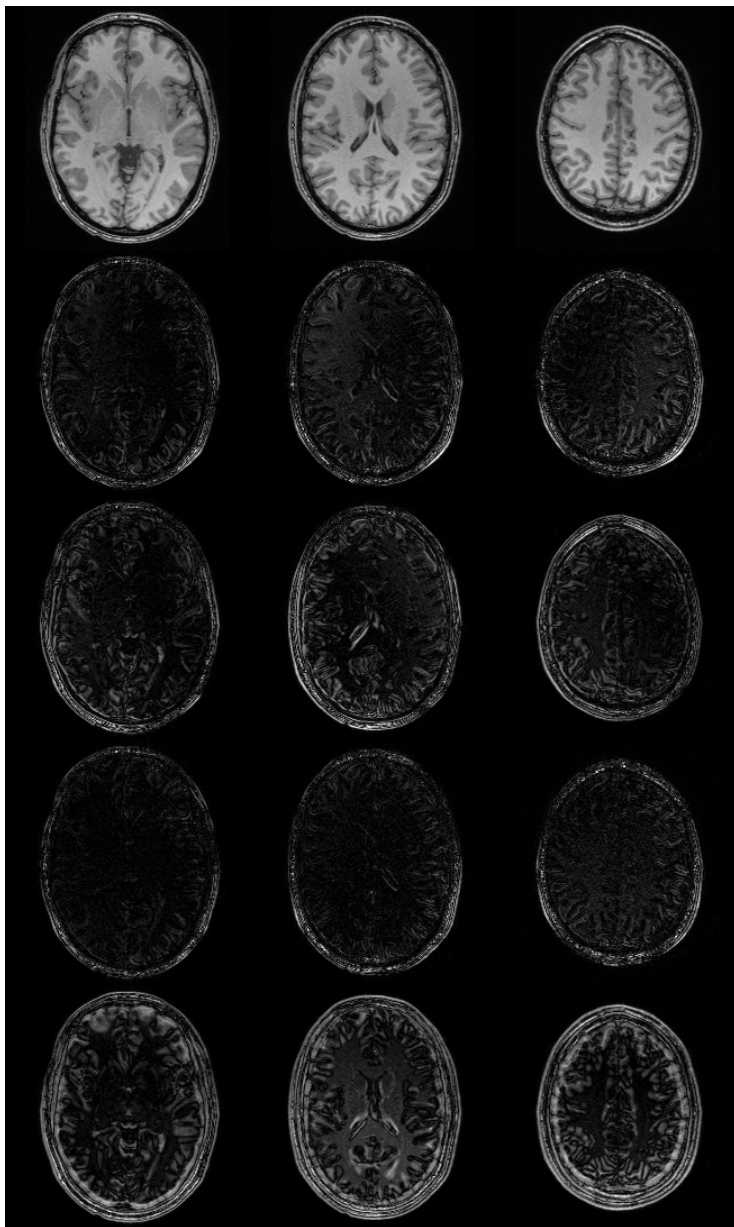
Figure 2.4: The top images shows the first MPRAGE scan of a scanning session out of five scans with different positions. The remaining images show the squared differences between the first scan and the subsequent scans, when not corrected for gradient non-linearities. The intensity differences with low spatial frequency are due to B_1 inhomogeneities. The intensity differences located near the rim of features are due to gradient non-linearities.
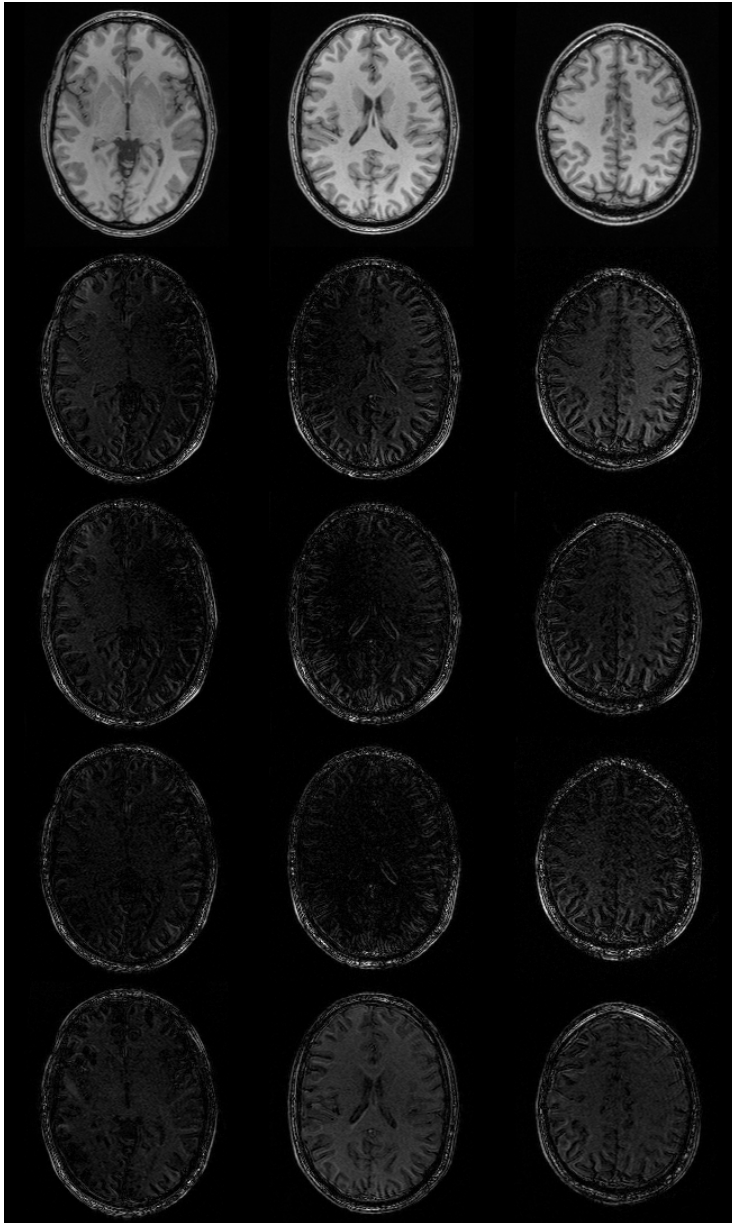
Figure 2.5: The top images shows the first MPRAGE scan of a scanning session out of five scans with different positions. The remaining images show the absolute differences between the first scan and the subsequent scans, when corrected for gradient non-linearities. The intensity differences with low spatial frequency are due to B1 inhomogeneities.

Image registration

Every MR image has a 4×4 spatial transformation matrix $\mathbf{M}$ associated with it, which maps voxel coordinates $\mathbf{x}$ to real world coordinates $\mathbf{y}$. The mapping is a simple matrix multiplication, $\mathbf{y} = \mathbf{M}\mathbf{x}$, or more elaborate:

$$\begin{pmatrix} y_1 \\ y_2 \\ y_3 \\ 1 \end{pmatrix} = \begin{pmatrix} m_{11} & m_{12} & m_{13} & m_{14} \\ m_{21} & m_{22} & m_{23} & m_{24} \\ m_{31} & m_{32} & m_{33} & m_{34} \\ 0 & 0 & 0 & 1 \end{pmatrix} \begin{pmatrix} x_1 \\ x_2 \\ x_3 \\ 1 \end{pmatrix} \tag{3.1}$$

This mapping of coordinates allows reorienting images without resampling, and also allows comparison of images with arbitrary resolutions and acquisition orientations.

Any spatial transformation matrix can be written as a product of a number of linear transformations; translations, rotations, scalings and shears. Each of these linear transformations is parametrized by three parameters, one for each spatial direction. Translations are the simplest, as it defines the mapping of origin between the coordinate systems

$$\begin{pmatrix} 1 & 0 & 0 & t_1 \\ 0 & 1 & 0 & t_2 \\ 0 & 0 & 1 & t_3 \\ 0 & 0 & 0 & 1 \end{pmatrix} \tag{3.2}$$

Rotations roll, pitch and yaw about the x, y and z axes respectively, are written as follows

$$
\begin{pmatrix}
1 & 0 & 0 & 0 \\
0 & \cos(u_1) & -\sin(u_1) & 0 \\
0 & \sin(u_1) & \cos(u_1) & 0 \\
0 & 0 & 0 & 1
\end{pmatrix}
\tag{3.3}
$$

$$
\begin{pmatrix}
\cos(u_2) & 0 & \sin(u_2) & 0 \\
0 & 1 & 0 & 0 \\
-\sin(u_2) & 0 & \cos(u_2) & 0 \\
0 & 0 & 0 & 1
\end{pmatrix}
\begin{pmatrix}
\cos(u_3) & -\sin(u_3) & 0 & 0 \\
\sin(u_3) & \cos(u_3) & 0 & 0 \\
0 & 0 & 1 & 0 \\
0 & 0 & 0 & 1
\end{pmatrix}
\tag{3.4}
$$

Scalings or Zooms, and finally shears

$$
\begin{pmatrix}
q_1 & 0 & 0 & 0 \\
0 & q_2 & 0 & 0 \\
0 & 0 & q_3 & 0 \\
0 & 0 & 0 & 1
\end{pmatrix}
\quad \text{and} \quad
\begin{pmatrix}
1 & s_1 & s_3 & 0 \\
0 & 1 & s_3 & 0 \\
0 & 0 & 1 & 0 \\
0 & 0 & 0 & 1
\end{pmatrix}
\tag{3.5}
$$

Any combination of translations and rotations defines a rigid body transformation, while adding scaling and shears defines a full affine transformation.[35]

Image transformation matrices are usually implicitly defined when positioning scans during image acquisition. The mapping of the transformation matrices is therefore from the individual images voxel coordinate systems to the scanner coordinate system. The scanner coordinate system is a right handed cartesian coordinate system with the z axis directed along the B_0 field, x along left/right, y along up/down, and has origin in the center of the bore.[1]

3.1   Optimization

Image registration (linear or non-linear) is really a non-linear optimization problem in that there is some function $O(\mathbf{q}, \mathbf{x})$ that depends in some non-linear fashion on a set of parameters $\mathbf{q}$ and the input data $\mathbf{x}$, and optimization determines the values of $\mathbf{q}$ that minimizes $O(\mathbf{q}, \mathbf{x})$ given $\mathbf{x}$. Methods for finding the parameters $\mathbf{q}$ come in many flavors, some require only the ability to calculate $O(\mathbf{q}, \mathbf{x})$ while other methods relies on the first, and possibly second, derivatives with respect to the parameters $\mathbf{q}$. Methods dependent on derivatives are usually faster and sometimes more robust, something that is especially important when there are a large number of unknown parameters.[88]

---

[1]The scanner coordinate system is defined in the DICOM standard, and the statement is only true for scanners conforming to these. [1]

The simplest and most used cost function is the "sum-of-squared differences" mentioned in section 3.2. Its use is limited to cases where the image intensities are very similar, as opposed to other cost-functions like e.g. normalised mutual information which are less sensitive to differences in contrast, also mentioned in section 3.2. However, the sum-of-squared differences cost-function has important computational advantages when searching for the parameters that minimize its value.[35]

Any image registration technique attempts to find a compromise between minimising the specified cost function, i.e. between making the images look as similar as possible, and making the deformations "reasonable". This compromise is formalised by a regularising function, which are functions of only the parameters $\mathbf{q}$ and not the data. The cost function is thereby split into a penalty function, that depends on both data and parameters, and a regularization function, only depending on the parameters.[88] The regularization function formalizes "reasonable" deformations, and are often based on concepts borrowed from mechanics, such as "membrane energy" and "bending energy". These are functions of the deformations themselves, that have a high value for sharp deformations and a small value for smooth deformations.

Newton's method for optimizations and related methods, such as Gauss-newton and Levenberg-Marquardt methods, utilizes the Taylor expansion of the cost function $O(\mathbf{q}, \mathbf{x})$ with respect to the parameters $\mathbf{q}$. Thus, provided that $O(\mathbf{q}, \mathbf{x})$ is twice-differentiable, and a reasonable starting estimate $\mathbf{q}^{(0)}$, the sequence defined by

$$\mathbf{q}^{(k+1)} = \mathbf{q}^{(k)} - \gamma \left[H O(\mathbf{q}^{(k)}, \mathbf{x}) \right]^{-1} \nabla O(\mathbf{q}^{(k)}, \mathbf{x}) \tag{3.6}$$

will converge towards an extremum of $O(\mathbf{q}^{(k)}, \mathbf{x})$. H denotes the Hessian, and related algorithms use different approximations of this to obtain a solution, as its exact calculation and inversion can be computationally intensive and numerically unstable.[88]

3.2 Coregistration

The scanner coordinate system is not optimal for voxel-wise statistical analysis of images due to differences in subject position during and between acquisitions. Therefore it is essential to obtain point correspondence between images by ensuring that the transformation matrices of all images of subjects refer to the same anatomical coordinate system. The process of determining these transformation matrices is generally called coregistration. In neurosurgery and neurological research one generally uses the Cartesian coordinate system known as stereotaxic space as an external, three-dimensional frame of reference. The most prominent stereotaxic space is most likely the Talairach coordinate system(see section 3.3)[113].

There are two steps involved in registering a pair of images together. There is the registration itself, whereby the optimal transformation is determined, and then there is the transformation which involves resampling the images in a new voxel coordinate system. Resampling of the images at arbitrary voxel coordinates is fundamental to the registration process, both in order to evaluate any objective function during optimization, and also to write the images once the optimal transformation has been determined. A common method for interpolation of images is to represent the voxel intensities as a linear combination of basis functions, typically b-splines of three or more degrees. Resampling then involves determining the parameters for the basis functions once, and evaluation at new points is an appropriate linear combination of the basis function. Resampling is then expressed as a simple convolution of the basis function coefficients.[35, 88]

Images of the same subject with similar contrasts between tissue types, can be coregistered by minimizing the mean squared difference between each of the images. The objective function being optimized is

$$\lambda_1 \sum_i \left(f\left(\mathbf{M}\mathbf{x}_i\right) - q g\left(\mathbf{x}_i\right)\right)^2 + \lambda_2 \sum_i \left(g\left(\mathbf{M}^{-1}\mathbf{x}_i\right) - q^{-1} f\left(\mathbf{x}_i\right)\right)^2 \tag{3.7}$$

q is an intensity scaling parameter accounting for the arbitrary scaling of MT image intensities. The objective function is made symmetric, to obtain more robust solutions [125, 126]. Gauss-Newton optimization algorithm has proven a good algorithm for rigid registration of images with similiar contrast. f and g are the resampling functions able to evaluate image intensities at arbitrary voxel positions in the respective images.[35]

Coregistration of images with different contrasts between tissue types, requires a different objective function derived from information theoretical measures such as entropy of joint probability distributions. This approach is required since there need not be a linear relationship between the image intensities. The entropy of joint probability distributions is written as

$$H\left(\mathbf{f},\mathbf{g}\right) = -\int_{-\infty}^{\infty}\int_{-\infty}^{\infty} P\left(\mathbf{f},\mathbf{g}\right)\log\left(P\left(\mathbf{f},\mathbf{g}\right)\right)d\mathbf{f}d\mathbf{g} \tag{3.8}$$

While the the marginalized entropies are given as

$$H\left(\mathbf{f}\right) \quad = \quad -\int_{-\infty}^{\infty} P\left(\mathbf{f}\right)\log\left(P\left(\mathbf{f}\right)\right)d\mathbf{f} \quad \text{and} \tag{3.9}$$

$$H\left(\mathbf{g}\right) \quad = \quad -\int_{-\infty}^{\infty} P\left(\mathbf{g}\right)\log\left(P\left(\mathbf{g}\right)\right)d\mathbf{g} \tag{3.10}$$

These enable the definition of normalized mutual information

$$\tilde{I}\left(\mathbf{f},\mathbf{g}\right) = \frac{H\left(\mathbf{f}\right)+H\left(\mathbf{g}\right)}{H\left(\mathbf{f},\mathbf{g}\right)} \tag{3.11}$$

These equations are easily discretized using histograms, and appropriate summations. The optimal rigid body transformation is then found using a Levenberg-Marquardt optimization algorithm, a stabilized version of the Gauss-Newton method used for the mean squared difference measure.[35] These methods for coregistration have been implemented in a number of freely available toolboxes, including FSL[58, 59] and SPM[5, 8, 63].

3.3 Spatial normalisation

Individual coordinate systems of different subjects are not immediately comparable, as a set of coordinates rarely will correspond to the same underlying neuroanatomical feature. When matching multiple subjects it is often more convenient to coregister each subjects brain to a common template using affine transformations, thus accounting for differences in size and global skewness. Either of the above mentioned objective functions can be appropriate depending on quality and contrast of the common template. Many studies rely on this simple approach of spatial normalisation for reporting neuroanatomical locations. More often spatial normalisation rely on additional nonlinear registration techniques, potentially requiring millions of parameters to describe the nonlinear transformations that warp an image into a standard space.[96]

The problem of spatial normalization, i.e. how to map a single subject's brain image into another brain or a template, is indeed not a trivial one. In practice it is often meaningless to even attempt an exact match between brains beyond a certain resolution. There is no one-to-one relationship between the cortical structures of one brain and those of another, so any registration method that attempts to match brains exactly must fold the brain to create artificial sulci and gyri. Even if an exact match is obtained, the solutions obtained by high-dimensional warping techniques may not be truly optimal. Hence any solution to the spatial normalization problem has to be a compromise between an exact match and warp complexity in order to obtain a valid point correspondence between subjects.[66]

Spatial normalization facilitates a wide range of statistical analyses, either voxel-based or via appropriate representations of neuroanatomical features derived from shape or geometric properties. Once a set of meaningful euclidian coordinates within a standard reference space has been obtained, results are readily incorporated into existing literature, brain atlases and databases.[82]

The most commonly adopted coordinate system within the brain imaging community is that described by the atlas of Talairach and Tournoux, 1988[113]. Use of the Ta-

lairach coordinate system and the accompanying atlas is heavily discussed[118], as it is based upon postmortem sections of a 60-year-old french female with a smaller than average brain size. This means that most other brains need to be considerably warped to conform to the small size of the atlas, introducing both bias and error. Furthermore, anatomical labeling of Brodmann areas was done visually using inconsistent slices[67]. Nonetheless, the Talairach atlas has proved an invaluable tool in modern neuroimaging, and has paved the way for more representative brain atlases including the MNI atlas from the Montreal Neurological Institute, used throughout this thesis.[29, 30]

Registering one image volume to another involves estimating a vector field (deformation field) that maps from coordinates of one image to those of the other. In this thesis, one image (the template image) is considered as fixed, and a mapping from this image to the second image (the source image) is estimated. The intensity at the i'th voxel of the template image is denoted $g(\mathbf{x}_i)$, where $\mathbf{x}_i$ is a vector describing the coordinates of the voxel. The deformation field spanning the domain of the template is denoted by $\mathbf{y}_i$ (or $\mathbf{y}(\mathbf{x}_i)$) at each point, and the intensity of the source image at this mapped point by $f(\mathbf{y}_i)$. The source image is transformed to match the template by resampling it at the mapped coordinates.[8]

Solutions to the very high dimensional spatial normalisation problem can be obtained in many ways. Often methods are tailored to specific features, such as subcortical structures or the cortical surface or tailored to specific types of analysis, fMRI or VBM[9, 32]. The approach used in the SPM software is based on a parametrization of the deformation field using cosine basis functions, see figure 3.1. In short the spatial transformation variables are written as

$$y_1(\mathbf{x}, \alpha) \;=\; x_1 + \sum_{m=1}^{M} \alpha_{m1} \phi_m(\mathbf{x}) \tag{3.12}$$

$$y_2(\mathbf{x}, \alpha) \;=\; x_2 + \sum_{m=1}^{M} \alpha_{m2} \phi_m(\mathbf{x}) \tag{3.13}$$

$$y_3(\mathbf{x}, \alpha) \;=\; x_3 + \sum_{m=1}^{M} \alpha_{m3} \phi_m(\mathbf{x}) \tag{3.14}$$

with

$$\phi_1(i) = \frac{1}{\sqrt{I}}, \quad \phi_m(i) = \sqrt{\frac{2}{I}} \cos\left(\frac{\pi(2i-1)(m-1)}{2I}\right) \quad i = 1\ldots I, m = 2\ldots M \tag{3.15}$$

Deformations are thus only defined by a few hundred parameters, forfeiting the potential precision of other non-linear registration methods. Deformations with high spatial frequencies cannot be modeled, since the deformations are restricted to the lowest spatial frequencies of the basis functions. This approach is unsuited for exact matches
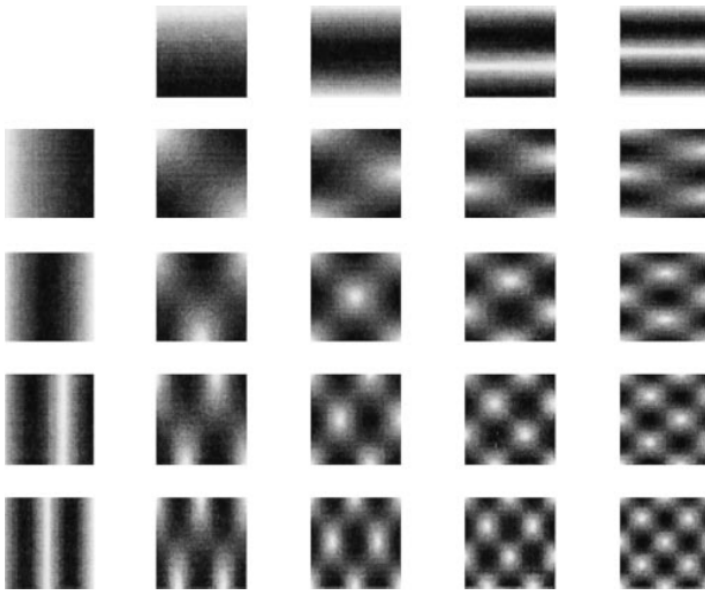
Figure 3.1: The lowest frequency two-dimensional cosine basis functions.[6]

between fine cortical structures, and does not encompass the whole range of detailed shape variability of neuroanatomical features found within the general population.[6, 10]

3.4 DARTEL

The DARTEL ("Diffeomorphic Anatomical Registration using Exponentiated Lie algebra") procedure utilizes a more sophisticated registration model, described in [9], to obtain a better spatial normalisation, with a higher degree of neuroanatomical correspondence between subjects. This model uses in the order of 6 000 000 parameters, providing plenty degrees of freedom to achieve much more precise intersubject alignment, and was developed specifically to counter the criticisms pertaining voxel based morphometry(see section 4.2). It has been shown that DARTEL outperforms ROI-based registration algorithms[135] and a number of other widely used and fully automated intersubject registration algorithms[66].

The DARTEL procedure is an iterative procedure initiated with rigidly aligned gray and

white matter segmentations of brain images. DARTEL creates a "flow field" for each of the subjects encoding how the individual images should be warped. The algorithm alternates between computing templates based on the average tissue probability maps from all subjects and subsequently updating the flow fields to best match the individual images to the latest template. As the images gradually become better aligned, the average tissue probability maps become increasingly sharp and gradually less smoothing is applied to the templates. Gray and white matter tissue maps are simultaneously aligned.

The computed average template need not be appropriately registered with the Talairach coordinate system nor MNI space, thus requiring further spatial normalisation to report the location of differences within a more established coordinate system. This can be achieved by using the spatial normalisation procedure described in section 3.3 on the average tissue probability maps.

3.5   High-dimensional warping

In the case of multiple images from the same subjects, it is often possible to obtain an one-to-one match between the images using non-linear registration, of at least some parts of the brain. The deformation field will in this case incorporate the dynamics of the subject's neuroanatomy during growth, aging, maturation, disease progression or treatment. Any singularities in the deformation field will occur due to localized neuroanatomical changes, such as disappearance or occurence of hemorrhagic lesions, occurrence of 'black hole' lesions often found in multiple sclerosis patients, or even as a result of surgical intervention. This quantitive and potentially very localized approach to the dynamics of neuroanatomy is at the core of the publications composing this thesis.

A high dimensional model has been implemented in SPM's high dimensional warping (HDW) toolbox, where a finite element approach is employed to estimate translations of each voxel. The toolbox uses bayesian statistics to obtain a maximum a posteriori (MAP) estimate of the deformation field describing the differences between the images. Priors describing the probability distributions of the deformation, are in this implementation assumed to have symmetric properties. This implies that the probability of obtaining a particular deformation field, is the same as obtaining its inverse. The details of the implementation can be found in [8, Chp. 4] and [4].

An example of a deformation field obtained using this toolbox is shown in figure 3.2.
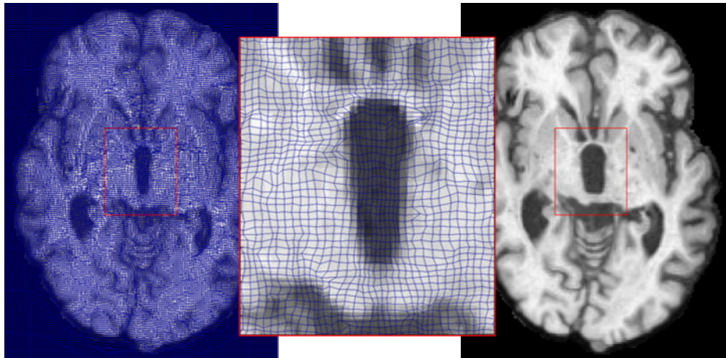
Figure 3.2: The deformation field illustrating the warping of one image to another.[101]

SPM's HDW toolbox was chosen because, it has been developed specifically with this purpose in mind, it computes a deformation field in reasonable time and has been successfully deployed in a number of studies[19, 31, 65]. There are a plethora of non-linear image registration techniques, related algorithms and implementations(see [66] for an evaluation of 14 non-linear deformation algorithms), many of which are equally applicable to detect localized neuroanatomical changes as SPM's HDW toolbox.

3.6 Smoothing

It is customary to smooth spatially normalized images by convolving with a 3D Gaussian kernel having FWHM ∼ 4-12mm. Smoothing of images both enhances statistics by noise cancellation, and somewhat compensates for imperfect anatomical correspondence between subjects. Furthermore, the fact that Gaussian random field theory is often used to control the family-wise error in mass-univariate hypothesis tests for significant effects require that data exhibit smoothness over several millimeters to become in agreement with the assumptions usually made in Gaussian random field theory[131]. Drawbacks of smoothing include compromised spatial resolution.

CHAPTER 4

Morphometry

A large number of approaches for morphometric analysis, i.e. characterization of neuroanatomical variability, exists, both within and between subjects. A simple approach involves subtracting images of single subjects acquired at different time points[11]. Most changes detected with this method will be related to pathology, provided that the images are properly coregistered (see section 3.2). Interpretation of results can be straight-forward for localized pathological changes, however many neurodegenerative diseases induce neuroanatomical changes that are too mild, diffuse, or topologically complex to be interpreted or even detected by this method (see figure 4.1 for an example).

The following sections cover two morphometry methods for quantitative and voxel-wise comparison of neuroanatomy throughout the brain, tensor-based morphometry (TBM) and voxel-based morphometry (VBM). Furthermore two methods for whole brain measures of morphometry are discussed.

Figure 4.1: Subtraction of images detect pathological changes. This subject sustained a severe traumatic brain injury, and has both diffuse and focal injuries.

4.1   Tensor-based morphometry (TBM)

Tensor based morphometry encodes any structural differences within a deformation field obtained from high-dimensional image registration, which can be further characterized by a number of statistical procedures. Methods utilizing these deformation fields to quantify neuroanatomical differences at each voxel are termed deformation based morphometry (DBM), or tensor based morphometr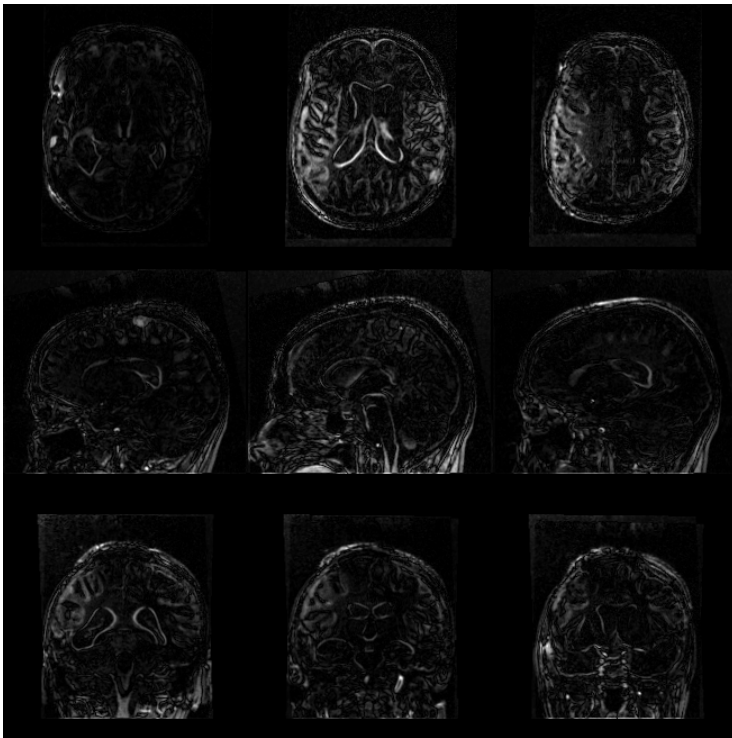y (TBM).[8] Deformation based morphometry refers to methods that identify differences in relative positions within subjects brains. Tensor based morphometry uses the deformation fields to identify differences in the local shape of brain structures.[35]

The deformation fields describe the spatial transformation that matches individual brains to each other or to a common template. The deformation fields that describe the spatial transformation to match individual brains to a common template, can also be studied on their own right. The deformation fields contain information about the individual image shapes, however the enormous neuroanatomical variability between normal subjects, makes interpretations less straight-forward.

Once an appropriate deformation field has been obtained, any further analysis is usually based upon the accompanying jacobian matrices. Each voxel contains information about the local stretching, shearing and rotation involved in the deformation, in the Jacobian matrix which is defined by:

$$\mathbf{J} = \begin{pmatrix} \frac{\partial y_1}{\partial x_1} & \frac{\partial y_1}{\partial x_2} & \frac{\partial y_1}{\partial x_3} \\ \frac{\partial y_2}{\partial x_1} & \frac{\partial y_2}{\partial x_2} & \frac{\partial y_2}{\partial x_3} \\ \frac{\partial y_3}{\partial x_1} & \frac{\partial y_3}{\partial x_2} & \frac{\partial y_3}{\partial x_3} \end{pmatrix} \tag{4.1}$$

The determinant of the jacobian matrices is directly related to local volume changes, before and after warping, and often appears as a normalization factor in differential geometry. If a region shrinks to half its original volume during the warping, then the intensity should be doubled so that the total signal is conserved. Analysis of the deformation fields is not limited to volumes, lengths, areas and other invariant tensor measures are potentially useful for localizing neuroanatomical changes or variability. Jacobian matrices of the deformation field can also be transformed in various ways, for example, by calculating strain tensors [4] or by the matrix logarithm [71, 127].

Spatial normalization of Jacobian determinant maps needs to be interpolated using logarithmic interpolation. This is achieved by simply taking the logarithm of the Jacobian determinants prior to spatial normalization, and exponentiating in normalized space. Furthermore the logarithmic of jacobian determinants is more symmetric and thus more appropriate for classical statistical analysis.[70]

The simplest form of TBM involves voxel-wise comparison of relative volumes derived from the Jacobian determinants of the deformation fields. Stastical inferences are made voxel-wise through use of spatial normalisation of such Jacobian determinant maps, as described in section 5, creating statistical parametric maps showing regional volume differences among poulations. This type of morphometry specifically looks at whether local growth or volume loss has occured between the time points of the scanning. The first paper discussed in chapter 6 uses this method. Alternatively the jacobian determinants can be combined with a VBM analysis to quantify local volume changes in units of gray matter tissue, as discussed in chapter 7.

TBM has been successfully utilized in studies of multiple sclerosis [116], maturation [54], HIV/AIDS [71, 72], Ageing and age-related diseases [19, 53, 55], and many others. The methods for TBM are not as standardized as methods for VBM. Each choice of intra-subject non-linear registration method spawns a new TBM method [20, 54, 85].

4.2   **Voxel-based morphometry (VBM)**

The direct voxel-wise comparison of local gray matter concentrations between subjects is termed voxel-based morphometry (VBM), and was introduced as a standardized method by John Ashburner & Karl Friston in [7].

The basic procedure for a VBM analysis involves the serial application of image intensity non-uniformity correction, tissue classification, spatial normalization of generated tissue probability maps, modulation with Jacobian determinants of the applied deformation field and finally spatial smoothing. Statistical inferences are then made upon resulting images of gray matter concentrations. Results obtained from a VBM analysis are heavily dependent on the specific image processing techniques employed, as well as good consistent image quality[12, 17]. The choice of tissue classification algorithm, spatial normalization method and statistical procedures all influence both anatomical specificity and statistical sensitivity.[10] To complicate matters further the entire procedure for VBM analysis is inherently circular.[13] Methods for tissue classification almost always rely on prior probability maps, which needs to be warped using spatial normalization methods. Spatial normalisation methods benefit greatly from the use of gray and white matter segmentations. Finally both methods rely on image intensity non-uniformity correction, which again benefit from both segmentations and spatial normalization. The circularity is resolved in SPM5, which implements a combined generative model for tissue classification, spatial normalisation and image intensity non-uniformity correction.[13] Estimation of the model parameters is an alternation between tissue classification, bias correction, and non-linear registration
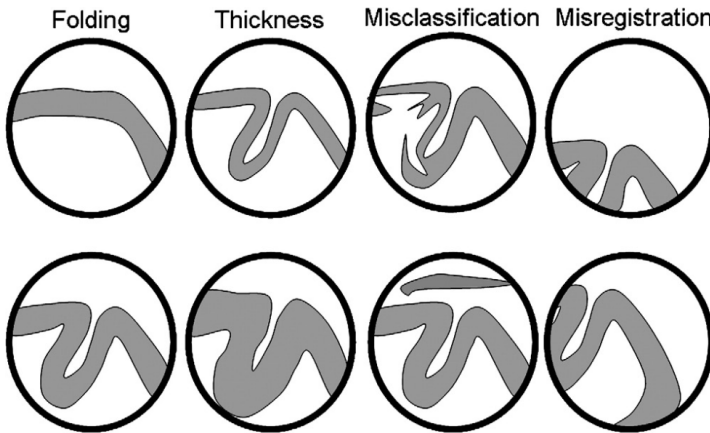
Figure 4.2: This illustrates how findings from a VBM study of gray matter could be interpreted. The top row shows situations where there would be less gray matter in a cortical region compared to the situation shown below it. From left to right, differences could be attributed to folding, thickness, misclassification or misregistration. Generally, the objective is to interpret differences in terms of thickness or folding.[10]

steps. This approach provides significantly better results than serial applications of each component.[13, 130] In order to preserve the volume of tissue from each structure, the warped images are multiplied, voxel-by-voxel with the Jacobian determinants of the deformations. Jacobian determinants encode relative volumes of tissue, before and after warping. For example, if a region shrinks to half its original volume during the warping, then the intensity would be doubled so that the total signal from that region is conserved. Figure 4.2 shows possible interpretations of findings in a VBM study of gray matter.

VBM has been successfully utilized in studies of ageing [42], age related diseases [22, 43], schizophrenia [60, 132, 133] and many other. The validity of VBM has been much discussed [12, 17, 84, 96], especially in relation to the employed spatial normalization routine. One of the criticisms of VBM has been that the precision of non-linear inter-subject registration using spatial basis functions is insufficient. For example, if the registration procedure systematically has problems with one population type, eg. elderly people with large ventricles, the anatomical differences detected by VBM may be real, but their localization and explanation in terms of gray matter volumetry may be incorrect. Specifically, any voxel-wise statistics are uninformative about group differences wherever the spatial normalization algorithm fails to register on robustly appearing image gradients. The method introduced in [7] is only valid far from all image gradients. These discussions has led to the development of the DARTEL procedure discssued in section 3.4.

4.3 Whole brain measures

Quantitative measurement of global changes in brain size and shape, especially to estimate atrophy in patients, provides a clinically useful measure. Structural Image Evaluation, using Normalisation, of Atrophy (SIENA) for longitudinal studies [110] and the cross-sectional variant SIENAX [111] has proven both robust and accurate. SIENA uses two brian images taken at different points in time, to estimate of percentage brain volume change (%BVC). SIENA works automatically by segmenting brain from non-brain in each image, and the external surface of the skull is used for rigid intra-subject registration. The surface of each brain is then estimated and the surface motion is estimated upon these. The mean perpendicular edge motion across the entire brain surface can then be converted into a percentage brain volume change estimate with subvoxel accuracy. Measurement error of %BVC has been reported to be approximately $\pm 0.2\%$ [111].

The cross-sectional variant, SIENAX, utilizes the same procedures as SIENA, however the second image is always the standard MNI template. Furthermore, it is not meaningful to report %BVC, instead global estimates of gray and white matter are reported.[111]

These methods were employed in [102, 134].

Statistics

Statistical inference in neuroimaging studies typically relies on classical/Fisher statistics testing using the hypothesis testing framework.[131] Hypothesis testing is generally done voxelwise using a mass-univarate approach, with significance levels sufficiently adjusted for multiple comparisons. A general linear model is fitted to the data in each voxel, thus obtaining statistical parameters which can be mapped into a stereotaxic space.[35]

5.1 Bayes' Theorem

Bayes' Theorem relates the direct probability of a generative model $\mathcal{M}$ with parameters $\boldsymbol{\theta}$ conditional on a given body of data $\mathbf{Y}$, $p(\mathcal{M}, \boldsymbol{\theta}|\mathbf{Y})$, to the inverse probability of the data conditional on the generative model, $p(\mathbf{Y}|\mathcal{M}, \boldsymbol{\theta})$ denoted the likelihood.

$$p(\mathcal{M}, \boldsymbol{\theta}|\mathbf{Y}) = \frac{p(\mathbf{Y}|\mathcal{M}, \boldsymbol{\theta})\, p(\mathcal{M}, \boldsymbol{\theta})}{p(\mathbf{Y})} \tag{5.1}$$

Despite its mathematical triviality, Bayes' Theorem is of great value in calculating conditional probabilities because inverse probabilities are typically both easier to ascertain and less subjective than direct probabilities. The probability of the model $p(\mathcal{M}, \boldsymbol{\theta})$ expresses the expectations about the model and parameters *prior* to observing the data

(hence typically denoted the prior). The probability of the data $p(\mathbf{Y})$ in the denominator is constant given $\mathbf{Y}$, and thus only serves as a normalisation factor and its direct calculation is most often avoided. $p(\mathbf{Y})$ can be calculated directly by summing/integrating the likelihood over all possible models and parameters involving substantial computational complexity.[52, 81]

5.2   The General Linear Model

The linear model is a pillar of modern statistics and is prominent in the analysis of neuroimaging data [18, 36, 37]. Given a set of input/predictor vectors $X^{\mathsf{T}} = (X_1, X_2, \ldots, X_K)$, the following model in matrix notation is used to predict the output Y at each voxel

$$\mathbf{Y} = \mathbf{X}\boldsymbol{\beta} + \boldsymbol{\epsilon} \tag{5.2}$$

Where $\mathbf{Y}$ denotes a $T \times N$ matrix containing the observed data series (of length T) as columns for each of the N voxels. $\mathbf{X}$ is a $T \times K$ matrix, denoted the design matrix, and $\boldsymbol{\beta}$ is a $K \times N$ parameter matrix (to be estimated). Finally, the $\boldsymbol{\epsilon}$ is the $T \times N$ residual matrix.

Assuming spatial independence and normally distributed residuals, ie. the spatially independent matrix variate normal distribution ($\boldsymbol{\epsilon} \sim \mathcal{N}_{T \times N}(\mathbf{0}, \mathbf{I}, \boldsymbol{\Sigma})$), the probability density is written as follows

$$p(\boldsymbol{\epsilon}|\boldsymbol{\Sigma}) = (2\pi)^{\frac{-TN}{2}} |\boldsymbol{\Sigma}|^{-N/2} \exp\left(-\frac{1}{2}\operatorname{Tr}\left[\boldsymbol{\epsilon}^{\mathsf{T}}\boldsymbol{\Sigma}^{-1}\boldsymbol{\epsilon}\right]\right) \tag{5.3}$$

Substituting $\mathbf{Y} - \mathbf{X}\boldsymbol{\beta}$ for $\boldsymbol{\epsilon}$ in the expression above, the probability is maximized by differentiating with respect to the each of parameters and equating to zero. The maximum likelihood estimate for the parameters $\boldsymbol{\beta}_{\mathrm{ML}}$ thereby becomes

$$\mathbf{X}^{\mathsf{T}}\boldsymbol{\Sigma}^{-1}\mathbf{X}\boldsymbol{\beta}_{\mathrm{ML}} = \mathbf{X}^{\mathsf{T}}\boldsymbol{\Sigma}^{-1}\mathbf{Y} \Rightarrow \boldsymbol{\beta}_{\mathrm{ML}} = (\mathbf{X}^{\mathsf{T}}\boldsymbol{\Sigma}^{-1}\mathbf{X})^{-1}\mathbf{X}^{\mathsf{T}}\boldsymbol{\Sigma}^{-1}\mathbf{Y} \tag{5.4}$$

This estimate is also known as the generalized least squares (GLS) or pre-whitened maximum likelihood estimate.[52] In the special case $\boldsymbol{\Sigma} = \mathbf{I}$, this maximum likelihood estimate is known as the ordinary least squares solution(OLS).[52]

The above expressions describe a multivariate model, however the assumed spatial independence essentially makes parameter estimation univariate. The remaining problem is to determine a good estimate of the covariance matrix $\boldsymbol{\Sigma}$. An often used estimate utilizes the residuals of the OLS solution, such that

$$\overline{\boldsymbol{\Sigma}} = \frac{1}{1-K}\boldsymbol{\epsilon}_{\mathrm{OLS}}^{\mathsf{T}} \otimes \boldsymbol{\epsilon}_{\mathrm{OLS}} \tag{5.5}$$

This estimate only has full rank and hence is invertible when $N >= T + K$. When $N < T + K$, the estimation of the covariance becomes an ill-posed problem due to the many free parameters. A specific structural form or a regularized version of Σ is often used to reduce this problem and handle such cases.[74, 128, 129]

Proper construction of the design matrix and the accompanying contrasts (see section 5.3) is essential for the application and interpretation of the general linear model. The design matrix is assumed to be deterministic, and each column represents independent variables which potentially describe the observed data in terms of other explanatory variables. Each column in the design matrix can come from a number of different sources

- Quantitative inputs; Age and weight are good examples.

- Transformations of quantitative input; log or square-root to model specific non-linear effects.

- Basis expansions, eg polynomial representation of quantitative inputs.

- Numeric coding of non-numeric inputs, eg binary encoding of gender. Factors with multiple levels are represented with an equal number of columns using binary encoding, eg. subjects in a repeated measures experiment.

- Interactions between variables, eg. Age$\times$Gender.

A column of ones is almost always included to model the intercept. In the case where $\mathbf{X}^\mathsf{T}\mathbf{X}$ is singular, the above expressions are modified by replacing the inverse by a pseudo inverse and K with the rank of $\mathbf{X}$. However, in this case the parameters of the model are not unique (in the sense that other parameters can produce the same residual) and interpretation of the parameters may be hampered.[23]

5.3   Hypothesis Testing

In the hypothesis testing framework, a null hypothesis is constructed reflecting how a test statistic would behave if the effect of interest was not present. If the test statistic is sufficiently extreme compared to the expected behavior, then the data does not support the null hypothesis and the alternative hypothesis is accepted. The most commonly used statistic is the student's t-test

$$t = \frac{\widehat{x} - \mu}{\widehat{\sigma}/\sqrt{n}} \tag{5.6}$$

Where x represents the quantity to be tested, μ is the value of x defined by the null hypothesis, $\widehat{\sigma}$ is the sample standard deviation and n is the residual degrees of freedom. The residual degrees of freedom is the total number of samples minus the degrees of freedom used to estimate the model. The t-test statistic is distributed according to the T-distribution with n degrees of freedom under the null hypothesis (no effect, Gaussian uncorrelated noise). When x is based on two samples (two-sample T-test/paired T-test) the denominator needs to be calculated assuming either equal sample size and variances (pooled-variance estimate), different sample sizes and equal variances, or different sample sizes and unequal variance through the Welch-Satterthwaite equation [97, 123].

An alternative test useful for testing the significance of a combination of effects is the F-test, here the ratio between the variance explained by two competing models (the null model and the alternative model) is tested.

$$F = \frac{(\text{RSS}_0 - \text{RSS}_1)/(K - K_0)}{\text{RSS}_1/(T - K - 1)} \qquad (5.7)$$

RSS_0 and RSS_1 denotes the residual sum of squares for least squares fit of general linear models with K_0 (the null model) and K (the alternative model) parameters respectively.

The general linear model allows for testing of linear combinations of effects through the contrast vector. A contrast vector $\mathbf{c}$ ($1 \times K$) defines the explanatory variables of interest, with which the voxel-wise t-test becomes

$$t_i = \frac{c\beta_i}{\widehat{\sigma}_i(c\beta_i)/\sqrt{n}}, \qquad (5.8)$$

The voxel-wise standard deviation estimate $\widehat{\sigma}_i(c^{\mathsf{T}}\beta_i)$ for this particular choice of contrast vector and covariance matrix is determined by

$$\widehat{\sigma}_i(c\beta_i) = \sqrt{\widehat{\sigma}_i^2 c(\mathbf{X}^{\mathsf{T}}\mathbf{\Sigma}^{-1}\mathbf{X})^{\dagger}c^{\mathsf{T}}} \qquad (5.9)$$

$\mathbf{X}^{\dagger}$ denotes the Moore-Penrose generalized/pseudo inverse of the matrix $\mathbf{X}$. More generally, $\mathbf{c}$ can be also a $(K - K_0) \times K$ matrix thereby defining an F-test. The voxel-wise F-test statistic is written

$$F_i = \frac{(\mathbf{c}\beta)^{\mathsf{T}}\left(\mathbf{c}(\mathbf{X}^{\mathsf{T}}\mathbf{\Sigma}^{-1}\mathbf{X})^{\dagger}c^{\mathsf{T}}\right)(\mathbf{c}\beta)/(K - K_0)}{\epsilon_1^{\mathsf{T}}\epsilon_1/(T - K - 1)} \qquad (5.10)$$

The voxelwise T- and F-statistics can be compared to the tabularized distributions to obtain a p-value, ie. the probability of observing an effect when the null hypothesis is true, commonly referred to as the uncorrected p-value.

5.4 Multiple comparisons

The uncorrected p-value from voxel-wise procedure for T- and F-tests attempt to control the voxel-wise false positives. However, when many voxels are considered this is not desirable as even a quite low false positive rate can result in many voxels being reported significant. The simple method of adjustment named after Bonferroni is based firmly within the classical tradition in applied statistics. Under the assumption that all tests are independent, the Bonferroni adjustment allow control of the so called family-wise error by simply multiplying the uncorrected p-value by the number of (independent) tests (The family-wise error refers to the probability of making one or more type-I errors). The Bonferroni adjustment is generally considered too conservative for neuroimaging studies, due to the fact that all voxels exhibit strong spatial dependence (especially after spatial smoothing).[130]

Spatial dependence can be taken into account through the use of Gaussian random field theory, which utilizes euler characteristics of regions above the statistical threshold to approximate proper statistical thresholds[130]. Alternatively the spatial extent of regions of significant voxels can be used to approximate a proper statistical threshold[38].

Another alternative is to control the expected overall false discovery rate (FDR), ie. the proportion of voxels declared significant which on average can be expected to be false positives[16, 39, 94]. Benjamini and Hochberg (1995) first proposed the notion of false discovery rate in [15], and here they showed a testing procedure which bounds FDR at a user-defined level α. The Benjamini-Hochberg procedure is based on p-values, and is calculated using the following algorithm

1. Fix the false discovery rate α and let $p(1) \leq p(2) \leq \cdots \leq p(N)$ denote the ordered p-values

2. Define $L = \max \{ j : p(j) < \alpha \cdot j/N \}$

3. Reject all hypotheses H_{0j} for which $p_j \leq p(L)$, the FDR rejection threshold.

Note that the FDR is not the same as type-I error, for which 0.05 is the customary threshold. The false discovery rate is the expected proportion of false positive among all the voxels that passes the threshold, thus $\alpha > 0.05$ might still be useful, especially if the study is exploratory in nature.[24].

The strong emphasis put on the null hypothesis unfortunately has a tendency to make hypothesis testing quite sensitive to the explicit assumptions made such as for exam-

ple normality. For instance variance estimates are quite sensitive to outliers making assumption of Gaussian residuals/normality important in especially F-tests.

5.5   Resampling methods for statistical inference

Classical parametric tests, as they are described in the previous sections, compare the observed statistics to their repective theoretical distributions, thereby indicating evidence of the experimental effect of interest. Resampling methods depart from theoretical distributions, instead inference is based upon estimates of the distributions obtained by resampling the data many times. The resampling method is closely tied to Monte Carlo simulations, which provides a solid theoretical background.[52]

Resampling in statistics comprises a number of different procedures with different objectives. Examples are, the randomization exact test also known as the permutation test, cross-validation techniques including *leave one out* cross-validation and bootstrap methods.[52] The permutation test was originally developed by R. A. Fisher[34] as a statistical significance test, although there were no computers in his days to automate such a laborious method. Cross-validation and to some extent bootstrapping was originally developed with model verification purposes.[52] The emergence of relatively inexpensive fast computers and the development of new sophisticated algorithms, have made resampling techniques practical for a wide range of problems.

A permutation test involves the random shuffling of observed data labels to determine how unusual an observed outcome is.[3] The basic idea of a permutation test, is easily demonstrated using data with two labels A and B whose sample means are $\bar{\mu}_A$ and $\bar{\mu}_B$. Suppose that we want to test, at some significance level, whether the data come from the same distribution. If random relabeling of the data doesn't change the means $\bar{\mu}_A$ and $\bar{\mu}_B$, we can infer that the labelling is of no consequence and hence the data comes from the same distribution. Algorithmically the permutation test proceeds as follows:

1. Record the statistic of interest for the observed data, eg. T- or F-test statistic.

2. Combine the observations from all the samples.

3. Shuffle them and relabel them in samples of the same sizes as the original samples.

4. Record the statistic of interest, eg. T- or F-test statistic.

5. Repeat 4-5 many many times.

6. Determine how often the resampled statistic of interest is as extreme as the observed value of the statistic. The p-value is determined as

$$p = \frac{\text{number of tests greater than or equal observed value} + 1}{\text{number of tests less than observed value} + 1} \qquad (5.11)$$

The above procedure is a Monte Carlo permutation test, also called a sampled or approximate permutation test. A permutation test in which all possible shufflings are systematically used is an exhaustive permutation test. A permutation test is thus simple, albeit time consuming. Monte Carlo permutation tests are asymptotically equivalent to an exhaustive permutation test, and are used when there are too many possible orderings of the data to allow complete enumeration. The number of Monte Carlo samples needed depends on the need for accuracy of the test, and depends on both the observed p-value and number of samples.[52]

An important assumption behind permutation testing is that the observations are exchangeable under the null hypothesis.[21] A notable exception to this is functional MRI data, which have intrinsic temporal correlations. If the labels are exchangeable under the null hypothesis, then the resulting exhaustive permutation tests yield exact significance levels.[35]

CHAPTER 6

Traumatic brain injury (TBI)

The subject of the first paper [102] is a longitudinal study of patients who sustained severe TBI, with a control group of healthy subjects for comparison (see appendix A for full article). Additional findings relating patterns of regional atrophy to clinical outcome in the cohort of patients is the subject of [106]. For a complete account of the clinical implications of the findings for the entire study see [101].

6.1   Symptoms

Severe TBI comprises a number of different injuries to the brain due to an external mechanical force to the craniofacial region. Severe TBI is often associated with focal brain lesions directly under the area of impact (in coup), as well as on the side opposite the impact (contre coup). Such focal lesions involve the superficial gray matter, occasionally with involvement of the underlying white matter, and are likely to be haemorrhagic. Traumatic axonal injuries (TAI) are another lesion type, which are diffuse or microscopic multi-focal lesions in white matter induced by sudden acceleration-deceleration and/or rotational forces, causing shearing of the axons. TAI is the most important cause of persistent vegetative state or death following TBI, and is also associated with long-term cognitive deficits, such as memory deficits, information processing and executive

functions. Secondary lesions types also occur, which are hypoxic-ischemic, due to compromised oxygen supply and/or compromised global perfusion. Secondary lesions are often avoidable if treated in due time.

6.2   Structural brain changes and TBI

Neuropathologists have long observed that the brains of patients with severe TBI months or years before death usually show conspicuous atrophy upon macroscopic examination. This is in accordance with common observations on repeated CT or MRI during rehabilitation, that the brain undergoes widespread atrophy concurrently with the clinical improvement. The underlying mechanisms for this atrophy, as well as the clinical implications for recovery, are poorly understood. Atrophy following severe TBI is not homogenously distributed, and knowledge of any regional distribution of late atrophy could potentially indicate the mechanism(s) accounting for the progressive volume loss. With the continuous rapid development of computing power, the application of increasingly sophisticated software for morphometric image analysis is made possible.[64]

6.3   Image processing

Conventional 3D high-resolution T1-weighted images was acquired at two time points at which the patients also were evaluated clinically. Patients were scanned ~ 8 weeks and ~ 12 months post-injury, and control subjects were scanned interleaved with patients. For 24 patients and 14 control subjects, sufficient-quality images were available at both time points. The images were processed to quantify both global volume changes, as well as regional volume changes. The data processing paths are schematized in figure 6.1, with 3 paths producing different measures of MRI morphometry.

As a rough estimate of the volume loss occurring before the first scan time point, patients were compared cross-sectionally to controls on global volume measures, using SIENAX. Normalized brain parenchymal volume (BPV) was on average 8.4% smaller in the patients than in the controls (mean $\pm$ SD: 1506 ml $\pm$ 85 ml and 1645 ml $\pm$ 85 ml, respectively). Visual inspections of segmentation showed misclassifications of white matter as gray matter in haemorrhagic areas, however this does not influence the BPV.

For quantitative evaluation of macrostructural changes over time, recent techniques suited for longitudinal studies SIENA and Tensor Based Morphometry were chosen.
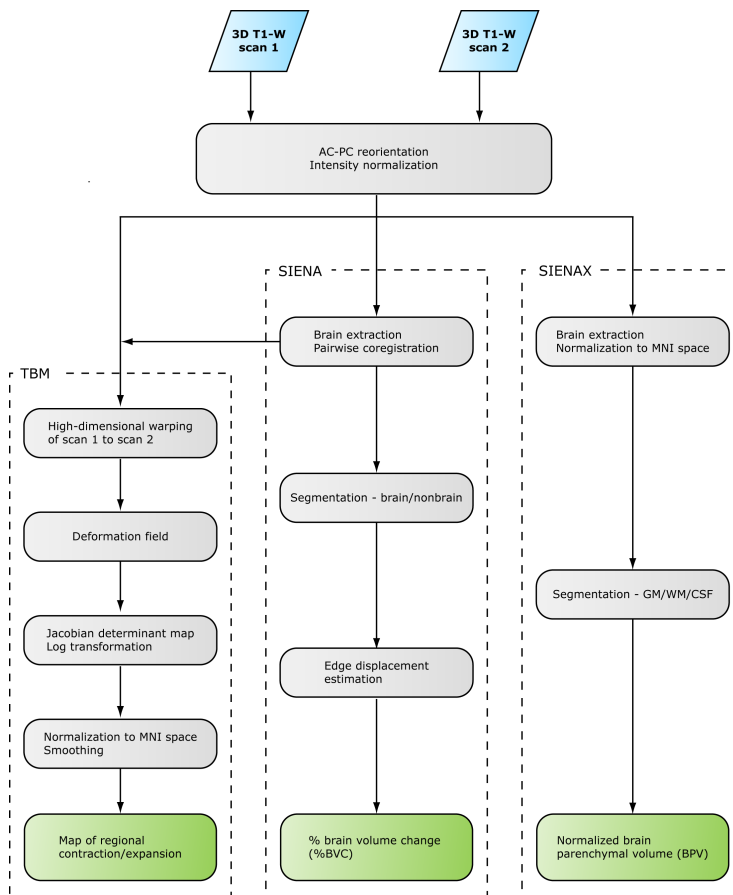
Figure 6.1: Overview of image processing for TBI morphometry. Subsequent statistical analyses are described in [102]. T1-W = T1-weighted; AC-PC = anterior commissure - posterior commissure; MNI = Montreal Neurological Institute; GM = gray matter; WM = white matter.
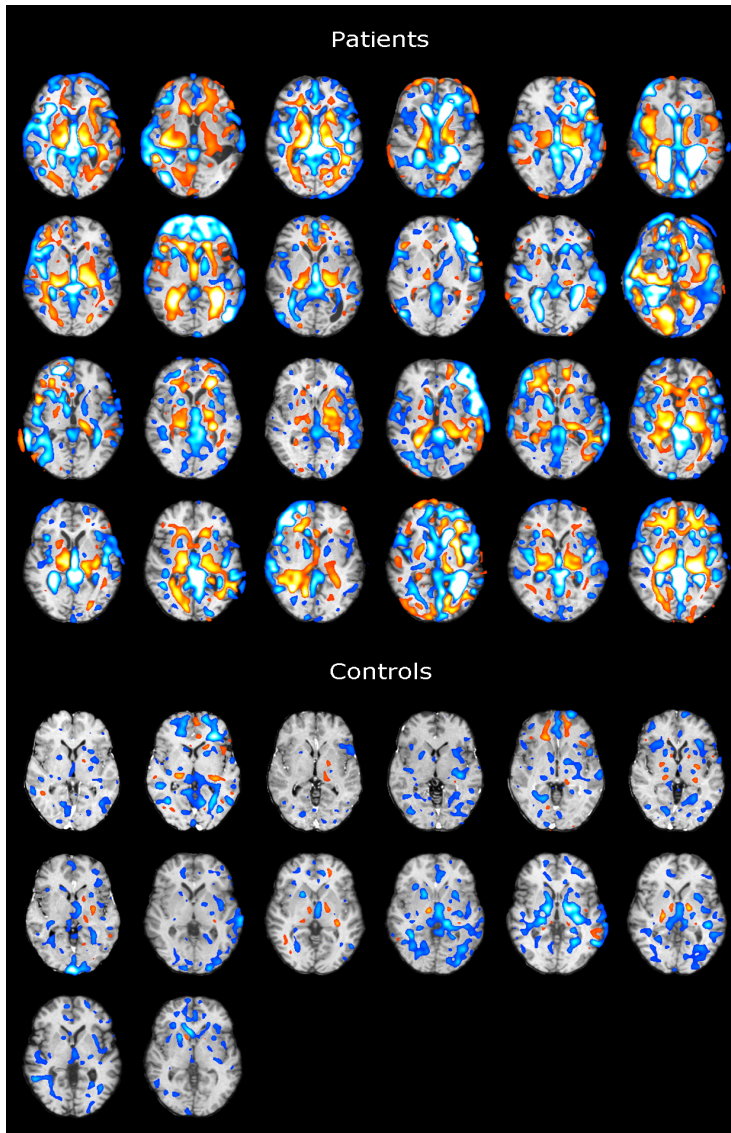
Figure 6.2: Individual TBM result images (one slice per subject) for the 24 patients and 14 controls. Normalized and smoothed log Jacobian determinant maps overlaid onto normalized T1-weighted images (scan 2). Longitudinal volume reduction is coded with hot colours, volume expansion with cold colours.
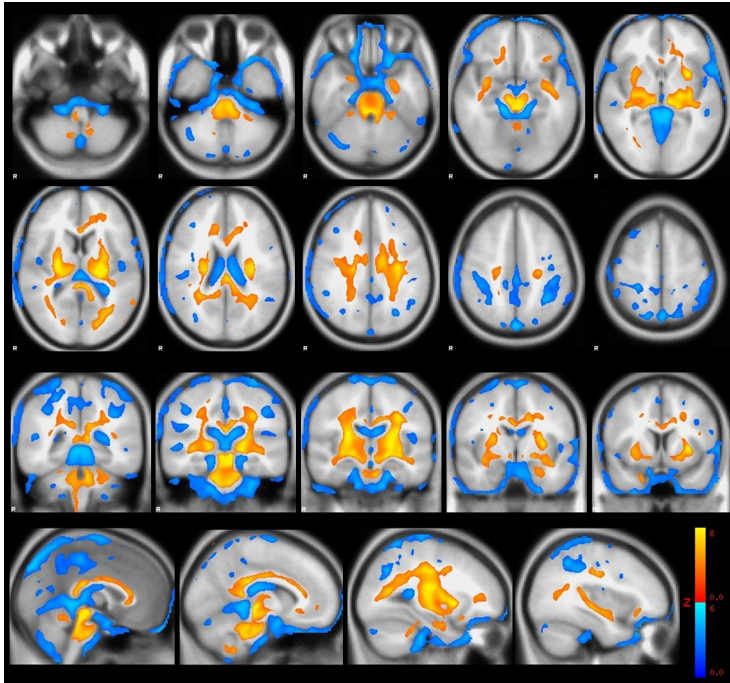
Figure 6.3: Regions of significant volume changes in TBI patients between ∼ 8 weeks and ∼ 12 months post-injury, as compared to controls, thresholded at false discovery rate (FDR) 0.05 (clusters of < 33.5 voxels rejected). Longitudinal volume reduction is coded with hot colours, volume expansion with cold colours. Results are overlaid onto the Montreal Neurological Institute (MNI) standard template.

These methods are thought to be more robust than traditional morphometric approaches for the analysis of structurally highly heterogeneous brains. During the scan interval, patients exhibited continued atrophy with percent brain volume change (%BVC), derived from SIENA, ranging between -0.6% and -9.4% (mean -4.0%, median -2.9%). In controls %BVC ranged between -0.9% and +0.3% (mean -0.18%, median -0.13%).[110, 111]

6.4 Results

As seen in figure 6.3, regional distribution of this late atrophy in patients (relative to controls), investigated using TBM, revealed widespread symmetric volume loss in the
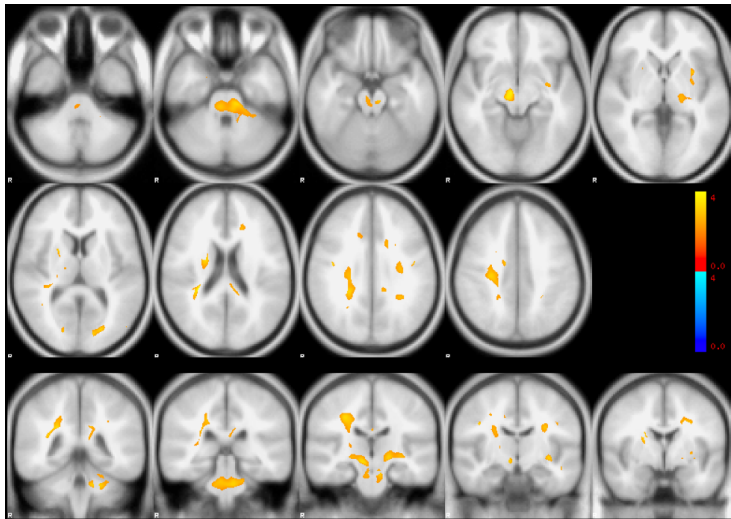
Figure 6.4: Areas in which patients with unfavourable outcome (GOS-E = 1–4; n = 8) exhibited more longitudinal volume change as compared to patients with favourable outcome (GOS-E = 5–8; n = 16), thresholded at FDR $p < 0.05$, uncorrected (clusters of < 33.5 voxels rejected). Longitudinal volume reduction is coded with hot colours, volume expansion with cold colours. Results are overlaid onto the MNI standard template.

brainstem and cerebellar peduncles, thalamus, putamen, internal and external capsules, inferior and superior longitudinal fasciculus, corpus callosum and corona radiata, with additional small clusters of volume loss mainly in the cerebellum and in the frontal lobes. Significant volume expansion was found in the ventricles and scattered in the subarachnoidal space (permutation test, FDR 0.05). Individual TBM result images for all subjects (one axial slice only) are displayed in figure 6.2.

6.5   Additional findings

Additional analysis of the TBM results of patients was made in order to investigate whether a different pattern of late atrophy would be found in patients with unfavourable outcome in comparison with patients with favourable outcome. Limited by the small number of subjects in each group (16 with favourable outcome and 8 with unfavourable outcome) it was expected that, if any detectable differences existed, there might be more extensive atrophy in the brainstem in patients with unfavourable outcome as compared to patients with favourable outcome, reflecting the supposedly more frequent oc-

currence of brainstem traumatic axonal injuries and extensive Wallerian degeneration with unfavourable outcome.

Statistical analysis was performed similarly as for the main TBM analysis (permutation test, same nuisance variables), however analysis was confied to the region that were significant in the main TBM analysis (permutation test, FDR 0.05). The results are seen in figure 6.4. Apart from clusters of volume expansion in the subarachnoidal CSF, this shows a generally asymmetrical pattern of small clusters of volume loss scattered mainly in deep white matter and brainstem. However, one bilateral cluster of volume reduction in the brainstem was found at the level of pons and the middle cerebellar peduncles, indicating more extensive volume loss over time in this area for patients with unfavourable outcome as compared to patients with favourable outcome.

6.6 Discussion

As discussed in section 4.2, similar limitations apply to the voxel-wise morphometric analyses performed in this study. The sensitivity to areas with high anatomical variability between subjects, such as cortical gyri and sulci, is less than to areas exhibiting little inter-subject variability[64, 117]. Combined with the frequent presence of focal lesions in frontal and temporal cortices, possibly complicating registration, the relative sparing of cortex observed in our group analysis in terms of volume loss over time could be a false-negative result. However, the individual TBM results only revealed cortical atrophy in a minority of the patients, thus suggesting white matter atrophy generally being more pronounced than cortical gray matter atrophy.

Most subjects in this patient population had visible focal lesions on conventional MRI. Possible confounding of focal lesions on the pattern of longitudinal volume loss found with TBM cannot be ruled out. In the cross-sectional TBM study [64], a subgroup analysis was performed for the patients without focal lesions, showing a pattern of volume loss comparable to that of the whole patient group. However, similar subgroup analysis was not made in the present study because of the small number of patients without focal lesions.

Certain limitations relate to the use of SIENAX and other segmentation algorithms for estimation of volume loss in the patients prior to the first scan. Although the patients and controls were fairly well matched with respect to demographic parameters, the assumption that brain volume of the patients prior to injury was comparable to that of the controls is a rough approximation. Further, the segmentation algorithm of SIENAX tended to misclassify focal lesions as gray matter, which prevented us from studying

gray and white matter separately. Since lesions were never misclassified as CSF, the sum of gray and white matter volume estimates was considered as a relatively valid estimate of parenchymal volume. However, in consideration of these limitations, the SIENAX results should be regarded only as rough estimations of initial volume loss.

Schizophrenia

The subject of the second and third paper [27, 28] was a morphological study of anti-psychotic-naïve first episode schizophrenia patients, with a control group of healthy subjects for comparison(see appendices B and C for full articles). For a complete account of the clinical implications of the findings for the entire study see [26].

7.1 Symptoms

Schizophrenia is a severe and heterogeneous mental illness affecting about 0.7 percent of the population[76]. The illness is characterized by a disintegration of the process of thinking, of contact with reality, and of emotional responsiveness[95, 119]. The origin of schizophrenia is a complex interaction of both genetic liability and environmental factors and the disorder is characterized by disturbances in brain biology and function[62, 114, 115]. People with the schizophrenia illness experience different symptoms, which are categorized into three broad categories: positive symptoms, negative symptoms, and cognitive symptoms.[83]

7.1.1   Positive symptoms

Positive symptoms are abnormal behavior patterns generally not seen in people without schizophrenia, such as hallucinations, delusions, thought or movement disorders[115]. The most prominent positive symptoms are hallucinations affecting either of the persons five senses; visual, auditory, olfactory, sensory or even taste[115]. Postive symptoms include

- Hallucinations are things a person sees, hears, smells, or feels that are oblivious to others, with "voices" being the most common type of hallucination in schizophrenia.

- Delusions are false beliefs that often stand out as bizarre and are a persistent part of the persons beliefs. Delusions include believes that people on television are directing special messages to them, or that radio stations are broadcasting their thoughts aloud to others. The person believes the delusions even after other people disprove that the beliefs, and any logical explanation will strengthen their false beliefs of conspiracy.

- Thought disorders are unusual or dysfunctional ways of thinking, making affected patient talk in a garbled way that is hard to understand, or abruptly stop speaking in the middle of a thought.

- Movement disorders appear as agitated body movements, or repetitive motions.

Positive symptoms can come and go, be severe and at other times hardly noticeable[115].

7.1.2   Negative symptoms

Negative symptoms are associated with disruptions of normal emotions and behavior patterns. Such symptoms are harder to recognize as part of the schizophrenia disorder as they are easily mistaken for other psychiatric illnessess such as depression or bipolar disorder[119]. Negative symptoms include:

- "Flat affect", ie a person's face does not move, or talks in a dull, monotonous voice.

- Lack of pleasure

- Lack of ability to begin and sustain planned activities

- Poverty of speech

People with negative symptoms need help with everyday tasks, from personal hygiene to food preparation. This often makes people suffering from schizophrenia seem lazy or unwilling to help themselves, but the problems are the negative symptoms caused by the illness[76].

7.1.3 Cognitive symptoms

Cognitive symptoms can be subtle, much like negative symptoms. Cognitive symptoms are thus as difficult to recognize as part of the disorder. Often, these symptoms are detected only when other tests are performed. Cognitive symptoms include

- Poor "executive functioning", ie. the ability to understand information and use it to make decisions.

- Trouble focusing or paying attention

- Problems with "working memory", ie. the ability to use information immediately after learning it.

Cognitive symptoms often make it hard to lead a normal life and earn a living. People with schizophrenia are often aware of their cognitive dysfunction, causing great emotional distress[76].

7.2 Structural brain changes in schizophrenia

The first MRI study of schizophrenia was conducted in 1984 [109] and despite negative findings, possibly due to small sample size (9 subjects) and poor resolution, numerous MRI studies have since confirmed early post-mortem findings[2]. MRI findings in chronic schizophrenia patients include reductions in total brain volume and gray matter volume reductions in severak sub-regions of the frontal, temporal (including amygdala-hippocampal complex, parahippocampal gyrus and superior temporal gyrus), parietal and occipital lobes, and in cerebellum. Subcortical abnormalities have been described in striatum, cavum septi pellucidi, anterior cingulate and thalamus.[41, 100]

The striatum, comprising the caudate nucleus, putamen, and nucleus accumbens, may constitute a specific region with regard to the pathophysiology of schizophrenia. These regions are involved in cognitive functions such as motivation and goal directed behaviour, and in sensorimotor coordination. Moreover, activation of the caudate nucleus and nucleus accumbens has been linked to reward processes. The caudate nucleus has been associated with language impairment and emotional processes such as romantic love.[26, 44]

Other regions of the brain are affected as well. Hippocampus volume reductions are not a characteristic of schizophrenia, but have been associated with numerous neuropsychiatric disorders. Hippocampus plays a vital role in processes of memory formation and stress and emotional regulation[40, 41]. Ventricular enlargement has been widely reported in schizophrenia, however ventricular enlargement has also been associated with various other neuropsychiatric disorders such as mild cognitive impairment and Alzheimers disease, delirium, late-life depression, bipolar disorder and alcoholism[100].

7.3   Image processing

In the present longitudinal study conventional 3D high-resolution T1-weighted and T2-weighted images were acquired at two time points at which the patients also were evaluated clinically. Patients were scanned at baseline and $\sim$ 6 months followup, and control subjects were scanned interleaved with patients.

The images were corrected for geometric distortions due to non-linearities in the scanner gradient system (see section 2.1) and subsequently processed using the VBM5 toolbox (see section 4.2). T2-weighted images were used to create brain masks to clean up segmentations.

Baseline images were spatially normalized using the DARTEL toolbox(see section 3.4). Using the final flow fields, the tissue maps were warped into average image space (DARTEL space) with 1 mm^3 interpolated (7th degree b-spline) isotropic voxels, and the voxel intensities were modulated using the Jacobian determinants of the warp deformations. Subsequently, the corresponding native T1-weighted images were warped into average image space without modulation, and an average T1-weighted image was calculated usable for regions-of-interest (ROI) delineation to be used small volume correction and extracting volume estimates.

For each subject, all follow-up T1-weighted images in native space were warped to individual subjects baseline T1-weighted images using the high-dimensional toolbox(see

section 3.5). The Jacobian determinant images of the resulting warp deformations were transformed to the DARTEL space with the previously generated DARTEL warps using logarithmic interpolation. Next, multiplying the corresponding baseline tissue maps with the Jacobian determinant images generated tissue maps for the follow-up images in DARTEL space.

7.4 Results of baseline study

Based on VBM analysis of 38 patients and 43 controls, volumes of hippocampus and caudate nucleus were decreased in patients as was hypothesized a priori. Any ventricular enlargement was absent, as well as global volume differences. The hippocampal volume reductions appeared influenced by a history of abuse. Exploratory analyses indicated reduced nucleus accumbens volumes in the patients.

After the baseline investigations the patients were treated with the second generation antipsychotic compound, quetiapine for 6 months in flexible doses according to their clinical need.

7.5 Results of followup study

Based on TBM analysis of 22 patients matched with 28 healthy control subjects, patients had significant volume loss in striatum and hippocampus, following six months of quetiapine treatment. The striatal volume loss was most pronounced in low quetiapine doses and less apparent in high doses. Conversely, hippocampal volume loss appeared more pronounced in high quetiapine doses than in low doses. Clinically, higher baseline positive symptoms were associated with more striatal and hippocampal volume loss over time.

7.6 Discussion

Global estimates of inter-cranial volume, parenchymal brain volume, gray or white matter volumes or atrophy estimated using SIENAX and SIENA did not reveal any significant volume differences between groups. The absence of brain parenchymal brain volume (BPV) reduction in the patients is in contrast to results in [112] and may reflect

that some of the patients included in this analysis had been exposed to first generation anti-psychotics, which may attenuate global gray matter loss[73].

Our finding of reduced caudate nucleus volume agrees with studies reporting absolute or significant caudate volume reductions in antipsychotic-naive schizophrenia patients. Thus, our findings add to the evidence that the caudate nucleus is a key structure in the pathophysiology of schizophrenia. The pathway to the observed volumetric reductions in the antipsychotic-naïve state is not clear but may be attributable to decreased metabolic rates in the basal ganglia. The magnitude of the caudate volume reductions in this study of about 5% are in line with the average caudate reduction in found in the literature.

MRI studies have previously associated striatal volume reductions with positive symptoms [25, 98], however the present study is the first to show that the severity of positive symptoms in the antipsychotic state may predict progressive striatal volume loss. The fact that no association between striatal volume and positive symptoms was observed at baseline, could indicate that in the earliest phase of schizophrenia the structural consequences of psychotic symptoms may occur with a delay in time.

Hippocampal activation has been associated with positive symptoms in at risk subjects for schizophrenia [124] and we speculate that the positive correlation between hippocampal volume loss and baseline positive symptoms could reflect a higher level of stress accompanying a psychotic state [91].

Although we did not find ventricular enlargement over time a significant correlation between ventricular increase and less negative symptom improvement was observed. As such our data are consistent with the growing body of evidence which has associated negative symptoms and poor prognosis with ventricular enlargement (for review, see [56]).

The mechanisms underlying these progressive brain dynamics, specific antipsychotic compounds and clinical symptoms warrant further clarification.

Discussion and conclusions

Computational neuroanatomy is a widely applicable technique, which is reflected in the diversity of neuroscientific questions addressed in the selected papers. The TBM procedure uses serial high-resolution MRI scans for studying (disease-related) structural anatomical changes over time. Specifically TBM is a highly automated image analysis technique that delineates local tissue gain or loss at a great spatial resolution. The applicability of TBM is clearly demonstrated in the papers presented in this thesis.

The first paper describes a study on the macrostructural brain changes during recovery after traumatic brain injuries. Traumatic brain injuries exhibit neuroanatomical changes that are obvious even to non-experts, however the diversity of the injuries as well as the gross pathological changes make it difficult to quantify changes over time in patients. Here TBM was utilized to characterize global and regional brain volume changes between two scan time points through a voxel-wise analysis. Despite remarkable clinical improvement in most patients, they all exhibited brain volume loss during the scan interval. Global volume change correlated with clinical injury severity, functional status at both time points, as well as 1-year outcome. The areas which underwent the most change were structures particularly susceptible to traumatic axonal injury such as copus callosum and regions in deep white matter and consequent Wallerian degeneration.

The second and third paper describe a study of the neurodegenerative consequences of schizophrenia and anti-psychotic drug treatment. Schizophrenia is associated with

subtle changes in the brain, which are undetectable by a non-expert, and as such provides a different challenge than the previous study. In the baseline study, VBM analysis combined with hypothesis driven regions of interest approach verified the presence of a morphological fingerprint in a first-episode schizophrenia sample with no prior lifetime anti-psychotic exposure. The follow-up study focused on medication effects over time and the results suggested differential dose-dependent effects on brain structure after exposure to only one anti-psychotic compound. TBM results among other things indicated that the severity of positive symptoms in first-episode schizophrenia patients may to some extend predict regional brain volume changes. This implies that early detection of symptoms of schizophrenia and relevant intervention may somewhat prevent regional brain deterioration and in turn improve the prognosis of the patients.

The image registration methods and statistical models used in the present thesis facilitated the remarkable spatial specificity and sensitivity of the results featured in the three selected papers. The neuroscientific questions addressed in each paper instigated different specialized image processing streams, built to characterize differences between brains, while considering neuroanatomical variability among subjects. The design, development and implementation of these complex image processing streams, required intricate understanding of the employed image registration and statistical methods.

In addition to TBI and schizophrenia, VBM and TBM have been successfully employed in numerous studies aimed to further our understanding of the brain in health and disease, including healthy aging and development during maturation and psychiatric disorders, e.g. autism, depression, tracking degenerative disease progression, and monitoring drug treatment effect. Additionally, such studies generally investigate how morphological characteristics are associated with for example specific cognitive measures, IQ, and genetic polymorphisms. Besides VBM and TBM several other complementary morphometric methods exist, such as cortical thickness measures and shape analysis of sub-cortical structures. Neuroimaging studies have become increasingly successful in combining multiple imaging modalities and computational methods to address neuroscientific questions. Indeed, it is important to note that most techniques, be it imaging modalities or computational methods, are complementary, emphasizing each other's qualities. Only in recent years have techniques, computational power and expertise consolidated and thereby reached the necessary level of sensitivity, reliability and feasibility.

Long-term global and regional brain volume changes following severe traumatic brain injury: a longitudinal study with clinical correlates

Long-term global and regional brain volume changes following severe traumatic brain injury: A longitudinal study with clinical correlates
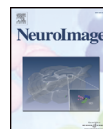
Annette Sidaros [a,b,c,*], Arnold Skimminge [a,d], Matthew G. Liptrot [a], Karam Sidaros [a], Aase W. Engberg [b], Margrethe Herning [a], Olaf B. Paulson [a,c,e], Terry L. Jernigan [a,c,f], Egill Rostrup [a,c,g]

[a] Danish Research Centre for Magnetic Resonance, Copenhagen University Hospital, Hvidovre, Denmark
[b] Brain Injury Unit, Department of Neurorehabilitation, Copenhagen University Hospital, Hvidovre, Denmark
[c] Faculty of Health Sciences, University of Copenhagen, Denmark
[d] Department of Informatics and Mathematical Modelling, Technical University of Denmark, Lyngby, Denmark
[e] Neurobiology Research Unit, Copenhagen University Hospital, Rigshospitalet, Denmark
[f] Laboratory of Cognitive Imaging, Department of Psychiatry, University of California, San Diego, CA, USA
[g] Department of Clinical Physiology, Copenhagen University Hospital, Glostrup, Denmark

ARTICLE INFO

ABSTRACT

Traumatic brain injury (TBI) results in neurodegenerative changes that progress for months, perhaps even years post-injury. However, there is little information on the spatial distribution and the clinical significance of this late atrophy. In 24 patients who had sustained severe TBI we acquired 3D T1-weighted MRIs about 8 weeks and 12 months post-injury. For comparison, 14 healthy controls with similar distribution of age, gender and education were scanned with a similar time interval. For each subject, longitudinal atrophy was estimated using SIENA, and atrophy occurring before the first scan time point using SIENAX. Regional distribution of atrophy was evaluated using tensor-based morphometry (TBM). At the first scan time point, brain parenchymal volume was reduced by mean 8.4% in patients as compared to controls. During the scan interval, patients exhibited continued atrophy with percent brain volume change (%BVC) ranging between −0.6% and −9.4% (mean −4.0%). %BVC correlated significantly with injury severity, functional status at both scans, and with 1-year outcome. Moreover, %BVC improved prediction of long-term functional status over and above what could be predicted using functional status at ~8 weeks. In patients as compared to controls, TBM (permutation test, FDR 0.05) revealed a large coherent cluster of significant atrophy in the brain stem and cerebellar peduncles extending bilaterally through the thalamus, internal and external capsules, putamen, inferior and superior longitudinal fasciculus, corpus callosum and corona radiata. This indicates that the long-term atrophy is attributable to consequences of traumatic axonal injury. Despite progressive atrophy, remarkable clinical improvement occurred in most patients.

© 2008 Elsevier Inc. All rights reserved.

Introduction

Traumatic brain injury (TBI) affects about 235 per 100,000 individuals each year in Europe (Tagliaferri et al., 2006) and is a major cause of death and severe morbidity worldwide. In survivors of severe TBI, long-term impairment of consciousness is usually attributable to traumatic axonal injury (TAI, also known as diffuse axonal injury). TAI results from rotational acceleration-deceleration causing shear strain deformation and subsequent disconnection of axons. It is characterized by microscopic lesions scattered throughout the white matter in particular, with certain regions being characteristically involved, namely the dorsolateral rostral brain stem, the corpus callosum and the subcortical parasagittal white matter. Other regions susceptible to TAI are the internal and external capsules, the deep grey matter, the cerebellum, various tracts in the brain stem and the cerebellar peduncles (Graham et al., 2002). It has been repeatedly observed in animals (Smith et al., 1997; Bramlett and Dietrich, 2002; Rodriguez-Paez et al., 2005) and in humans (Graham et al., 2002) that TBI results in widespread brain atrophy that progresses over several months and perhaps even years post-injury. While it is remarkable that atrophy continues in the chronic phase of TBI, concurrently with clinical recovery, the clinical significance of this late atrophy remains unclear. The progressive degeneration is thought to involve Wallerian degeneration of the white matter tracts disrupted by TAI, but other mechanisms such as apoptosis, inflammation, excitotoxicity, and prolonged hypoperfusion may also play a role (Bramlett and Dietrich,

2002; Rodriguez-Paez et al., 2005). Characterising the spatial distribution of late atrophy might contribute to the understanding of its pathogenesis.

Few longitudinal MRI studies have quantitatively examined progressive atrophy following TBI and the correlation to clinical parameters. In seven patients with mild to moderate TBI, scanned twice at least 3 months (up to 2.5 years) apart, MacKenzie et al. reported a longitudinal change in brain parenchymal volume of on average −4.16% (relative to −1.49% in healthy controls) and found greater volume loss in patients with initial loss of consciousness than in those without loss of consciousness (MacKenzie et al., 2002). However, in this study early and late atrophy were conflated since the time from injury to the first scan varied between 7 and 430 days. Recently, Trivedi et al. (2007) published a study applying SIENA (Smith et al., 2002) to evaluate global brain volume change between approximately 79 and 409 days post-TBI in 37 patients with TBI ranging from mild to severe. The authors found a change in brain volume of mean −1.43% (relative to +0.1% in healthy controls), with greater decline in brain volume being associated with longer duration of post-injury coma. However, relation to outcome was not reported.

Characterising quantitatively the regional distribution of late atrophy following TBI is challenging, especially because focal lesions often coexist with diffuse lesions, causing regional distortions in brain shape and intensity inhomogeneities which complicate procedures such as registration and tissue segmentation. Until recently, previous studies on TBI have been based on regions-of-interest (for a review, see Bigler, 2001) or on voxel-based morphometry (Gale et al., 2005; Tomaiuolo et al., 2005; Salmond et al., 2005; Bendlin et al., in press). However, recent advances in computational techniques for nonlinear image registration have allowed for an unbiased and more precise registration that does not necessarily rely on tissue segmentation, thus overcoming some of the major limitations of traditional volumetric approaches. One such approach is tensor-based morphometry (TBM), which determines the deformation field required to warp the early image to match the late image within subject (or in cross-sectional studies, the deformation field required to warp the image to a study-specific template). Regional volume change is quantified by taking the Jacobian determinant at each voxel (Ashburner et al., 2000). One cross-sectional TBM study on TBI was very recently published (Kim et al., 2008). The population consisted of 29 patients with moderate to severe TBI, scanned once at least 3 months (ranging between 4 months and 27.5 years) following injury. The authors found localized volume loss most prominently in the thalamus, the midbrain, the corpus callosum, the cingulate cortex, and the caudate. Significant volume increase was found mainly in the ventricles. However, as this study was not based on serial scans, and as the time from injury to MRI varied considerably between patients, no conclusions could be drawn about the time course of the structural changes.

In the present prospective longitudinal study, we examined the morphological changes occurring between two time points, approximately 8 weeks and 12 months post-injury, in 24 patients with severe TBI, comparing them to 14 healthy matched controls scanned with a similar time interval. We used SIENA to provide an estimate of global atrophy between scans, and TBM to investigate the regional distribution of late volume change. Additionally we used SIENAX (Smith et al., 2002) to estimate global atrophy occurring before the first scan time point, in order to compare this with the late atrophy. We hypothesized that the most pronounced late volume change would be found within regions susceptible to TAI (listed at the beginning of this introduction) as well as along the affected white matter tracts (as a consequence of secondary Wallerian degeneration). Further, we expected that the extent of global brain volume change from first to second scan would be larger in patients with longer duration of coma/post-traumatic amnesia and with poorer functional status and outcome.

Materials and methods

Subjects

Twenty-six adult patients with severe TBI were evaluated for this study. As two patients were subsequently excluded because of motion artefacts in the MR images, the final TBI group comprised 24 patients. Fourteen healthy control subjects were selected to match the patient group with respect to age, sex and education. Both patients and controls had two MR scans with an interval of 345±42 days (mean±SD). Group comparisons of age, sex, education and scan interval are listed in Table 1.

Patients were recruited from the Brain Injury Unit at Copenhagen University Hospital, Hvidovre, Denmark, to which they were admitted for subacute rehabilitation. Patients were referred from neuro-intensive units, and admitted for rehabilitation only if Glasgow Coma Scale score (GCS; Teasdale and Jennett, 1974) was still subnormal after cessation of sedation. Severe TBI was defined as a post-resuscitation GCS <8 measured within 24 h post-injury and prior to the initiation of paralytics or sedatives. Patients were excluded from the present study if they had any previous history of TBI or other neurological disorder, if contraindications to MRI or to sedation during MRI were present, or if the first MRI could not be performed within 12 weeks post-trauma for safety or practical reasons. Controls had no history of significant TBI or other neurological disorder.

The study was approved by the local Scientific Ethics Committee (KF 01-038/03), meeting criteria of the Helsinki Declaration. Informed consent was obtained from the participants or, for patients with impaired consciousness, from next of kin.

Clinical assessments

For all patients, clinical data were documented in medical files, and ratings were performed by trained staff, neurologists, and neuropsychologists. Cause of trauma was either motor vehicle accident ($n=16$), fall ($n=7$) or assault ($n=1$). Accidents with any direct involvement of a motor vehicle (including pedestrian or bicyclist hit by car) were classified as motor vehicle accident. Neurosurgery was defined as surgery that involved craniotomy, excluding insertion of ICP monitoring devices. The number of days from TBI until GCS >8 was registered as a measure of coma duration, and the Galveston Orientation and Amnesia Test (Levin et al., 1979) was repeatedly applied to establish duration of post-traumatic amnesia (PTA). Both were regarded as measures of injury severity. The Functional Independence Measure (FIM; Granger et al., 1986) was documented regularly, including at both scan time points (sum score ranging from 18 indicating "total assist", to 126 indicating "complete independence"). Functional outcome at ~12 months post-TBI was evaluated using the 8-point Glasgow Outcome Scale Extended (GOS-E; Wilson et al., 1998), ranging from 1=dead to 8=good recovery (upper). For dichotomized outcome, the commonly used division into unfavourable outcome (GOS-E=1–4) and favourable outcome (GOS-E=5–8) was applied, distinguishing whether or not patients were able to live independently.

Image acquisition

All patients and controls were scanned on the same 1.5 T MRI scanner (Magnetom Vision; Siemens Medical Solutions, Erlangen, Germany) using a standard circular-polarized head coil. During the study period, MRI sessions for patients and controls were interleaved in time, and no major upgrades were carried out on the scanner during the study.

A 3D sagittal T1-weighted sequence (MPRAGE, TR/TE/TI=13.5/7/ 100 ms, flip angle 15°, isotropic 1 mm resolution) was acquired in all

Table 1
Group comparisons of demographics and scan interval

	Patients ($n=24$)	Controls ($n=14$)	Group differences
Age, at scan 1 (years) [mean (SD)]	33.2 (13.5)	31.2 (8.1)	$P>0.5$[a]
Sex: M/F	18/6	9/5	$P>0.7$[b]
Education (years) [mean (SD)]	13.3 (3.1)	13.7 (2.7)	$P>0.6$[a]
Scan interval (days) [mean (SD)]	343 (47)	348 (30)	$P>0.6$[b]

[a] Independent-samples *t*-test.
[b] Fishers Exact test.

subjects at both scan time points. For patients, additional conventional sequences included: axial T2-weighted images (spin-echo, TR/TE=5400/99 ms, 27 contiguous, 5 mm thick slices, 0.5×0.5 mm in-plane resolution), coronal T2*-weighted gradient-echo images (TR/TE=544/15 ms, 34 contiguous, 5 mm thick slices, 0.9×0.9 mm in-plane resolution), axial and sagittal FLAIR (TR/TE/TI=9000/110/2500 ms, 34 contiguous, 5 mm thick slices, 0.9×0.9 mm in-plane resolution). All the structural images were evaluated by a neuroradiologist (M.H.) for identification and classification of lesions.

All patients were referred for the first MRI for clinical purposes. The majority of patients ($n=19$) were sedated for this scan, since they were unable to cooperate due to decreased level of consciousness or cognitive impairment. Intravenously administered propofol was used for sedation, and patients were monitored by anaesthesiology staff. Oxygen supply and mechanical ventilation were provided when necessary.

For the follow-up scan, subjects were repositioned as close as possible to their position in the previous scan. For ethical reasons patients were sedated only if a follow-up MRI was requested for clinical purposes and patients were unable to cooperate for MRI. While 4 patients were sedated for the follow-up MRI, 20 were fully cooperative without sedation. Two additional non-sedated patients were excluded from this study due to motion artefacts in the follow-up images. All the remaining images were judged of good quality.

Image processing

Preprocessing: global volume changes

The 3D T1-weighted images were first reoriented manually to the anterior–posterior commissure (AC–PC) orientation, and resliced to 1 mm³ voxels. Intensity normalisation within and between scans was performed using N3 and MRI Normalise from the MNI toolbox (www.bic.mni.mcgill.ca).

We used SIENA, available in the FSL 3.3 toolbox (www.fmrib.ox.ac.uk/fsl), to evaluate global brain volume change between the two scan time points for each subject. Additionally we applied SIENAX (also within FSL) for an estimation of brain parenchymal volume, normalized for head size, at the first scan time point. These methods have been described in detail elsewhere (Smith et al., 2001; Smith et al., 2002). In brief, SIENA starts by extracting brain and skull images from the two-timepoint whole-head input data. The two brain images are then aligned to each other (using the skull images to constrain the registration scaling); both brain images are resampled into the space halfway between the two. (This intermediate result was later entered into the TBM analysis, see below). Then segmentation is carried out in order to find brain/non-brain edge points. Perpendicular edge displacement, between the two time points, is estimated at these edge points, and the mean edge displacement is converted into a global estimate of percentage brain volume change (%BVC) from first to second scan. Measurement error of %BVC is reported to be approximately ±0.20% (Smith et al., 2002).

In SIENAX, brain and skull images are extracted, and the brain image is affine-registered to an MNI standard template (using the skull image to determine registration scaling, to be used as a normalisation for head size). Next, segmentation with partial volume estimation is carried out in order to calculate the total volume of brain tissue: normalised brain parenchymal volume (BPV).

Preprocessing: regional volume changes

We used TBM to evaluate the regional distribution of brain volume change between the two scan time points. Following the intensity

Table 2
Clinical characteristics and global brain volume results for the 24 patients

Patient no.	Age at scan1 (years)	Sex	Cause of trauma	Neurosurgery	Duration of coma (days)	Duration of PTA (days)	TBI to scan1 (days)	TAI grade[a]	Focal lesions[b]	FIM at scan1	FIM at scan2	GOS-E at ~1 year	BPV at scan1	%BVC
1	23	F	Fall	–	>FU	>FU	58	2	–	18	18	2	1406	−9.42
2	21	F	MVA	+	12	39	64	2	+	79	117	4	1536	−5.29
3	34	M	MVA	–	126	>FU	81	3	–	18	30	3	1471	−8.80
4	40	F	Fall	+	9	>FU	64	2	+	18	20	3	1263	−7.02
5	40	M	Assault	–	4	88	50	0	–	87	122	6	1405	−1.16
6	60	M	Fall	+	21	>FU	46	2	+	34	35	3	1543	−7.21
7	28	M	MVA	–	24	66	69	3	–	122	125	8	1595	−4.08
8	54	M	Fall	–	14	119	45	2	+	60	125	5	1429	−1.80
9	23	M	MVA	+	18	47	81	2	+	117	124	6	1584	−2.56
10	24	M	MVA	–	1	39	36	1	–	93	125	5	1549	−0.62
11	65	M	Fall	–	3	39	42	1	+	116	120	6	1449	−2.60
12	31	M	MVA	+	7	48	40	2	+	38	102	5	1609	−6.28
13	37	M	MVA	+	14	40	69	1	+	117	122	7	1535	−2.74
14	22	M	MVA	–	7	31	55	2	–	120	125	7	1587	−1.78
15	19	M	MVA	–	2	23	37	1	–	113	124	7	1673	−1.28
16	41	F	MVA	+	10	65	41	2	+	55	113	5	1537	−3.73
17	26	M	MVA	–	22	65	77	1	+	106	124	6	1500	−1.87
18	22	M	MVA	–	9	178	79	2	–	18	103	4	1543	−2.45
19	23	M	MVA	–	11	107	55	3	+	23	111	4	1515	−5.58
20	18	F	MVA	–	15	66	62	3	+	24	105	4	1443	−2.69
21	40	M	Fall	+	10	84	48	2	+	100	117	5	1484	−1.63
22	53	M	Fall	+	5	171	39	3	+	18	111	5	1443	−6.80
23	27	M	MVA	–	10	77	47	2	–	49	113	5	1498	−2.98
24	26	F	MVA	–	4	58	29	2	–	59	126	8	1557	−4.75

MVA = motor vehicle accident; >FU = exceeds ~1 year follow-up; PTA = post-traumatic amnesia; FIM = functional independence measure; GOS-E = Glasgow outcome scale, extended; BPV = brain parenchymal volume; %BVC = percent brain volume change. See text for details.
[a] According to location of microhaemorrhages on T2*-W images (0=none, 1=subcortical only, 2=callosal, 3=brainstem).
[b] Parenchymal lesions excluding TAI (mainly contusions).

normalisation and initial registration steps from SIENA, described above, we then applied the high dimensional warping available in the SPM2 'Deformation toolbox' (www.fil.ion.ucl.ac.uk/spm) to these images. This TBM analysis estimates the deformation field that would warp the early T1 image to match the late T1 image within each subject (Ashburner et al., 2000). From this deformation field the amount of regional expansion or contraction is extracted by taking the Jacobian determinant at each point, thus generating a Jacobian determinant map in alignment with the late image. Following logarithmic transformation of the Jacobian determinant values (Leow et al., 2007) regional contraction corresponded to positive values and regional expansion to negative values. The non-skull-stripped follow-up T1 images were then normalized in SPM2 to the MNI standard space, and this transformation was applied to the log-transformed Jacobian determinant maps. Finally, these images were smoothed with an 8 mm Gaussian kernel.

Statistical analysis: global volume changes

The outputs from SIENA and SIENAX, %BVC and BPV respectively, were analysed group-wise using the non-parametric Mann Whitney *U*-test. Correlation analyses with clinical and conventional imaging variables were performed using the Spearman's rho. Prediction of functional status at follow-up by BPV and FIM at the first scan and % BVC was assessed using linear regression.

Statistical analysis: regional volume changes

For statistical analysis of TBM results, we used a permutation test (Randomise, available in FSL). Unlike the general linear model, permutation tests do not rely on the assumption that data are normally distributed (Nichols and Holmes, 2001). To compare patients and controls, a design matrix was constructed that included the nuisance variables age, sex, education and scan interval. Calculations were performed voxel-wise with 10,000 permutations, and a whole-brain correction for multiple comparisons was applied using a false discovery rate (FDR) of 0.05. Clusters with a radius of <2 mm (volume <33.5 mm^3) were rejected for display purposes. Anatomy atlas tools available in FSL were used to help identify anatomical regions.

Results

Global volume changes

Already at the first scan time point ~8 weeks post-trauma, normalized BPV, derived from SIENAX, was 8.4% lower in patients
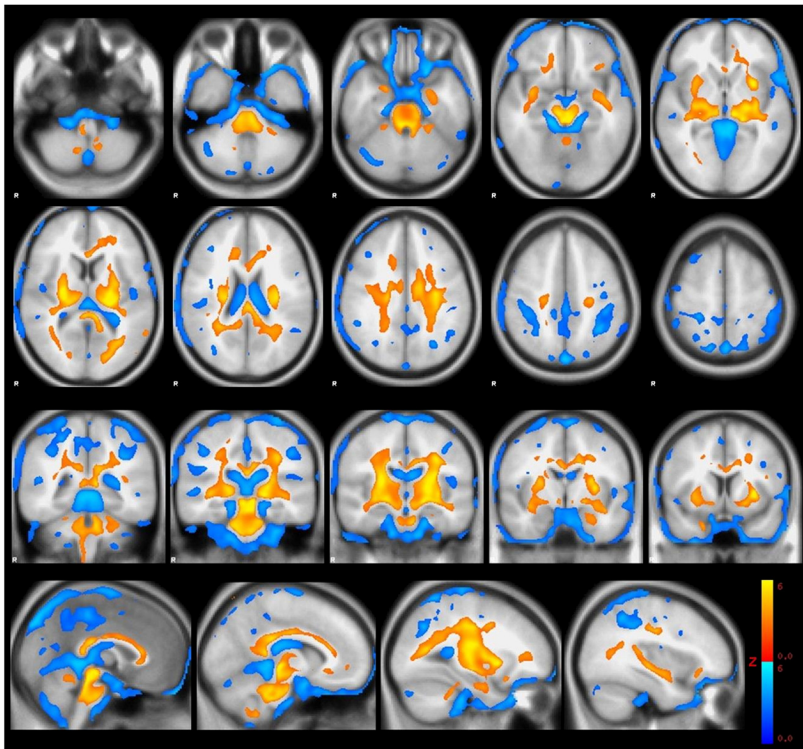
Fig. 1. Regions of significant volume changes in TBI patients between ~8 weeks and ~12 months post-injury, as compared to controls, thresholded at false discovery rate (FDR) 0.05 (clusters of <33.5 voxels rejected). Longitudinal volume reduction is coded red/yellow, volume expansion is coded blue. Results are overlaid onto the MNI standard template.

than controls (mean±SD: 1506 ml±85 ml vs. 1645 ml±85 ml, $P<0.0001$, Mann–Whitney U-test).

During the ~11 months scan interval %BVC, derived from SIENA, ranged between −0.6% and −9.4% (mean −4.0%, median −2.9%) in patients, compared to between −0.9% and +0.3% (mean −0.18%, median −0.13%) in controls (patients vs. controls: $P<0.000001$, Mann–Whitney U-test).

For each patient, Table 2 lists BPV and %BVC together with selected demographic, clinical and conventional imaging variables. There was a significant correlation between BPV and %BVC when all subjects were considered ($r=0.57$, $P<0.001$, Spearman's rho); however this correlation was not significant for either patients or controls separately. No significant correlations were found between %BVC and scan interval, age or gender. All but one patient had microhaemorrhages on T2*-weighted images, indicating TAI. Graded according to location (Graham et al., 2002), TAI grade correlated with %BVC ($r=-0.59$, $P<0.01$, Spearman's rho), but not with BPV.

To check for the robustness of SIENAX for these traumatized brains, we also applied SIENAX on the follow-up scans, again comparing to controls, and calculated the differences (in %) between BPV at the first and second scan (data not shown). These values were roughly comparable to the %BVC derived from SIENA, indicating that the estimates from SIENAX were reliable, at least as rough estimates of BPV.
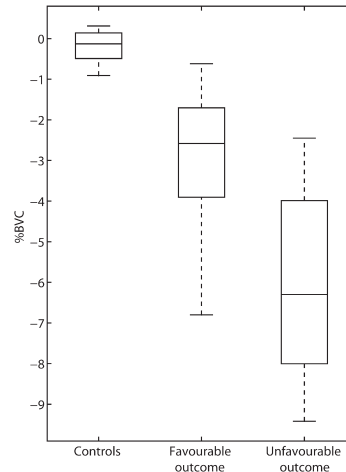
Regional volume changes

TBM, with whole-brain correction for multiple comparisons, identified regions with significant volume loss or volume expansion over time in patients as compared to controls. Fig. 1 shows the differences between patients and controls using an FDR of 0.05. At this threshold, a large coherent cluster of volume loss extended from the brain stem and cerebellar peduncles and bilaterally through the thalamus, internal capsule, external capsule, putamen, inferior and superior longitudinal fasciculus, corpus callosum (genu, body and splenium) and corona radiata. Small clusters of significant volume loss were also found, mainly in the cerebellum and in the frontal lobes. Significant longitudinal volume expansion in patients compared to controls was found in the ventricles and scattered in the subarachnoidal space (with a large cluster at the fundus of the intraparietal sulcus). In general the pattern of volume loss as well as volume expansion was relatively symmetric. The statistical strength of volume loss, reaching its maximum in the tectum mesencephali ($Z=6.86$), exceeded that of volume expansion (maximum $Z=5.07$). Details of significant volume loss are found in Table 3.

Fig. 2. Box and whiskers plot of %BVC in patients with favourable ($n=16$) and unfavourable ($n=8$) outcome ($P<0.01$, Mann–Whitney U-test). Control values ($n=14$) are displayed for comparison. %BVC = percent brain volume change.

Correlation with clinical variables

Injury severity

BPV at the first scan correlated significantly with duration of PTA ($r=-0.59$, $P<0.01$, Spearman's rho), however not with duration of coma. Both duration of coma and PTA correlated significantly with %BVC between the two scan time points ($r=-0.45$, $P<0.05$ and $r=-0.53$, $P<0.01$, respectively, Spearman's rho).

Functional status and outcome

BPV at the first scan correlated significantly with concomitantly evaluated FIM ($r=0.46$, $P<0.05$, Spearman's rho). Also %BVC between the two scan time points was significantly correlated with FIM evaluated both at the first and at the second scan time point ($r=0.62$, $P=0.001$ and $r=0.68$, $P<0.001$ respectively, Spearman's rho).

Table 3
Clusters of significant volume loss in patients compared to controls at false discovery rate (FDR) 0.05

	Anatomical region	Tissue type	Side	MNI coordinates of voxel of maximum significance			PeakZ	Cluster size (voxels)
				x	y	z		
1	Large coherent cluster in the brain stem and cerebellar peduncles, extending bilaterally through internal capsule, thalamus, putamen, external capsule, inferior and superior longitudinal fasciculus, corpus callosum, corona radiata	WM+GM	L/R	−1	−31	−16	6.86	129013
2	Cerebellum	GM	L	−8	−50	−54	4.06	963
3	Frontal orbital cortex	GM	L	−29	18	−18	3.54	736
4	Cerebellum	GM	R	10	−62	−52	3.74	508
5	Frontal orbital cortex	GM	R	9	20	−21	3.04	301
6	Cerebellum	GM	R	25	−53	−23	3.05	212
7	Frontal lobe, subcortical WM	WM	L	−43	10	18	3.13	178
8	Frontal lobe, cortex/subcortical WM	WM+GM	L	−42	29	2	3.77	148
9	Middle temporal gyrus	GM	L	−60	−56	10	3.40	122
10	Superior corona radiata	WM	R	23	8	38	2.72	110
11	Lateral occipital cortex	GM	L	−50	−77	13	3.06	61

Coordinates of each cluster maximum are reported. Cluster maximum for cluster 1 corresponds to tectum mesencephali.
GM = grey matter; WM = white matter; L = left; R = right.

With respect to 1-year outcome, BPV at the first scan did not differ significantly between favourable and unfavourable outcome groups (Mann–Whitney U-test). However, BPV correlated significantly with the full scale GOS-E ($r=0.48$, $P<0.05$). Late volume change (%BVC between the two scan time points) was significantly different between outcome groups (Fig. 2; $P<0.01$, Mann–Whitney U-test) and also correlated significantly with the full scale GOS-E ($r=0.55$, $P<0.01$).

In a linear regression model with FIM at the follow-up scan as the dependent variable, FIM at the initial scan significantly predicted late FIM, as one would expect ($P<0.001$). Adding BPV at the first scan did not improve the model. However, adding %BVC to the model improved prediction of late FIM (increment $F=4.7$ and parameter estimate $P<0.001$ for %BVC), with pronounced late atrophy predicting lower FIM at follow-up, and vice versa.

Discussion

We studied late atrophy occurring between ~8 weeks and ~12 months following severe TBI, using TBM to evaluate the regional distribution of volume change and SIENA to estimate individual global atrophy. Additionally, SIENAX was used to estimate global atrophy occurring prior to the first time point. In patients, as compared to controls, significant atrophy during the scan interval was found in: a large coherent cluster in the brain stem and cerebellar peduncles extending bilaterally through the thalamus, internal capsule, external capsule, putamen, inferior and superior longitudinal fasciculus, corpus callosum and corona radiata; and in smaller clusters mainly in the cerebellum and the frontal lobe. At ~8 weeks post-injury brain volume was already reduced by mean 8.4% in patients as compared to controls, but an additional mean 4.0% (median 2.9%) volume loss occurred in patients during the scan interval. The magnitude of this late volume loss was significantly correlated with injury severity (duration of coma and PTA), with FIM at both scan time points, and with 1-year GOS-E.

Global volume changes

We found a highly significant decline in brain volume during the late subacute and chronic phases of TBI. This is in agreement with the recent study by Trivedi et al. also using SIENA (Trivedi et al., 2007). While our patient population represented very severely injured survivors of TBI (Engberg et al., 2006), Trivedi studied a population of mixed injury severity ranging from mild to severe TBI. This probably explains why we found a greater decline in brain volume (mean −4.0%, median −2.9%) compared to their study (mean −1.43%). However, part of this difference may also be due to the fact that the time from TBI to the first scan was slightly shorter in our study (55 days, range=29–81 days compared to 79 days, range=39–109 days).

All but one patient in the present study had microhaemorrhages on conventional T2*-weighted images, indicating the presence of TAI. In accordance with the view that general atrophy post-TBI is mainly caused by TAI, we found that TAI grade, as evaluated on T2*-weighted images, correlated with %BVC. However, a similar correlation could not be found for initial atrophy estimated by BPV.

To relate longitudinal decline in brain volume to the early atrophy occurring between the time of injury and the first scan time point (the first ~8 weeks post-injury), we used SIENAX, comparing brain volume in patients at the first scan time point to that of the controls. With SIENAX we found that BPV in patients at the first scan time point was on average 8.4% smaller than BPV in controls. While this should be regarded as a fairly rough estimate (see subsection Limitations), it clearly indicates that the rate of decline in brain volume is much higher in the acute/early subacute phase post-trauma than at later stages. Obviously our study does not allow further conclusions to be made about the time course of atrophy following TBI, as we cannot know whether the late atrophy occurred gradually during the whole scan interval, or whether the degenerative process ended already after

a few months. However, animal studies suggest a gradual volume decrease up to at least 1 year post-trauma (Rodriguez-Paez et al., 2005). Future human studies with multiple scan time points should be conducted to better characterize the time course of the progressive atrophy following TBI.

Regional volume changes

The pattern of late atrophy observed in patients as compared to controls corresponds well to those regions known from neuropathological and biomechanical studies to be susceptible to TAI or to consequences of TAI (Graham et al., 2002; Maxwell et al., 1997). The continuous involvement of the corticospinal tract from the corona radiata through the posterior limb of the internal capsule, crus cerebri and pons is likely to represent Wallerian degeneration secondary to TAI. These results suggest that the progressive atrophic process following TBI is a direct consequence of TAI. The highest level of significance was found for the tectum mesencephali, which is one area particularly susceptible to TAI.

The results of the present study are mainly in agreement with the findings of the single available TBM study on TBI (Kim et al., 2008). When comparing these two studies, one should bear in mind that while we investigated the regional distribution of late atrophy only, the study by Kim et al. was not longitudinal and therefore did not distinguish between early and late atrophy. In both studies, the statistical strength of volume loss was generally higher than that of volume expansion. As concluded by Kim et al. this suggests that using ventricular enlargement to indirectly measure atrophy is not the most sensitive measure. Like in the study by Kim et al. we found significant volume loss (at FDR 0.05) in the brainstem, thalamus, corpus callosum, putamen and cerebellum. However, the volume loss was more widespread in our study and included the entire corticospinal tract from corona radiata to pons as one coherent cluster. Additionally we found significant volume loss in the external capsule, inferior and superior longitudinal fasciculus and in the cerebellar peduncles. Unlike Kim et al. we did not find volume loss in the caudate. While in both studies significant volume expansion was found in CSF, Kim et al. also found apparent volume expansion in some white matter areas including the internal capsule, which they interpreted as secondary to heavy atrophy of surrounding areas.

Some of the discrepancies between the present study and the study by Kim et al. are likely to be due to differences in injury severity, as Kim et al. included patients with both moderate and severe TBI. It is possible that there are also some differences in the regional distribution of the atrophy occurring in the acute/early subacute phase compared to the late atrophy in the late subacute/chronic phase. One should also bear in mind the somewhat random nature of the injuries in the individual TBI patients, which inadvertently is another source of variability between studies. Finally, discrepancies may also be related to methodological differences in the two studies. Importantly, in the cross-sectional study by Kim et al., every brain was warped to a population-specific template based on both controls and patients, while in our longitudinal study warping was performed within subject.

In a very recent longitudinal study, Bendlin and co-workers (Bendlin et al., in press) measured regional volume changes in patients with moderate TBI using voxel-based morphometry (VBM). Their study design is somewhat similar to ours, but differs in some key elements. Firstly, there is a difference in injury severity of the TBI patients. Secondly, as opposed to VBM, TBM is based on intra-subject volume change. Thirdly, VBM relies on segmented white matter and grey matter maps, whereas our TBM analysis has the advantage of not relying on tissue segmentation (in our dataset tissue segmentation tended to misclassify focal lesions, see subsection Limitations). Despite these differences, our results are largely in agreement with the findings of Bendlin et al. who reported longitudinal volume losses

in corona radiata, corpus callosum, internal and external capsules, superior and inferior longitudinal fasciculus, cingulum, inferior fronto-occipital fasciculus, corticospinal tract, cerebellar peduncles, thalamus, and pallidum, as well as small areas with volume loss in the cerebellar white matter, right post-central and precentral gyri, supplementary motor area, and putamen.

Clinical significance of progressive atrophy

One of the advantages of the prospective longitudinal design used in this study is that it allowed us not only to scan the patients with a uniform time interval, but also to collect clinical data at predefined time points, including outcome evaluation about 1 year post-injury. We found several correlations between clinical variables and the degree of late global atrophy. In agreement with the study by Trivedi et al., we found a significant correlation between duration of coma and %BVC, although duration of coma was defined slightly differently in the two studies. Another indicator of injury severity, duration of PTA, also correlated significantly with %BVC in our study. These findings are not surprising given that the extent of TAI is likely to be a major determinant of %BVC as well as of the severity of impairment of consciousness reflected by duration of coma or PTA.

Furthermore, we found significant correlations between %BVC and functional status (as evaluated by FIM) at both scan time points, and between %BVC and 1-year GOS-E. These findings, however, do not necessarily imply that late volume loss *per se* is a determinant of functional status and outcome. It might be that the extent of TAI is the major determinant of both %BVC and clinical function including long-term clinical outcome. The consequences of TAI may involve cellular processes other than atrophy, which also might account for some of the clinical consequences following TAI.

Using linear regression, we determined which parameters predicted functional status at the follow-up scan. We found that inclusion of %BVC dramatically improved upon the predictive performance offered by the ~8 week FIM values alone. Thus, a higher rate of volume loss during the scan interval was associated with poorer functional status at follow-up, controlling for the degree of functional impairment present at the first scan time point. It should be noted, however, that the four most severely injured patients (patient no. 1, 3, 4 and 6 in Table 2, who all had PTA >1 year) stood out from the rest, causing the correlation between %BVC and FIM at ~12 months to be driven mainly by these subjects. Larger studies are clearly needed to confirm the observed relationship between atrophy and functional impairment.

For the majority of patients, decline in brain volume occurred concurrently with remarkable clinical improvement, as for example reflected in the median FIM-value which increased from 60 (18–122) at the time of the first scan to 117 (18–126) at the second scan. This apparent paradox indicates that some regenerative processes must occur despite the macroscopic degeneration. From animal studies evidence is accumulating that neuroplastic changes, such as axonal sprouting and synaptic reorganization, accompany functional recovery following TBI (reviewed e.g. by Levin 2003; Albensi and Janigro 2003, Dancause 2006) and may even be enhanced by pharmacological procedures (see e.g. Priestley 2007). In humans, using diffusion tensor imaging, we recently found that diffusion abnormalities following severe TBI, supposedly reflecting disruption of axonal micro-architecture, partly normalise during clinical recovery, particularly in patients with good outcome (Sidaros et al., 2008). Metabolite abnormalities, as measured by MR proton spectroscopy, also have been found to recover over time to near normal levels in good outcome patients (Holshouser et al., 2006; Signoretti et al., 2008).

Limitations

The use of SIENAX is based on the assumption that brain volume of the patients prior to injury was comparable to that of the controls.

Since the groups were matched with respect to age, sex and education, this may be a reasonable approximation. Even if it had been feasible to acquire another MRI in the very acute phase following trauma, oedema would have greatly confounded longitudinal volume comparisons.

In principle, clearing of brain oedema between scans could be responsible for an apparent loss of brain volume over time. However, we found no radiological evidence of oedema at the first MRI (evaluated on T2-weighted and FLAIR images), consistent with the experience that oedema resolution usually occurs within the first four weeks post-injury, i.e. before the first scan time point of this study. Furthermore, the fact that BPV was found to be substantially lower in patients than controls at the first scan time point, strongly argues that oedema had resolved at that point and thus did not mediate the observed longitudinal decline in brain volume.

Grey matter/white matter segmentation tended to misclassify focal lesions as grey matter, regardless of original tissue type. This prevented us from studying grey and white matter atrophy separately. However, lesioned tissue was never misclassified as CSF, and the sum of grey matter and white matter volume estimates, derived from SIENAX, were therefore regarded as valid estimates of BPV.

One limitation related to voxel-wise morphometric approaches such as TBM is that the sensitivity to areas with high anatomical variability between subjects, such as cortical gyri and sulci, is less than to areas exhibiting little inter-subject variability. In a TBI population, the correct warping of cortical areas is even further complicated by the occurrence of focal lesions, which are often cortical in location. Therefore, we cannot exclude the possibility that the observed relative sparing of cortical areas, in terms of late atrophy, could be a false-negative result. On the other hand, we did not expect cortical atrophy to be a prominent feature in comparison with white matter atrophy, because local cortical atrophy due to focal lesions would vary in location between patients and thus be unlikely to emerge as significant in a voxel-wise group analysis. The possibility of more widespread cortical thinning, e.g. secondary to TAI with retrograde degeneration, would probably be below the limit of detection by TBM. Future studies, using for example cortical thickness mapping, might elucidate a possible cortical involvement in the degenerative process following TBI.

Finally, another limitation of our study is that we did not acquire MRI at more than two time points. Future studies using multiple data acquisitions at shorter time intervals would allow for a more detailed description of the time course of atrophy following TBI.

Conclusions

In this prospective longitudinal study of late volume changes following severe TBI we have demonstrated that the most pronounced atrophy is found in regions susceptible to TAI or to consequences of TAI, suggesting that TAI is a major factor responsible for late degeneration. We have further shown associations between the extent of global atrophy and clinical parameters, including duration of coma and PTA, and 1-year outcome. Interestingly, in most patients these long-term degenerative changes occurred concurrently with functional improvement, suggesting that macroscopic tissue loss is less important than supposedly microscopic neuroplastic processes in determining clinical function.

References

Albensi, B.C., Janigro, D., 2003. Traumatic brain injury and its effects on synaptic plasticity. Brain Inj. 17 (8), 653–663.

Ashburner, J., Andersson, J.L., Friston, K.J., 2000. Image registration using a symmetric prior — in three dimensions. Hum. Brain Mapp. 9 (4), 212–225.

Bendlin, B.B., Ries, M.L., Lazar, M., Alexander, A.L., Dempsey, R.J., Rowley, H.A., et al., in press. Longitudinal changes in patients with traumatic brain injury assessed with diffusion-tensor and volumetric imaging. Neuroimage. doi:10.1016/j.neuroimage.2008.04.254.

Bigler, E.D., 2001. Quantitative magnetic resonance imaging in traumatic brain injury. J. Head Trauma Rehabil. 16 (2), 117–134.

Bramlett, H.M., Dietrich, W.D., 2002. Quantitative structural changes in white and gray matter 1 year following traumatic brain injury in rats. Acta Neuropathol. 103 (6), 607–614.

Dancause, N., 2006. Neurophysiological and anatomical plasticity in the adult sensorimotor cortex. Rev. Neurosci. 17 (6), 561–580.

Engberg, A.W., Liebach, A., Nordenbo, A., 2006. Centralized rehabilitation after severe traumatic brain injury — a population-based study. Acta Neurol. Scand. 113 (3), 178–184.

Gale, S.D., Baxter, L., Roundy, N., Johnson, S.C., 2005. Traumatic brain injury and grey matter concentration: a preliminary voxel based morphometry study. J. Neurol. Neurosurg. Psychiatry 76 (7), 984–988.

Graham, D.I., Gennarelli, T.A., McIntosh, T.K., 2002. Trauma. In: Lantos, G.A.P.L. (Ed.), Greenfield's Neuropathology, seventh ed., vol. 1. Arnold Publishers, London, pp. 823–898.

Granger, C.V., Hamilton, B.B., Keith, R.A., Zielesny, M., Sherwin, F.S., 1986. Advances in functional assessment for medical rehabilitation. Top. Geriatr. Rehabil. 1, 59–74.

Holshouser, B.A., Tong, K.A., Ashwal, S., Oyoyo, U., Ghamsary, M., Saunders, D., et al., 2006. Prospective longitudinal proton magnetic resonance spectroscopic imaging in adult traumatic brain injury. J. Magn. Reson. Imaging 24 (1), 33–40.

Kim, J., Avants, B., Patel, S., Whyte, J., Coslett, B.H., Pluta, J., et al., 2008. Structural consequences of diffuse traumatic brain injury: a large deformation tensor-based morphometry study. Neuroimage 39 (3), 1014–1026.

Leow, A.D., Yanovsky, I., Chiang, M.C., Lee, A.D., Klunder, A.D., Lu, A., et al., 2007. Statistical properties of Jacobian maps and the realization of unbiased large-deformation nonlinear image registration. IEEE Trans. Med. Imaging 26 (6), 822–832.

Levin, H.S., 2003. Neuroplasticity following non-penetrating traumatic brain injury. Brain Inj. 17 (8), 665–674.

Levin, H.S., O'Donnell, V.M., Grossman, R.G., 1979. The Galveston Orientation and Amnesia Test. A practical scale to assess cognition after head injury. J. Nerv. Ment. Dis. 167 (11), 675–684.

MacKenzie, J.D., Siddiqi, F., Babb, J.S., Bagley, L.J., Mannon, L.J., Sinson, G.P., et al., 2002. Brain atrophy in mild or moderate traumatic brain injury: a longitudinal quantitative analysis. AJNR Am. J. Neuroradiol. 23 (9), 1509–1515.

Maxwell, W.L., Povlishock, J.T., Graham, D.L., 1997. A mechanistic analysis of nondisruptive axonal injury: a review. J. Neurotrauma 14 (7), 419–440.

Nichols, T.E., Holmes, A.P., 2001. Nonparametric permutation tests for functional neuroimaging: a primer with examples. Hum. Brain Mapp. 15 (1), 1–25.

Priestley, J.V., 2007. Promoting anatomical plasticity and recovery of function after traumatic injury to the central or peripheral nervous system. Brain 130 (Pt. 4), 895–897.

Rodriguez-Paez, A.C., Brunschwig, J.P., Bramlett, H.M., 2005. Light and electron microscopic assessment of progressive atrophy following moderate traumatic brain injury in the rat. Acta Neuropathol. 109 (6), 603–616.

Salmond, C.H., Chatfield, D.A., Menon, D.K., Pickard, J.D., Sahakian, B.J., 2005. Cognitive sequelae of head injury: involvement of basal forebrain and associated structures. Brain 128 (Pt. 1), 189–200.

Sidaros, A., Engberg, A.W., Sidaros, K., Liptrot, M.G., Herning, M., Petersen, P., et al., 2008. Diffusion tensor imaging during recovery from severe traumatic brain injury and relation to clinical outcome: a longitudinal study. Brain 131 (Pt. 2), 559–572.

Signoretti, S., Marmarou, A., Aygok, G.A., Fatouros, P.P., Portella, G., Bullock, R.M., 2008. Assessment of mitochondrial impairment in traumatic brain injury using high-resolution proton magnetic resonance spectroscopy. J. Neurosurg. 108 (1), 42–52.

Smith, D.H., Chen, X.H., Pierce, J.E., Wolf, J.A., Trojanowski, J.Q., Graham, D.I., et al., 1997. Progressive atrophy and neuron death for one year following brain trauma in the rat. J. Neurotrauma 14 (10), 715–727.

Smith, S.M., De Stefano, N., Jenkinson, M., Matthews, P.M., 2001. Normalised accurate measurement of longitudinal brain change. J. Comput. Assist. Tomogr. 25 (3), 466–475.

Smith, S.M., Zhang, Y., Jenkinson, M., Chen, J., Matthews, P.M., Federico, A., et al., 2002. Accurate, robust and automated longitudinal and cross-sectional brain change analysis. Neuroimage 17 (1), 479–489.

Tagliaferri, F., Compagnone, C., Korsic, M., Servadei, F., Kraus, J., 2006. A systematic review of brain injury epidemiology in Europe. Acta Neurochir. (Wien) 148 (3), 255–268.

Teasdale, G., Jennett, B., 1974. Assessment of coma and impaired consciousness. A practical scale. Lancet 2 (7872), 81–84.

Tomaiuolo, F., Worsley, K.J., Lerch, J., Di Paola, M., Carlesimo, G.A., Bonanni, R., et al., 2005. Changes in white matter in long-term survivors of severe non-missile traumatic brain injury: a computational analysis of magnetic resonance images. J. Neurotrauma 22 (1), 76–82.

Trivedi, M.A., Ward, M.A., Hess, T.M., Gale, S.D., Dempsey, R.J., Rowley, H.A., et al., 2007. Longitudinal changes in global brain volume between 79 and 409 days after traumatic brain injury: relationship with duration of coma. J. Neurotrauma 24 (5), 766–771.

Wilson, J.T., Pettigrew, L.E., Teasdale, G.M., 1998. Structured interviews for the Glasgow Outcome Scale and the Extended Glasgow Outcome Scale: guidelines for their use. J. Neurotrauma 15 (8), 573–585.

Hippocampal and Caudate Volume Reductions in Antipsychotic-Naïve First Episode Schizophrenia

Research Paper

Hippocampal and caudate volume reductions in antipsychotic-naive first-episode schizophrenia

Bjørn H. Ebdrup, MD, PhD; Birte Glenthøj, MD, DMSc; Hans Rasmussen, PhD; Bodil Aggernaes, MD, PhD; Annika R. Langkilde, MD, PhD; Olaf B. Paulson, MD, DMSc; Henrik Lublin, MD, DMSc; Arnold Skimminge, MSc; William Baaré, PhD

Ebdrup, Glenthøj, Rasmussen, Aggernaes, Lublin — Center for Neuropsychiatric Schizophrenia Research and Center for Clinical Intervention and Neuropsychiatric Schizophrenia Research, Psychiatric Center Glostrup, Copenhagen University Hospital, Glostrup; Ebdrup, Langkilde, Paulson, Skimminge, Baaré — Danish Research Centre for Magnetic Resonance, MR-Department, Copenhagen University Hospital Hvidovre, Hvidovre; Paulson, Baaré — Center for Integrated Molecular Brain Imaging and Neurobiology Research Unit, Copenhagen University Hospital, Rigshospitalet, Copenhagen, Denmark

Background: Enlarged ventricles and reduced hippocampal volume are consistently found in patients with first-episode schizophrenia. Studies investigating brain structure in antipsychotic-naive patients have generally focused on the striatum. In this study, we examined whether ventricular enlargement and hippocampal and caudate volume reductions are morphological traits of antipsychotic-naive first-episode schizophrenia. **Methods:** We obtained high-resolution 3-dimensional T_1-weighted magnetic resonance imaging scans for 38 antipsychotic-naive first-episode schizophrenia patients and 43 matched healthy controls by use of a 3-T scanner. We warped the brain images to each other by use of a high-dimensional intersubject registration algorithm. We performed voxel-wise group comparisons with permutation tests. We performed small volume correction for the hippocampus, caudate and ventricles by use of a false discovery rate correction ($p < 0.05$) to control for multiple comparisons. We derived and analyzed estimates of brain structure volumes. We grouped patients as those with ($n = 9$) or without ($n = 29$) any lifetime substance abuse to examine the possible effects of substance abuse. **Results:** We found that hippocampal and caudate volumes were decreased in patients with first-episode schizophrenia. We found no ventricular enlargement, differences in global volume or significant associations between tissue volume and duration of untreated illness or psychopathology. The hippocampal volume reductions appeared to be influenced by a history of substance abuse. Exploratory analyses indicated reduced volume of the nucleus accumbens in patients with first-episode schizophrenia. **Limitations:** This study was not a priori designed to test for differences between schizophrenia patients with or without lifetime substance abuse, and this subgroup was small. **Conclusion:** Reductions in hippocampal and caudate volume may constitute morphological traits in antipsychotic-naive first-episode schizophrenia patients. However, the clinical implications of these findings are unclear. Moreover, past substance abuse may accentuate hippocampal volume reduction. Magnetic resonance imaging studies addressing the potential effects of substance abuse in antipsychotic-naive first-episode schizophrenia patients are warranted.

Introduction

Magnetic resonance imaging (MRI) studies have demonstrated the presence of structural brain abnormalities in multiple brain regions in chronic schizophrenia patients compared with healthy controls.[1] Although, volume changes have also been observed in various brain regions in first-episode schizophrenia patients,[2] only hippocampal volume reduction and ventricular enlargement are consistently present, as shown in 2 recent meta-analyses.[3,4] Inconsistencies among studies are probably because of differences in methods, samples sizes and sample composition (e.g., studies vary

in the inclusion criteria regarding previous exposure to antipsychotic medications and substance abuse or dependence).

Numerous studies point toward hippocampal involvement in schizophrenia (for reviews see[5,6]). Volumetric reductions in hippocampus, however, are not pathognomonic for schizophrenia, but they have been associated with numerous neuropsychiatric disorders, including substance abuse.[7] Moreover, typical and atypical antipsychotics may affect hippocampal volumes differently.[8] In antipsychotic-naive patients, significant hippocampal reductions have been reported,[9] although not consistently.[10] The clinical implications of hippocampal involvement in antipsychotic-naive schizophrenia patients are unclear. However, hippocampal reductions may be associated with illness duration and psychopathology.[11]

Ventricular enlargement is also not specific for schizophrenia.[12] Nevertheless, recent studies suggest that ventricular enlargement may progress during the course of the disease and may be related to outcome[13] or antipsychotic treatment.[14]

Studies investigating minimally medicated and antipsychotic-naive schizophrenia patients have often focused on the striatum, which consists of the caudate nucleus, putamen and nucleus accumbens.[15] Striatal volume reductions are not consistently found in medicated first-episode patients, likely because antipsychotic treatment in itself can induce alterations in the striatum (for review see[16]). Nevertheless, a recent meta-analysis of voxel-based structural MRI studies in first-episode patients found the presence of caudate nucleus reductions as compared with chronic schizophrenia patients.[2] Moreover, nonpsychotic children of psychotic individuals have been shown to have smaller caudate nuclei.[17] Absolute volume reductions in the putamen and nucleus accumbens[15,18,19] have also been observed, although significant changes have only been observed in the putamen.[18] Significantly increased putamen volumes have also been reported.[9]

Although the clinical implications of structural striatal changes in schizophrenia are unresolved, caudate volume changes have been associated with illness duration and positive symptoms.[20] Also, a positive correlation was found between putamen surface contractions and affective flattening.[18]

Structural changes already observed in antipsychotic-naive schizophrenia patients are likely not because of hospitalization, chronicity or antipsychotic treatment. However, schizophrenia patients commonly have a past or present history of substance abuse or dependence. Both alcoholism[21,22] and cannabis abuse[23,24] have been associated with grey matter changes in frontal, temporal and subcortical regions as well as ventricular changes. Some studies have dealt with this issue by excluding patients with comorbid substance abuse or dependence.[25-27] However, the criteria used are not uniform among studies and encompass exclusion because of substance dependence[20], "significant abuse"[19] or abuse within a 6-month period,[28] as well as no mention of abuse.[9,10,29]

The primary aim of our study was to investigate whether the presence of hippocampal reduction, ventricular enlargement and caudate reduction is a morphologic trait in first-episode antipsychotic-naive schizophrenia patients compared with matched healthy controls. Regional voxel-wise and volumetric analyses were performed after high-dimensional

intersubject warping of all patients' brains.[30] Region-of-interest (ROI) masks of the hippocampus, ventricles and caudate were created to test our a priori hypotheses. Moreover, associations with clinical measures were explored. Finally, we tested for possible effects of any lifetime substance abuse.

Methods

The study was conducted in accordance with the declaration of Helsinki II and approved by the ethics committee of the Capital Region (H-KF-01–78/97). After complete description of the study to the participants, written informed consent was obtained.

Participants

Initially, 43 patients and 43 healthy controls, matched for age, sex and parental socio-economic status, underwent MRI scans. Patients were recruited as part of a first-episode schizophrenia study conducted in the Capital Region of Copenhagen, Denmark (Psychiatric Centres Amager, Ballerup, Bispebjerg, Gentofte, Glostrup and Rigshospitalet). We included patients aged 18–45 years with a diagnosis of schizophrenia, no prior exposure to antipsychotic medication and no medical or neurologic comorbidity. The DSM-IV diagnoses were based on the Schedules for Clinical Assessment in Neuropsychiatry (SCAN), version 2.1.[31] We also included patients who used benzodiazepines (to reduce agitation and anxiety). Use of antidepressants was recorded. Patients with any lifetime substance abuse are denoted Pt_{ab}, patients with no lifetime substance abuse diagnosis are denoted Pt_{non-ab} and the total patient sample is denoted Pt_{all}.

The controls were recruited from the community and had no prior or present psychiatric disorder, had never used psychotropic medication and had no first-degree relatives with a psychiatric disorder, as determined by SCAN interviews. Both patients and controls had normal physical and neurologic examinations, no history of major head injury (loss of consciousness), no mental retardation, no contraindications on MRI or any nonpsychiatric disorder. We assessed handedness by use of the Edinburgh Inventory.[32] A neuroradiologist (A.L.) examined the MRI scans, which were free of pathology. We excluded controls with substance abuse or dependence.

Clinical measures

Trained raters assessed psychopathology with the Positive and Negative Syndrome Scale (PANSS),[33] and the interviews were recorded on DVDs for validation purposes. In a random subset of 10 PANSS recordings, an intraclass correlation of 0.92 in a 2-way mixed effect model was achieved.

We defined the duration of untreated illness as the time between the first unspecific symptoms related to psychosis to the date of the MRI scan. Symptoms had to be associated with a decline in a previous stable level of function. We collected data about the duration of untreated illness with the best-estimate approach[25] with information from the SCAN interview, clinical records and relatives, if possible.

Image acquisition

We acquired high-resolution 3-dimensional (3-D) T_1-weighted, sagittal, magnetization-prepared rapid-gradient echo (MPRAGE) scans of each patient's whole head (echo time 3.93 ms, repetition time 1540 ms, inversion time 800 ms, flip angle 9°, field of view 256 mm, matrix 256 × 256, 1 × 1 × 1 mm voxels, 192 slices) and 2-dimensional (2-D) T_2-weighted, axial, turbo spin echo (TSE) scans of the whole brain (echo time one 17 ms, echo time two 100 ms, repetition time 9000 ms, flip angle 150°, field of view 220 mm, matrix 256 × 256, GRAPPA acceleration factor 2, 30 reference lines, 0.9 × 0.9 × 3 mm voxels, 50 slices). We used a Siemens Magnetom Trio 3-T scanner with an 8-channel head coil (Invivo Corporation).

Image processing

We corrected the images for spatial distortions owing to nonlinearity in the gradient system of the scanner[34] and processed the images using the VBM5 toolbox (http://dbm .neuro.uni-jena.de/vbm/vbm5-for spm5/) in SPM5 (Wellcome Department of Cognitive Neurology, University College London, UK), which includes a unified segmentation algorithm,[35] and a hidden Markov random field method.[36] We used the T_2-weighted images to automatically create brain masks in native space. We derived brain masked grey and white and cerebral spinal fluid tissue maps in native space from the T_1 images. We used these masks, together with the affine part of the spatial transformation from native to Montreal Neurological Institute (MNI) space, in Diffeomorphic Anatomical Registration Through Exponentiated Lie Algebra (DARTEL)[30] using default settings, allowing for high-dimensional intersubject registration. Recently, it has been shown that DARTEL can successfully register the hippocampus across patients.[37] Using the final flow fields that parameterize the deformations, brain masked grey matter, white matter and cerebral spinal fluid images were warped into average image space (DARTEL space) and modulated with the Jacobian determinant of the applied deformation fields to correct for local volume changes following the high dimensional intersubject warping. We used voxel-wise analyses to test for differences in regional tissue volume. We smoothed these tissue images with an 8-mm full-width at half-maximum Gaussian kernel. We visually checked the quality of the images generated at each processing stage.

Regions of interest

We created the following ROI masks on the average of DARTEL warped MPRAGE images for all participants. The delineation landmarks were as follows: hippocampus,[38] ventricles, lateral and third ventricle,[39] caudate nucleus, nucleus accumbens and putamen.[15]

Volumetric brain measures

We acquired intracranial volume estimates by integrating and adding image intensity values of modulated and warped grey matter, white matter and cerebral spinal fluid images. Total brain volume was acquired by integrating and adding grey matter and white matter image intensity values. Total ROI volumes were acquired to investigate whether local voxel-wise differences were reflected in whole ROI volume differences, and to generate percent difference estimates. We derived hippocampal, caudate and accumbens volume estimates by integrating image intensity values of modulated and warped grey matter images within the hippocampus, caudate and accumbens masks, respectively. We derived ventricle estimates by integrating image intensity values of modulated and warped cerebral spinal fluid images within the ventricle masks. Because the grey matter tissue of the putamen was only partially classified, we derived putamen volume estimates by integrating intensity values of modulated and warped binary image volumes within the putamen mask.

Statistical analyses

We used the Statistical Package for the Social Sciences (SPSS) to analyze demographic and volumetric data. We tested the distribution of all continuous data for normality with the Shapiro–Wilk test. Age, duration of untreated illness, cerebral spinal fluid and ventricle volumes were not normally distributed. Logarithmic transformation only normalized the distribution of duration of untreated illness. We tested age, cerebral spinal fluid and ventricle volumes nonparametrically with the Mann–Whitney U test. We tested handedness and sex differences with the Fisher exact test and socioeconomic status with the Pearson χ^2 test. Because the Pt_{ab} group only consisted of 9 patients, the Mann–Whitney U test was used to compare clinical data (PANSS scores and duration of untreated illness) between the 2 subgroups. We identified potential outliers with the Grubb outlier test.[40]

We used analysis of covariance to compare Pt_{all} and controls for volumetric estimates of intracranial volume, total brain volume, grey matter and white matter. We entered age, sex and intracranial volume as covariates. Intracranial volume was only corrected for age and sex. We used the Mann–Whitney U test to test for group differences in cerebral spinal fluid volume after the effects of age, sex and intracranial volume had been regressed out. We used the latter approach to test differences for in intracranial volume, total brain volume, grey matter, white matter and cerebral spinal fluid volumes between Pt_{non-ab} and Pt_{ab}.

In the voxel-wise analyses of group differences, age, sex and intracranial volume were covariates. We first tested for differences between Pt_{all} and controls. Subsequently, planned comparisons tested for differences between Pt_{non-ab} and controls, Pt_{ab} and controls, and Pt_{non-ab} and Pt_{ab}. We estimated general linear models nonparametrically using Randomize, version 2.1, part of the FSL library of tools (www.fmrib.ox.ac.uk/fsl/randomise/ index.html) with 10 000 permutations. We used small volume correction, applying ROI masks, to test our a priori hypotheses of hippocampal reduction, ventricle enlargement and caudate reduction. A false discovery rate threshold of 0.05 was used to correct for multiple comparisons. The clinical data (positive,

negative and total PANSS scores, and duration of untreated illness) were used as covariates in separate analyses.

We analyzed group differences in total hippocampal, ventricles, caudate, accumbens and putamen volume estimates with SPSS using a repeated-measures analysis of variance with group (Pt_{all} and control or Pt_{non-ab} and control) as the between-subjects factors, and hemisphere (left and right) as the within-subjects variable. Age, sex and intracranial volume were covariates. We tested for volumetric differences of ROIs between Pt_{ab} and controls and Pt_{non-ab} and Pt_{ab} by use of the Mann–Whitney U test, after regressing out age, sex and intracranial volume effects. We calculated the percentage ROI volume differences using corrected volumes adjusted for age, sex and intracranial volume.

All tests were 2-tailed, and the significance level was set to $p < 0.05$.

Results

Demographic characteristics

Of the 43 patients with first-episode schizophrenia, we excluded 5 patients from further analyses (3 whose diagnoses were adjusted to schizotypal personality disorder and 2 with artifacts on their MRI scans). Of the 38 patients included, 9 fulfilled the DSM-IV criteria for lifetime substance abuse. Three of the 9 patients had no history of abuse for the past year, and 5 patients had no abuse for the past month. Diagnoses were based on excessive intake of alcohol ($n = 3$), cannabis ($n = 2$), alcohol and cannabis ($n = 3$) and central stimulants ($n = 1$). One patient had smoked cannabis on a few occasions in the month before the MRI scan. All participants had a negative urine screening result for substance intake. In total, there were 9 patients with any lifetime substance abuse side-diagnosis (Pt_{ab}), 29 patients with no lifetime substance abuse diagnosis (Pt_{non-ab}). Demographic and clinical characteristics are shown in Table 1.

There were no differences between Pt_{all} and control groups for age ($Z = -0.51$, $p = 0.61$), sex (Fisher exact test, $p > 0.99$), handedness (Fisher exact test, $p > 0.99$) and parental socioeconomic status ($\chi^2_2 = 1.85$, $p = 0.40$). Likewise, the 2 patient subgroups, Pt_{ab} and Pt_{non-ab} did not differ in age, sex, handedness or parental socio-economic status ($p > 0.21$). Compared with Pt_{non-ab}, the Pt_{ab} group had more benzodiazepines prescribed in the investigation period (Fisher exact test, $p = 0.02$) and a tendency toward higher PANSS positive scores ($Z = -1.84$, $p = 0.07$). There was no difference in antidepressant exposure between the 2 patient groups (lifetime exposure: Fisher exact test, $p = 0.66$; current treatment: Fisher exact test, $p = 0.13$), and there was no difference between PANSS negative, PANSS total or duration of untreated illness ($p > 0.76$).

Global brain volumes

There were no volumetric differences in intracranial volume, total brain volume, grey matter, white matter or cerebral

Table 1: Demographic characteristics, clinical data and global brain volumes for antipsychotic-naive first-episode schizophrenia patients and healthy controls

Characteristic	Pt_{ab},† $n = 9$	Pt_{non-ab}, $n = 29$	All patients, $n = 38$	Healthy controls, $n = 43$
	Group; mean (SD)*			
Age, yr, mean (SD) [range]	28.0 (4.4) [20–35]	25.7 (5.6) [18–37]	26.2 (5.4) [18–37]	26.9 (5.7) [18–38]
Sex, male:female	6:3	20:9	26:12	30:13
Handedness, right:left, no. of patients	9:0	36:3	35:3	39:4
Parental socio-economic status, high/moderate/low, no. of patients	3/4/2	18/10/1	21/14/3	30/11/2
Benzodiazepine prescription,‡ no. of patients	8	12	20	—
Antidepressant use, lifetime, § no. of patients	3	6	9	—
Antidepressant use, current,¶ no. of patients	3	3	6	—
Positive and Negative Syndrome Scale[33] score				
Positive	21.6 (4.6)	18.5 (3.8)	19.2 (4.2)	—
Negative	21.8 (6.0)	21.8 (7.1)	21.8 (6.8)	—
Total	81.9 (16.5)	79.5 (14.9)	80.1 (15.1)	—
Duration of untreated illness, wk	188.0 (193.3)	174.5 (229.4)	178.0 (219.0)	—
Absolute, uncorrected volume, cm³				
Intracranial	1619.7 (188.3)	1517.9 (159.9)	1542.0 (170.1)	1552.6 (124.3)
Total brain	1320.4 (155.9)	1242.1 (139.5)	1260.7 (145.3)	1271.4 (109.1)
Total grey matter	792.7 (85.3)	760.7 (79.8)	768.3 (81.1)	777.0 (64.0)
Total white matter	527.6 (74.7)	481.4 (64.9)	492.4 (69.3)	494.3 (50.9)
Cerebrospinal fluid	299.4 (53.8)	275.7 (36.3)	281.3 (41.6)	281.2 (45.9)

Pt_{ab} = patients with any lifetime DSM-IV substance abuse diagnosis; Pt_{non-ab} = patients with no lifetime substance abuse diagnosis; SD = standard deviation.
*Unless otherwise indicated.
†The Pt_{ab} group comprised those with alcohol abuse, in sustained full remission, ($n = 2$); alcohol abuse, on agonist therapy ($n = 1$); cannabis abuse, in a controlled environment, ($n = 1$); other abuse, sustained full remission ($n = 1$); other abuse, moderate ($n = 1$); other abuse, in a controlled environment ($n = 2$); other abuse, early partial remission ($n = 1$). Diagnoses were based on excessive intake of alcohol ($n = 3$), cannabis ($n = 2$), alcohol and cannabis ($n = 3$) and central stimulants ($n = 1$).
‡Number of patients with any prescription of benzodiazepines in the investigation period.
§Antidepressants lifetime: selective serotonin reuptake inhibitors ($n = 7$), noradrenergic and specific serotonergic antidepressant ($n = 1$), unknown antidepressant ($n = 1$).
¶Antidepressants, current: selective serotonin reuptake inhibitors ($n = 5$), noradrenergic and specific serotonergic antidepressant ($n = 1$).

spinal fluid between the Pt_{all} and control groups ($p > 0.23$) or between the 2 patient subgroups ($p > 0.14$) (Table 1).

Regional brain analyses

Results for the voxel-wise analyses are shown in Table 2. Absolute, uncorrected volume estimates for ROIs are presented in Table 3.

Hippocampus
The voxel-wise analyses revealed significant bilateral reductions in hippocampal grey matter in the Pt_{all} group as compared with the control group. This difference was accounted for by Pt_{ab} rather than by Pt_{non-ab} (Fig. 1). Direct comparison of the 2 patient groups showed significantly reduced hippocampal grey matter in the Pt_{ab} group.

The results of the volumetric analyses paralleled those of the voxel-wise analysis. The significant main effect of group, $Pt_{all} \times$ control ($F_{1,76} = 4.26$, $p = 0.042$), was accounted for by Pt_{ab} ($Pt_{ab} \times$ control; $Z = -3.28$, $p = 0.001$), rather than by Pt_{non-ab} ($Pt_{non-ab} \times$ control; $F_{1,67} = 0.63$, $p = 0.43$). Moreover, those in the Pt_{ab} group had significantly smaller hippocampus volumes than those in the Pt_{non-ab} group ($Z = -2.73$, $p = 0.006$). The comparison of Pt_{all} and

control did not reveal a hemisphere × group interaction ($F_{1,76} = 2.61$, $p = 0.11$) or hemisphere effect ($F_{1,76} = 0.31$, $p = 0.58$). The group differences represented corrected hippocampal volume reductions of 2.4% between Pt_{all} and control, 6.5% between Pt_{ab} and control, and 0.1% between Pt_{non-ab} and control (Fig. 2).

Ventricles
Neither the voxel-wise nor the volumetric analyses revealed ventricle differences between any of the groups ($p > 0.38$ in the volumetric analyses). Grubbs test detected one outlier in the control group. Visual inspection of this participant's MRI scan indicated no pathology or artifact. Exclusion of this outlier did not change the results. The results of exploratory analyses of group differences for the third and the lateral ventricle volumes separately were not significant.

Caudate nucleus
The voxel-wise analyses revealed significantly reduced caudate grey matter bilaterally in the Pt_{all} group compared with the control group. This difference was primarily because of Pt_{non-ab} rather than Pt_{ab} (Fig. 3) However, the 2 patient groups did not significantly differ from each other.

The analyses of caudate nucleus volume paralleled the

Table 2: Results of the voxel-wise analyses for antipsychotic-naive first-episode schizophrenia patients and healthy controls

Mask	Contrast*	Side	Z score	p value†	x	y	z	Cluster size, mm³
Hippocampus	$Pt_{all} < HC$	Left	3.65	0.004‡	−26	−12	−28	987
		Right	3.99	0.004‡	25	−17	−25	2270
	$Pt_{ab} < HC$	Left	3.99	0.002‡	−26	−13	−28	1930
		Right	3.39	0.002‡	22	−14	−27	2760
	$Pt_{non-ab} < HC$	Right	2.74	0.35	30	−17	−22	—
	$Pt_{ab} < Pt_{non-ab}$	Left	3.43	0.031‡	−24	−15	−26	1320
		Right	2.79	0.033‡	24	−10	−20	572
Ventricles	$Pt_{all} > HC$	Left	2.71	0.87	−28	−68	6	—
	$Pt_{ab} > HC$	Left	2.11	0.98	−28	−68	6	—
	$Pt_{non-ab} > HC$	Left	3.45	0.34	−34	−51	1	—
	$Pt_{ab} > Pt_{non-ab}$	Left	2.10	0.91	−15	4	25	—
Caudate nucleus	$Pt_{all} < HC$	Left	3.10	0.030‡	−14	17	2	2950
		Right	2.59	0.033‡	10	17	−5	2700
	$Pt_{ab} < HC$	Left	2.58	0.17	−10	20	−1	—
	$Pt_{non-ab} < HC$	Left	3.11	0.023‡	−15	−5	−25	3460
		Right	2.86	0.023‡	12	3	18	3060
	$Pt_{ab} < Pt_{non-ab}$	Left	0.93	0.93	−21	21	0	—
Nucleus accumbens	$Pt_{all} < HC$	Left	2.90	0.08	−12	14	−6	—
	$Pt_{ab} < HC$	Left	1.81	0.40	−13	14	−6	—
	$Pt_{non-ab} < HC$	Left	3.16	0.018‡	−10	16	−7	375
		Right	2.75	0.018‡	10	14	6	168
	$Pt_{ab} < Pt_{non-ab}$	Right	0.72	0.89	14	16	−11	—
Putamen	$Pt_{all} < HC$	Left	2.62	0.16	−24	6	−11	—
	$Pt_{ab} < HC$	Right	3.08	0.099	33	3	0	—
	$Pt_{non-ab} < HC$	Left	2.56	0.76	−14	8	−10	—
	$Pt_{ab} < Pt_{non-ab}$	Right	2.94	0.13	33	1	−1	—

HC = healthy controls; MNI = Montreal Neurological Institute; Pt_{ab} = patients with any lifetime DSM-IV substance abuse diagnosis; Pt_{all} = all patients; Pt_{non-ab} = patients with no lifetime substance abuse diagnosis.
*All significant contrasts are displayed. For nonsignificant contrasts, only the voxel with the lowest p value is displayed.
†p values are false discovery rate (FDR)–corrected ($p < 0.05$).
‡Significant after FDR correction.

Ebdrup et al.

voxel-wise results. There was a significant main effect of group, $Pt_{all} \times$ control ($F_{1,76} = 8.94$, $p = 0.004$). This group difference was primarily accounted for by Pt_{non-ab} ($Pt_{non-ab} \times$ control; $F_{1,67} = 6.88$, $p = 0.01$), although there was a tendency toward caudate volume reduction in Pt_{ab} ($Pt_{ab} \times$ control; $Z = -1.90$, $p = 0.06$). There was no volumetric difference between the 2 patient groups ($Z = -0.17$, $p = 0.99$). There was no hemisphere $\times$ group interaction when comparing the Pt_{all} and control groups ($F_{1,76} = 0.62$, $p = 0.44$) or hemisphere effect ($F_{1,76} = 3.24$, $p = 0.076$). The group differences represented corrected caudate volume reductions of 5.1% between Pt_{all} and control, 5.1% between Pt_{non-ab} and control, and 5.0% between Pt_{ab} and control (Fig. 4).

Nucleus accumbens and putamen

Exploratory voxel-wise analyses of the nucleus accumbens revealed a tendency for reduced grey matter in the Pt_{all} group compared with the control group. This tendency appeared to be driven by Pt_{non-ab}, rather than by Pt_{ab}. However, the 2 patient groups did not significantly differ from each other. Analyses of nucleus accumbens volume showed a significant main effect of group ($Pt_{all} \times$ control; $F_{1,76} = 6.82$, $p = 0.011$). This group difference seemed to be accounted for by Pt_{non-ab} ($Pt_{non-ab} \times$ control; $F_{1,67} = 7.58$, $p = 0.008$), rather than by Pt_{ab} ($Pt_{ab} \times$ control; $Z = -0.88$, $p = 0.38$).

Voxel-wise exploratory analyses of the putamen did not reveal any differences between Pt_{all} and control, Pt_{non-ab} and control or Pt_{ab} and control. Exploratory analyses of putamen volume did not reveal any group main effects ($Pt_{all} \times$ control: $F_{1,76} = 0.42$, $p = 0.52$; $Pt_{non-ab} \times$ control: $F_{1,67} = 0.044$, $p = 0.83$; $Pt_{ab} \times$

control: $Z = -1.27$, $p = 0.20$). When comparing the hemisphere $\times$ group interactions for the Pt_{all} and control groups ($F_{1,67} = 1.25$, $p = 0.27$ and $F_{1,67} = 0.001$, $p = 0.97$ for the accumbens and putamen, respectively). Hemisphere effects ($F_{1,67} = 0.18$, $p = 0.73$ and $F_{1,67} = 0.012$, $p = 0.33$ for the accumbens and putamen, respectively) were absent.

Whole brain

Exploratory voxel-wise whole brain analyses did not reveal any group differences in regional grey matter, white matter or cerebral spinal fluid volumes.

Clinical measures

Neither the voxel-wise nor the volumetric analyses revealed significant associations between PANSS scores or duration of untreated illness and hippocampal, ventricle or striatal structure volumes. However, we observed a weak tendency of longer duration of untreated illness to be associated with reduced hippocampal volume in the Pt_{all} group ($F_{1,32} = 2.55$, $p = 0.13$). Associations with other brain regions, as examined with exploratory whole brain voxel-wise analyses, were absent. There were no significant associations between clinical measures and global brain measures (intracranial volume, total brain volume, grey matter, white matter or cerebral spinal fluid).

Discussion

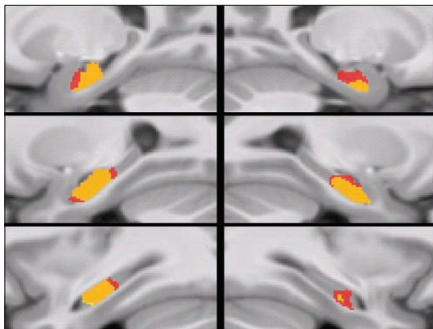As we had hypothesized, this study revealed significant hip-

Table 3: Absolute, uncorrected volume estimates for regions of interest for antipsychotic-naive first-episode schizophrenia patients and healthy controls

Brain region	Group; absolute, uncorrected brain volume, mm³, mean (SD)			
	Pt_{ab}, $n = 9$	Pt_{non-ab}, $n = 29$	All patients, $n = 38$	Healthy controls, $n = 43$
Hippocampus				
Left	4235 (396)	4330 (390)	4307 (388)	4458 (387)
Right	4205 (424)	4260 (379)	4247 (385)	4331 (370)
Total	8440 (809)	8590 (756)	8554 (760)	8789 (717)
Ventricles				
Left	8063 (3755)	7008 (2890)	7258 (3094)	7372 (4226)
Right	7173 (2030)	6812 (3635)	6898 (3301)	7078 (4149)
Third	488 (184)	397 (140)	418 (154)	432 (147)
Total	15 725 (5508)	14217 (6267)	14574 (6058)	14882 (8112)
Caudate nucleus				
Left	3531 (370)	3374 (428)	3411 (416)	3598 (354)
Right	3611 (333)	3454 (410)	3491 (395)	3690 (368)
Total	7142 (698)	6828 (833)	6902 (805)	7288 (718)
Nucleus accumbens				
Left	358 (52)	337 (42)	342 (45)	356 (40)
Right	381 (50)	359 (38)	364 (42)	383 (39)
Total	739 (100)	697 (78)	707 (84)	739 (76)
Putamen				
Left	4117 (536)	4165 (492)	4153 (496)	4200 (376)
Right	4408 (522)	4388 (479)	4393 (482)	4444 (390)
Total	8525 (1055)	8553 (967)	8546 (974)	8643 (759)

Pt_{ab} = patients with any lifetime DSM-IV substance abuse diagnosis; Pt_{all} = all patients; Pt_{non-ab} = patients with no lifetime substance abuse diagnosis; SD = standard deviation.

pocampal and caudate volume reductions in a relatively large cohort of antipsychotic-naive first-episode schizophrenia patients compared with matched healthy controls. Ventricular enlargement was absent. No differences in global volumes were found, and no significant associations between tissue volumes and psychopathology or duration of untreated illness were observed.

Our data support the growing body of evidence that indicates that the hippocampal volume is significantly reduced at the onset of schizophrenia.[3,4,6] The observed corrected volume reduction of 2.4% in the schizophrenia patients, Pt_{all}, compared with the control participants was somewhat smaller than the 8.2% reduction reported in a recent meta-analysis of data from first-episode schizophrenia patients.[4] However, the patients in the present study had never taken antipsychotics, whereas most of the studies included in the meta-analysis included medicated patients.[4] It has been suggested that previous exposure to first-generation antipsychotics may not protect against progressive reductions in hippocampal volume reduction.[8] Moreover, the meta-analysis also included studies that did not account for substance abuse or dependence. Interestingly, the hippocampal volume reduction in our study appeared most pronounced in patients with a lifetime substance abuse diagnosis (Pt_{ab}), accounting for a corrected volume reduction of 6.5% as compared with controls, whereas the reduction among patients without a history of abuse (Pt_{non-ab}) was only 0.1%. However, this study was not a priori designed to test for potential effects of substance abuse; thus, interpreting the results
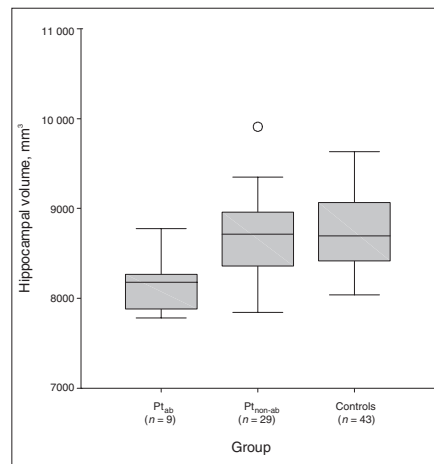
about the effects of abuse must be done cautiously.

Indeed, the absolute, uncorrected volumes (Table 3) suggest that both patient groups might have reduced hippocampal volumes compared with controls. Our findings of higher PANSS positive scores and more frequent prescriptions of benzodiazepines among the Pt_{ab} patients suggests that stress could also have influenced hippocampal volumes.[7] To our knowledge, no studies have associated benzodiazepine use with volumetric brain changes in schizophrenia. Finally, genetic variants prevalent in the normal population may contribute to morphologic variations in schizophrenia;[41] hence, the differences between the small patient subgroups observed in this study could reflect random genetic profiles rather than past substance abuse.

Our finding of reduced caudate nucleus volume agrees with studies reporting absolute[15] or significant[9,25,26,29,42,43] caudate reductions in antipsychotic-naive schizophrenia patients. Thus, our findings add to the evidence that the caudate nucleus is a key structure in the pathophysiology of schizophrenia.[44] The pathway to the observed volumetric reductions in the antipsychotic-naive state is not clear but may be attributable to decreased metabolic rates in the basal ganglia.[45] The magnitude of the caudate volume reductions in

Fig. 1: Voxel-wise hippocampal grey matter volume reductions in first-episode schizophrenia patients for the right (**right, mirrored**) and left hemispheres (**left**). Voxel-wise nonparametric statistic results showing areas were all schizophrenia patients had smaller hippocampal grey matter volumes than healthy controls (yellow), areas where patients with any lifetime substance abuse had smaller volumes than healthy controls (red), and the overlap of the 2 contrasts (orange). Displayed voxels survived a false discovery rate–corrected ($p < 0.05$) small volume correction restricted to the hippocampus. Results are projected on sagittal slices of the average of all DARTEL-warped magnetization-prepared rapid-gradient echo images. From top to bottom, the images are 18, 23 and 28 mm, respectively, from the midsagittal plane.

Fig. 2: Boxplot of hippocampal volumes in schizophrenia patients with any lifetime substance abuse (Pt_{ab}), patients with no lifetime substance abuse (Pt_{non-ab}) and matched healthy controls. Volumes are corrected for age, sex and intracranial volume. In the box-and-whisker plot, the central box represents the values from the lower to upper quartile. The transverse line in the box represents the median corrected volume. The vertical line extends from the minimum to the maximum value, excluding outside values. Outside values are defined as values smaller or larger than the lower quartile minus 1.5 times the interquartile range and are displayed as separate points (?). No outliers were identified.

this study of about 5% are in line with the average caudate reduction in the study by Glenthoj and colleagues.[15] In the present study, caudate volume reductions were significant in the Pt_{non-ab} group and were also apparent in Pt_{ab}, suggesting only a modest, if any, effect of abuse on caudate volumes.

Ventricular enlargement has consistently been observed in first-episode schizophrenia[3,4] and has also been reported in antipsychotic-naive patients.[39,43] Nevertheless, ventricular enlargement was absent in the present cohort, and, as such, our data suggest that ventricular enlargement may not occur until a later stage of the disease[13] or may be related to antipsychotic medication use.[14]

In our voxel-wise analyses, the nucleus accumbens volume appeared reduced at a trend-level in the Pt_{all} group as compared with the control group. However, in the volumetric analyses, this reduction was significant. Volume reductions in the nucleus accumbens have previously been found in antipsychotic-naive schizophrenia patients,[15,18,19] but, to the best of our knowledge, significant accumbens volume reductions have not been reported. Still, limited conclusions can be drawn from our finding because it emerged from exploratory analyses. Moreover, the accumbens reductions were only partially supported by the voxel-wise analysis. In agreement with most[15,18,25,27,46] but not all[19,26] reports on the putamen, we also observed decreased absolute, uncorrected putamen volumes in patients; however, this was not significant when corrected for age, sex and intracranial volume. Only 1 study reported putamen volumes to be significantly reduced,[18]

rendering the issue of structural changes in the putamen in antipsychotic-naive schizophrenia patients unresolved.

We observed no significant differences in corrected global brain volumes (intracranial volume, total brain volume, grey matter, white matter and cerebral spinal fluid) in the patients as compared with the controls. The absence of total brain volume reduction in the patients is in contrast to the findings by Steen and colleagues[4] and could reflect that some of the patients included in the meta-analysis had been exposed to first-generation antipsychotics, which may attenuate global grey matter loss.[47]

It is unclear whether reductions in the hippocampus and caudate nucleus in antipsychotic-naive schizophrenia are associated with psychopathology and illness duration. Although not significant, our observation of a weak association between longer duration of untreated illness and reduced hippocampal volume is in line with those of Matsumoto and colleagues,[11] suggesting that hippocampal changes may occur during the transition to psychosis.[48] Associations between structural abnormalities and clinical variables presumably reflect underlying pathophysiologic disturbances in neurotransmission, metabolism and genetic variance, and different mechanisms may underlie positive and negative symptoms.[49] Studies investigating the relations between volumetric measures and clinical variables have yielded inconsistent results likely attributable to differences in clinical samples, image acquisition and processing and anatomic delineation protocols.

We found no altered asymmetry between patients and

Fig. 3: Voxel-wise caudate grey matter volume reductions in patients with first-episode schizophrenia in the right (**right, mirrored**) and left (**left**) hemispheres. Voxel-wise nonparametric statistic results showing areas were all patients had smaller caudate nucleus grey matter volumes than healthy controls (yellow), areas where patients with no lifetime substance abuse diagnosis had smaller volumes than healthy controls (purple) and the overlap of the 2 contrasts (orange). Displayed voxels survived a false discovery rate–corrected ($p < 0.05$) small volume correction restricted to the caudate nucleus. Results are projected on sagittal slices of the average of all DARTEL warped magnetization-prepared rapid-gradient echo images. From top to bottom, the images are 13, 18 and 23 mm, respectively, from the midsagittal plane.
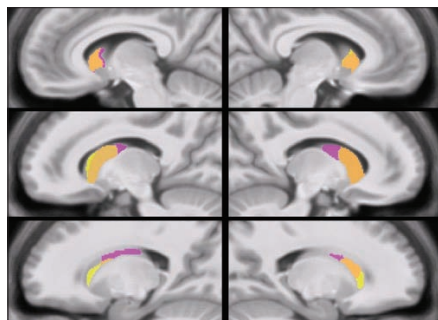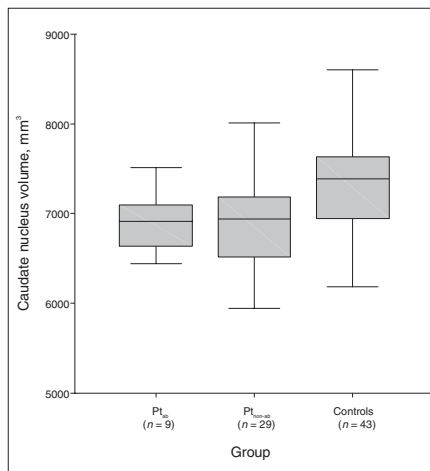
Fig. 4: Boxplot of caudate nucleus volumes in schizophrenia patients with any lifetime substance abuse (Pt_{ab}), patients with no lifetime substance abuse (Pt_{non-ab}) and matched healthy controls. Volumes are corrected for age, sex and intracranial volume. See Figure 2 for information about interpretation of the boxplot.

controls, hence we have not replicated our previous finding of altered asymmetry of the caudate nucleus in an independent group of 19 antipsychotic-naive patients.[15]

Limitations

The present study is limited with respect to elucidating the possible role of drug abuse on volumetric measures because it was not a priori designed to test for differences between patients with or without a lifetime substance abuse diagnosis. Moreover, even though we have assessed all DSM-IV diagnoses with a validated instrument (SCAN 2.1), we cannot exclude the possibility that some of the patients in the Pt$_{non-ab}$ group may have had a past period of excessive drug use, which we were not informed of. Additionally, because of the small number of patients with abuse and the various types of abuse, we cannot make causal inferences about the impact of lifetime substance abuse on brain structure in first-episode schizophrenia patients. Nevertheless, comorbid substance abuse has previously been associated with morphologic changes, including in the hippocampus.[22,23]

Another limitation was the unequal size of the patient subgroups. This was addressed by the use of nonparametric statistical analyses, which makes no assumptions about the distribution of the data. Notably, the volumetric analyses confirmed the differences detected by the voxel-wise analyses, hereby ruling out the possibility that the voxel-wise results were based on random local minima.

Conclusion

Our study indicates that reduced hippocampus and caudate nucleus volumes may constitute morphologic traits in first-episode antipsychotic-naive schizophrenia patients. However, the clinical implications of these findings are still unclear. Moreover, a history of substance abuse may accentuate hippocampal volume reductions. Magnetic resonance imaging studies explicitly addressing the potential effects of any lifetime substance abuse in antipsychotic-naive first-episode schizophrenia patients are warranted.

References

1. Shenton ME, Dickey CC, Frumin M, et al. A review of MRI findings in schizophrenia. *Schizophr Res* 2001;49:1-52.
2. Ellison-Wright I, Glahn DC, Laird AR, et al. The anatomy of first-episode and chronic schizophrenia: an anatomical likelihood estimation meta-analysis. *Am J Psychiatry* 2008;165:1015-23.
3. Vita A, De Peri L, Silenzi C, et al. Brain morphology in first-episode schizophrenia: a meta-analysis of quantitative magnetic resonance imaging studies. *Schizophr Res* 2006;82:75-88.
4. Steen RG, Mull C, McClure R, et al. Brain volume in first-episode schizophrenia: systematic review and meta-analysis of magnetic resonance imaging studies. *Br J Psychiatry* 2006;188:510-8.
5. Gur RE, Keshavan MS, Lawrie SM. Deconstructing psychosis with human brain imaging. *Schizophr Bull* 2007;33:921-31.
6. Boos HB, Aleman A, Cahn W, et al. Brain volumes in relatives of patients with schizophrenia: a meta-analysis. *Arch Gen Psychiatry* 2007;64:297-304.
7. Geuze E, Vermetten E, Bremner JD. MR-based in vivo hippocampal volumetrics: 2. Findings in neuropsychiatric disorders. *Mol Psychiatry* 2005;10:160-84.
8. Chakos MH, Schobel SA, Gu H, et al. Duration of illness and treatment effects on hippocampal volume in male patients with schizophrenia. *Br J Psychiatry* 2005;186:26-31.
9. Salgado-Pineda P, Baeza I, Perez-Gomez M, et al. Sustained attention impairment correlates to gray matter decreases in first episode neuroleptic-naive schizophrenic patients. *Neuroimage* 2003;19:365-75.
10. Laakso MP, Tiihonen J, Syvalahti E, et al. A morphometric MRI study of the hippocampus in first-episode, neuroleptic-naive schizophrenia. *Schizophr Res* 2001;50:3-7.
11. Matsumoto H, Simmons A, Williams S, et al. Structural magnetic imaging of the hippocampus in early onset schizophrenia. *Biol Psychiatry* 2001;49:824-31.
12. Kempton MJ, Geddes JR, Ettinger U, et al. Meta-analysis, database, and meta-regression of 98 structural imaging studies in bipolar disorder. *Arch Gen Psychiatry* 2008;65:1017-32.
13. Van Haren NE, Pol HE, Schnack HG, et al. Progressive brain volume loss in schizophrenia over the course of the illness: evidence of maturational abnormalities in early adulthood. *Biol Psychiatry* 2008;63:106-13.
14. Crespo-Facorro B, Roiz-Santianez R, Perez-Iglesias R, et al. Effect of antipsychotic drugs on brain morphometry. A randomized controlled one-year follow-up study of haloperidol, risperidone and olanzapine. *Prog Neuropsychopharmacol Biol Psychiatry* 2008;32:1936-43.
15. Glenthoj A, Glenthoj BY, Mackeprang T, et al. Basal ganglia volumes in drug-naive first-episode schizophrenia patients before and after short-term treatment with either a typical or an atypical antipsychotic drug. *Psychiatry Res* 2007;154:199-208.
16. Scherk H, Falkai P. Effects of antipsychotics on brain structure. *Curr Opin Psychiatry* 2006;19:145-50.
17. Rajarethinam R, Upadhyaya A, Tsou P, et al. Caudate volume in offspring of patients with schizophrenia. *Br J Psychiatry* 2007;191:258-9.
18. Ballmaier M, Schlagenhauf F, Toga AW, et al. Regional patterns and clinical correlates of basal ganglia morphology in non-medicated schizophrenia. *Schizophr Res* 2008;106:140-7.
19. Gunduz H, Wu H, Ashtari M, et al. Basal ganglia volumes in first-episode schizophrenia and healthy comparison subjects. *Biol Psychiatry* 2002;51:801-8.
20. Crespo-Facorro B, Roiz-Santianez R, Pelayo-Teran JM, et al. Caudate nucleus volume and its clinical and cognitive correlations in first episode schizophrenia. *Schizophr Res* 2007;91:87-96.
21. Pfefferbaum A, Sullivan EV, Rosenbloom MJ, et al. A controlled study of cortical gray matter and ventricular changes in alcoholic men over a 5-year interval. *Arch Gen Psychiatry* 1998;55:905-12.
22. Nagel BJ, Schweinsburg AD, Phan V, et al. Reduced hippocampal volume among adolescents with alcohol use disorders without psychiatric comorbidity. *Psychiatry Res* 2005;139:181-90.
23. Rais M, Cahn W, Van Haren N, et al. Excessive brain volume loss over time in cannabis-using first-episode schizophrenia patients. *Am J Psychiatry* 2008;165:490-6.
24. Yucel M, Solowij N, Respondek C, et al. Regional brain abnormalities associated with long-term heavy cannabis use. *Arch Gen Psychiatry* 2008;65:694-701.
25. Keshavan MS, Rosenberg D, Sweeney JA, et al. Decreased caudate volume in neuroleptic-naive psychotic patients. *Am J Psychiatry* 1998;155:774-8.

26. Shihabuddin L, Buchsbaum MS, Hazlett EA, et al. Dorsal striatal size, shape, and metabolic rate in never-medicated and previously medicated schizophrenics performing a verbal learning task. *Arch Gen Psychiatry* 1998;55:235-43.

27. Lang DJ, Kopala LC, Vandorpe RA, et al. An MRI study of basal ganglia volumes in first-episode schizophrenia patients treated with risperidone. *Am J Psychiatry* 2001;158:625-31.

28. Shihabuddin L, Buchsbaum MS, Hazlett EA, et al. Striatal size and relative glucose metabolic rate in schizotypal personality disorder and schizophrenia. *Arch Gen Psychiatry* 2001;58:877-84.

29. Corson PW, Nopoulos P, Andreasen NC, et al. Caudate size in first-episode neuroleptic-naive schizophrenic patients measured using an artificial neural network. *Biol Psychiatry* 1999;46:712-20.

30. Ashburner J. A fast diffeomorphic image registration algorithm. *Neuroimage* 2007;38:95-113.

31. Wing JK, Babor T, Brugha T, et al. SCAN. Schedules for Clinical Assessment in Neuropsychiatry. *Arch Gen Psychiatry* 1990;47:589-93.

32. Oldfield RC. The assessment and analysis of handedness: the Edinburgh inventory. *Neuropsychologia* 1971;9:97-113.

33. Kay SR, Fiszbein A, Opler LA. The Positive and Negative Syndrome Scale (PANSS) for schizophrenia. *Schizophr Bull* 1987;13:261-76.

34. Jovicich J, Czanner S, Greve D, et al. Reliability in multi-site structural MRI studies: effects of gradient non-linearity correction on phantom and human data. *Neuroimage* 2006;30:436-43.

35. Ashburner J, Friston KJ. Unified segmentation. *Neuroimage* 2005; 26:839-51.

36. Cuadra MB, Cammoun L, Butz T, et al. Comparison and validation of tissue modelization and statistical classification methods in T1-weighted MR brain images. *IEEE Trans Med Imaging* 2005;24:1548-65.

37. Yassa MA, Stark CE. A quantitative evaluation of cross-participant registration techniques for MRI studies of the medial temporal lobe. *Neuroimage* 2009;44:319-27.

38. Baare WF, van Oel CJ, Hulshoff Pol HE, et al. Volumes of brain structures in twins discordant for schizophrenia. *Arch Gen Psychiatry* 2001;58:33-40.

39. Cahn W, Hulshoff Pol HE, Bongers M, et al. Brain morphology in antipsychotic-naive schizophrenia: a study of multiple brain structures. *Br J Psychiatry Suppl* 2002;43:s66-72.

40. Grubbs F. Procedures for detecting outlying observations in samples. *Technometrics* 1969;11:1-21.

41. Meisenzahl EM, Rujescu D, Kirner A, et al. Association of an interleukin-1beta genetic polymorphism with altered brain structure in patients with schizophrenia. *Am J Psychiatry* 2001;158:1316-9.

42. Ettinger U, Kumari V, Chitnis XA, et al. Volumetric neural correlates of antisaccade eye movements in first-episode psychosis. *Am J Psychiatry* 2004;161:1918-21.

43. Chua SE, Cheung C, Cheung V, et al. Cerebral grey, white matter and CSF in never-medicated, first-episode schizophrenia. *Schizophr Res* 2007;89:12-21.

44. Abi-Dargham A, Gil R, Krystal J, et al. Increased striatal dopamine transmission in schizophrenia: confirmation in a second cohort. *Am J Psychiatry* 1998;155:761-7.

45. Buchsbaum MS, Hazlett EA. Positron emission tomography studies of abnormal glucose metabolism in schizophrenia. *Schizophr Bull* 1998;24:343-64.

46. Gur RE, Maany V, Mozley PD, et al. Subcortical MRI volumes in neuroleptic-naive and treated patients with schizophrenia. *Am J Psychiatry* 1998;155:1711-7.

47. Lieberman JA, Tollefson GD, Charles C, et al. Antipsychotic drug effects on brain morphology in first-episode psychosis. *Arch Gen Psychiatry* 2005;62:361-70.

48. Velakoulis D, Wood SJ, Wong MT, et al. Hippocampal and amygdala volumes according to psychosis stage and diagnosis: a magnetic resonance imaging study of chronic schizophrenia, first-episode psychosis, and ultra-high-risk individuals. *Arch Gen Psychiatry* 2006;63:139-49.

49. Nesvag R, Saetre P, Lawyer G, et al. The relationship between symptom severity and regional cortical and grey matter volumes in schizophrenia. *Prog Neuropsychopharmacol Biol Psychiatry* 2009;33:482-90.

JPN's top 10 Articles, February 2010 (based on Web views on PubMed Central)

1. **How to increase serotonin in the human brain without drugs**
   Young
   J Psychiatry Neurosci 2007;32(6):394–9

2. **Are SAMe and 5-HTP safe and effective treatments for depression?**
   Young
   J Psychiatry Neurosci 2003;28(6):471

3. **L-Tyrosine to alleviate the effects of stress?**
   Young
   J Psychiatry Neurosci 2007;32(3):224

4. **Treatment plans and interventions for depression and anxiety disorders**
   Antony
   J Psychiatry Neurosci 2001;26(5):422

5. **Animal models of schizophrenia: a critical review**
   Marcotte et al.
   J Psychiatry Neurosci 2001;26(5):395–410

6. **Ecological momentary assessment: what it is and why it is a method of the future in clinical psychopharmacology**
   Moskowitz and Young
   J Psychiatry Neurosci 2006;31(1):13–20

7. **Antidepressant effects of exercise: Evidence for an adult-neurogenesis hypothesis?**
   Ernst et al.
   J Psychiatry Neurosci 2006;31(2):84–92

8. **Conversion sensory symptoms associated with parietal lobe infarct: case report, diagnostic issues and brain mechanisms**
   Ramasubbu
   J Psychiatry Neurosci 2002;27(2):118–22

9. **How do the atypical antipsychotics work?**
   Anath et al.
   J Psychiatry Neurosci 2001;26(5):385–94

10. **A review of olanzapine-associated toxicity and fatality in overdose**
    Chue and Singer
    J Psychiatry Neurosci 2003;28(4):253–61

Regional brain changes in antipsychotic-naïve first-episode schizophrenia patients treated with quetiapine: Relation to dose and psychopathology

CINP

Progressive striatal and hippocampal volume loss in initially antipsychotic-naive, first-episode schizophrenia patients treated with quetiapine: relationship to dose and symptoms

**Bjørn H. Ebdrup[1,2,3], Arnold Skimminge[3], Hans Rasmussen[1,2], Bodil Aggernaes[1],
Bob Oranje[1,2], Henrik Lublin[1,2], William Baaré[3,4] and Birte Glenthøj[1,2]**

[1] *Centre for Neuropsychiatric Schizophrenia Research, CNSR, Psychiatric Centre Glostrup, Copenhagen University Hospital, Glostrup, Denmark*
[2] *Centre for Clinical Intervention and Neuropsychiatric Schizophrenia Research, CINS, Psychiatric Center Glostrup, Copenhagen University Hospital, Glostrup, Denmark*
[3] *Danish Research Centre for Magnetic Resonance, DRCMR, MR Department, Copenhagen University Hospital Hvidovre, Hvidovre, Denmark*
[4] *Center for Integrated Molecular Brain Imaging, CIMBI, Copenhagen, Denmark*

Abstract

First-generation antipsychotics have been associated with striatal volume increases. The effects of second-generation antipsychotics (SGAs) on the striatum are unclear. Moreover, SGAs may have neuroprotective effects on the hippocampus. Dose-dependent volumetric effects of individual SGAs have scarcely been investigated. Here we investigated structural brain changes in antipsychotic-naive, first-episode schizophrenia patients after 6 months treatment with the SGA, quetiapine. We have recently reported on baseline volume reductions in the caudate nucleus and hippocampus. Baseline and follow-up T1-weighted images (3 T) from 22 patients and 28 matched healthy controls were analysed using tensor-based morphometry. Non-parametric voxel-wise group comparisons were performed. Small volume correction was employed for striatum, hippocampus and ventricles. Dose-dependent medication effects and associations with psychopathology were assessed. Patients had significant bilateral striatal and hippocampal loss over the 6-month treatment period. When compared to controls the striatal volume loss was most pronounced with low quetiapine doses and less apparent with high doses. *Post-hoc* analyses revealed that the striatal volume loss was most pronounced in the caudate and putamen, but not in accumbens. Conversely, hippocampal volume loss appeared more pronounced with high quetiapine doses than with low doses. Clinically, higher baseline positive symptoms were associated with more striatal and hippocampal loss over time. Although patients' ventricles did not change significantly, ventricular increases correlated with less improvement of negative symptoms. Progressive regional volume loss in quetiapine-treated, first-episode schizophrenia patients may be dose-dependent and clinically relevant. The mechanisms underlying progressive brain changes, specific antipsychotic compounds and clinical symptoms warrant further research.

Received 22 March 2010; Reviewed 15 May 2010; Revised 15 June 2010; Accepted 18 June 2010

Key words: Brain imaging (MRI), hippocampus, psychopathology, schizophrenia, second-generation antipsychotic (SGA), striatum.

Introduction

Magnetic resonance imaging (MRI) studies have shown widespread progressive brain alterations during the

Address for correspondence: Dr B. H. Ebdrup, Center for Neuropsychiatric Schizophrenia Research, CNSR, Center for Clinical Intervention and Neuropsychiatric Schizophrenia Research, CINS, Psychiatric Center Glostrup, University Hospital Glostrup, DK-2600 Glostrup, Denmark.
Tel.: +45 2630 0522   *Fax*: +45 4323 4653
Email: bebdrup@cnsr.dk

course of schizophrenia. These brain changes seem to occur most dramatically in the early stages of the disease; however, it is still unclear to what extend specific regional changes are related to antipsychotic medication and psychopathology (Arango *et al.* 2008; Borgwardt *et al.* 2009; Hulshoff Pol & Kahn, 2008).

A growing body of evidence indicates that first-generation antipsychotic (FGA) compounds may induce striatal hypertrophy possibly linked to the blockade of the dopamine D_2 receptors and the

induction of extrapyramidal side-effects (Lieberman *et al.* 2008; Navari & Dazzan, 2009; Scherk & Falkai, 2006; Smieskova *et al.* 2009; Vita & De Peri, 2007).

Although second-generation antipsychotic (SGA) compounds also target the D_2 receptors, SGAs may not cause volume increases (Chakos *et al.* 1994; Dazzan *et al.* 2005; Smieskova *et al.* 2009) and they may even decrease striatal volumes (Crespo-Facorro *et al.* 2008). Notably, SGAs do not constitute a homogeneous category (Leucht *et al.* 2009) and both preclinical (Andersson *et al.* 2002; Lidow & Goldman-Rakic, 1997; Tarazi *et al.* 2001) and clinical (Crespo-Facorro *et al.* 2008; Markianos *et al.* 2001) studies indicate differential effects depending on the specific SGA administered, emphasizing the importance of investigating individual antipsychotic compounds preferably in antipsychotic-naive patients.

Among SGAs, both clozapine and quetiapine have been shown to reverse volumetric increases caused by FGAs in striatum (Scheepers *et al.* 2001; Stip *et al.* 2008). Interestingly, both compounds are characterized by a low affinity and a loose binding (a fast k_{off}) for dopamine D_2 receptors and a broad receptor profile (Kapur & Seeman, 2001; Kessler *et al.* 2006). However, clozapine is not recommended as a first choice in first-episode schizophrenia patients (Kerwin, 2007). The biochemical mechanisms underlying the antipsychotic effect of quetiapine are not fully understood. Some have argued that the effect may be mediated solely via a transiently high D_2 occupancy (Kapur *et al.* 2000; Tauscher-Wisniewski *et al.* 2002), while others have proposed that a weak D_2 antagonism in combination with a potent 5-HT$_{2A}$ antagonism underlie the effect (Meltzer *et al.* 2003; Meltzer & Huang, 2008). Interestingly, in a positron emission tomography (PET) study employing the 5-HT$_{2A}$ specific radioligand fluorine 18-labelled altanserin in a subset of the present cohort of first-episode schizophrenia patients treated with quatiapine, higher 5-HT$_{2A}$ occupancy was associated with a reduction in positive symptoms. Moreover, the optimal clinical effect associated with 5-HT$_{2A}$ occupancy was obtained with occupancies between 60% and 70%, corresponding to moderate doses of 336–538 mg/d (Rasmussen *et al.* 2010). These observations could suggest that in doses higher than $\sim$538 mg/d (70% 5-HT$_{2A}$ occupancy) the antipsychotic effect of quetiapine may predominantly be mediated through dopaminergic blockade. Until now, longitudinal studies investigating dose-dependent effects of antipsychotic monotherapy on striatal volumes are largely absent (for an exception see Glenthoj *et al.* 2007). Hypothetically, dose-dependent involvement of serotonergic and dopaminergic

systems, respectively, may induce differential striatal alterations.

Investigations of the relationship between progressive striatal brain changes and symptom improvement have yielded inconsistent results. The aforementioned caudate volume reduction associated with clozapine treatment was significantly related to positive and general symptom improvement (Scheepers *et al.* 2001). In contrast, left-sided caudate and putamen volume increases have been associated with positive symptom improvement after 4 wk treatment with either FGAs or SGAs (Taylor *et al.* 2005).

Administration of SGAs early in the course of schizophrenia may protect against progressive global grey-matter (GM) loss and ventricular enlargement which in turn may improve symptoms and the functional outcome (Hulshoff Pol & Kahn, 2008; Lieberman *et al.* 2008). The hippocampus, in particular, is a plastic region which is highly susceptible to neuropsychiatric stress (Geuze *et al.* 2005). Both in chronic as well as in first-episode schizophrenia patients hippocampal volume reductions have been consistently found (Shenton *et al.* 2001; Steen *et al.* 2006; Vita *et al.* 2006). This has prompted the question as to whether antipsychotic compounds, and in particular SGAs, may protect against hippocampal volume loss (Angelucci *et al.* 2000; Bai *et al.* 2003; Halim *et al.* 2004). In preclinical studies quetiapine has been shown to increase brain-derived neurotrophic factor (BDNF) expression (Park *et al.* 2006; Xu *et al.* 2002), to reduce neurodegeneration induced by global cerebral ischaemia (Bi *et al.* 2009; Yan *et al.* 2007), and to reverse stress-induced suppression of neurogenesis (Luo *et al.* 2005) in hippocampus.

The present study encompasses follow-up MRI data on a cohort of antipsychotic-naive, first-episode schizophrenia patients after 6 months treatment with quetiapine. Twenty-two patients and 28 matched healthy control subjects (HC) participated. At baseline the patients ($n=38$) compared to HC ($n=43$) displayed *a-priori* hypothesized volume reductions in the caudate nucleus and the hippocampus, albeit no enlargement of the ventricles (Ebdrup *et al.* 2010). In the current study, we used tensor-based morphometry (TBM) to explore striatal volume changes after $\sim$6 months of treatment. We explicitly tested if high quetiapine doses were associated with relative striatal volume increases compared to low doses. Moreover, we investigated whether quetiapine had a preserving effect on hippocampus and ventricle volumes. Finally, associations between structural changes and psychopathology were explored.

Table 1. Demographics, clinical data and global brain volumes

	Time-point	Lo$_{que}$ ($n=13$)	Hi$_{que}$ ($n=9$)	Pt$_{all}$ ($n=22$)	HC ($n=28$)
Age (yr)	B	26.2 (5.7)	27.8(5.1)	26.2 (5.4)	28.4 (6.0)
Gender (male/female)	–	8/5	7/2	15/7	21/7
Handedness (right/left)	–	13/0	8/1	21/1	26/2
P-SES (high/moderate/low)	–	7/6/0	2/5/2	9/11/2	19/7/27
MR scan interval (months)	–	7.3 (1.1)	7.2 (0.8)	7.3 (1.0)	7.7 (2.3)
Quetiapine (mean dose)	F	352.3 (103.3)	807.2 (178.3)	538.4 (265.7)	–
Benzodiazepines (yes/no)[a]	L	7/6	9/0	16/6	–
	F	0/13	3/6	3/19	–
Antidepressants (yes/no)[b]	L	2/11	3/6	5/17	–
	F	1/12	2/7	3/19	–
Weight (kg)	B	73.9 (21.0)	76.4 (10.3)	74.9 (17.1)	75.8 (9.6)
	F	80.2 (22.3)	86.3 (12.6)	82.7 (18.8)	76.7 (10.9)
Substance abuse (yes/no)[c]	L	1/12	4/5	5/17	–
DUI (wk)[d]	B	266.8 (296.1)	133.6 (174.5)	178 (219.0)	–
PANSS positive score	B	19.2 (3.0)	20.7 (5.3)	19.8 (4.0)	–
	F	14.5 (3.7)	15.2 (4.6)	14.8 (4.0)	–
PANSS negative score	B	21,9 (6.4)	21.1 (7.8)	21.6 (6.8)	–
	F	19.8 (4.9)	18.9 (5.4)	19.4 (5.0)	–
PANSS total score	B	80.5 (13.3)	79.8 (19.6)	80.2 (15.8)	–
	F	70.8 (17.1)	68.4 (20.0)	69.9 (17.8)	–
Intracranial volume (ICV)	B	1509.3 (142.7)	1612.2 (240.0)	1555.4 (190.4)	1576.5 (105.9)
Total brain volume (TBV)	B	1226.1 (128.0)	1296.4 (128.0)	1254.9 (159.5)	1277.4 (100.8)
	F	1228.2 (119.9)	1298.5 (179.3)	1257.0 (147.4)	1268.9 (94.5)
Total grey matter (GM)	B	753.8 (73.3)	779.4 (113.1)	764.3 (90.1)	778.1 (63.1)
	F	755.0 (69.1)	778.5 (101.8)	764.6 (82.6)	771.8 (57.6)
Total white matter (WM)	B	472.2 (60.7)	517.1 (90.3)	490.6 (75.7)	499.3 (43.5)
	F	473.2 (58.2)	520.1 (84.9)	492.3 (72.4)	497.1 (42.8)

Lo$_{que}$, Patients treated with quetiapine <538 mg/d; Hi$_{que}$, patients treated with quetiapine ≥538 mg/d; Pt$_{all}$, all patients; HC, healthy control subjects; B, Baseline; F, Follow-up; L, Lifetime; P-SES, parental socioeconomic status; PANSS, Positive and Negative Syndrome Scale.

Volumes of ICV, TBV, GM, WM and CSF are in cm³ (S.D.).

[a] Number of patients having any prescription of benzodiazepines.

[b] Number of patients in antidepressant treatment. At follow-up the three patients were treated with: selective serotonin re-uptake inhibitors ($n=2$); noradrenergic and specific serotonergic antidepressant ($n=1$).

[c] Number of patients with any lifetime diagnosis of substance abuse. None of the patients abused in the investigation period.

[d] DUI, Duration of untreated illness at baseline.

Method

The study was conducted in accordance with the Declaration of Helsinki II and approved by the Ethics Committee of the Capital Region, Copenhagen (H-KF-01-78/97). After complete description of the study to the subjects, written informed consent was obtained.

Participants

Twenty-two patients and 28 HC participated in the follow-up study. Demographic and clinical characteristics are given in Table 1. All participants were re-examined with MRI and psychopathology was re-assessed with the Positive and Negative Syndrome Scale (PANSS; Kay *et al.* 1987) by trained raters (intra-class correlation=0.92). After the baseline examinations, the patients were treated with quetiapine according to their clinical need (mean=538; S.D.=265 mg/d) in an intended treatment period of 6 months (mean=7.3, S.D.=1.0 months).

Baseline data on 38 patients and 43 age-, gender- and parental socioeconomic status- (P-SES) matched HC has been reported elsewhere (Ebdrup *et al.* 2010). Briefly, patients were recruited from the Capital Region of Copenhagen, Denmark. Inclusion criteria were: a diagnosis of schizophrenia, no prior exposure to antipsychotic medication, age between 18–45 yr, and no medical or neurological comorbidity. DSM-IV

4   *B. H. Ebdrup et al.*

diagnoses were based on the Schedules for Clinical Assessment in Neuropsychiatry (SCAN) version 2.1 (Wing *et al.* 1990). Diagnoses were confirmed by regular clinical contacts during the treatment period. Benzodiazepines were allowed to reduce agitation and anxiety. Use of antidepressants was registered. None of the patients received anti-cholinergic medication. Duration of untreated illness (DUI) was defined as the time between the first unspecific symptoms related to psychosis and the date of the MRI scan. Symptoms had to be associated with a decline in a previous stable level of functioning. DUI data were collected as a best-estimate approach (Keshavan *et al.* 1998) with information from the SCAN interview, clinical records and relatives when possible. Of the 38 patients included at baseline, nine fulfilled lifetime DSM-IV criteria for substance abuse. At follow-up, 5/22 patients had a lifetime history of substance abuse, but none abused in the treatment period. Further, at follow-up all subjects had a negative urine screening for substance intake. Extrapyramidal side-effects (EPS) were evaluated with The Extrapyramidal Symptom Rating Scale (ESRS; Chouinard & Margolese, 2005).

HC were recruited from the community. Both patients and HC had normal physical and neurological examinations and MRI scans were without pathology.

Medication

As described in the Introduction, PET data from our group have indicated that the antipsychotic effect of quetiapine is associated with up to 70% 5-HT$_{2A}$ occupancy corresponding to ~538 mg/d (Rasmussen *et al.* 2010). We hypothesized that higher quetiapine doses act primarily through D$_2$ blockade. The mean quetiapine dose in this study was 538 mg/d and was suitable for testing if high doses would be associated with relative striatal volume increases compared to low doses. Accordingly, to test for medication effects the patients were *a-priori* split into a high quetiapine (Hi$_{que}$) ($\geq$538 mg) (n=9) and a low quetiapine (Lo$_{que}$) (<538 mg) (n=13) group. Cumulative quetiapine intake was also calculated (mean=111.8 g, S.D.=62.5), but since this correlated strongly with the mean dose (ρ=0.97) only data on the mean dose are presented here.

Image acquisition and processing

Details of the MRI acquisition protocol and processing of the images have been presented elsewhere (Ebdrup *et al.* 2010). Briefly, high-resolution 3D T1-weighted, sagittal, magnetization-prepared rapid gradient echo (MPRAGE) scans and 2D T2-weighted, axial, turbo-spin echo scans were acquired of the whole head at two time-points on a Siemens Magnetom Trio 3 T MR scanner (Siemens, Germany) with an eight-channel head coil. Images were gradient un-warped (Jovicich *et al.* 2006) and processed using the VBM5 toolbox (http://dbm.neuro.uni-jena.de/vbm/vbm5-forspm5/) in SPM5 (Wellcome Department of Cognitive Neurology, University College London, UK). T2-weighted images were used to create brain masks in native space. Brain-masked GM and white-matter (WM) tissue maps were used for high-dimensional inter-subject registration by means of DARTEL ('diffeomorphic anatomical registration through exponentiated lie algebra'; Ashburner, 2007). The brain-masked GM, WM, and CSF images were warped into average image space (DARTEL space) and modulated with the Jacobian determinant (JD) of the applied deformation fields to correct for local volume changes following the inter-subject warping.

To determine volumetric changes from baseline to follow-up, follow-up bias-corrected and intensity-normalized T1 images in average image space were warped to their baseline counterparts using high-dimensional intra-subject warping (Ashburner *et al.* 2000). To evaluate volume changes over time the resulting intra-subject JD image was transformed with the natural logarithm and warped into DARTEL space. The volume of each tissue class at follow-up was calculated by the following formula:

$$\text{GM}_{\text{DARTEL}} * (1 - \exp[\log(\text{JD}_{\text{intra-subject}}, \text{DARTEL})]).$$

The volume change from baseline to follow-up was calculated by subtraction of baseline and follow-up images.

Regions of interest (ROIs)

ROI masks were created using the average of DARTEL-warped MPRAGE images of all subjects to test our specific hypotheses (Ebdrup *et al.* 2010). Used delineation landmarks are referenced: striatum (comprised of masks of caudate nucleus, nucleus accumbens, putamen) (Glenthoj *et al.* 2007), hippocampus (Baare *et al.* 2001), ventricles (comprised of lateral and third ventricle) (Cahn *et al.* 2002).

Volumetric brain measures

Total brain volume (TBV) and intracranial volume (ICV) were estimated by integrating and adding image-intensity values of modulated and warped GM and WM (TBV), and CSF (ICV) images. ROI volumes were acquired to investigate whether local voxel-wise

changes were reflected in whole ROI volume changes. ROI volume estimates were derived by integrating image intensity values of modulated and warped images within the specific ROI (for details see Ebdrup *et al.* 2010). Global and regional volume estimates are given in Tables 1 and 3, respectively.

Statistical analyses

Statistical Package for the Social Sciences software (SPSS Inc., USA) was used to analyse demographic and volumetric data. The distribution of continuous data was tested for normality with the Shapiro–Wilk test. Age and volumetric changes in ROIs (caudate nucleus, nucleus accumbens, putamen, hippocampus, ventricles) were not normally distributed, thus group comparisons were performed non-parametrically with the Mann–Whitney U test. Handedness and gender differences were tested with Fisher's exact test and socioeconomic status with Pearson's χ^2 test. Potential outliers were identified with Grubbs' outlier test (Grubbs, 1969). Differences in PANSS scores between patient groups were tested with the Student's t test.

In the voxel-wise analyses we tested how groups differed on volumetric changes over time (baseline – follow-up) and in volumes at follow-up. We first tested for differences between all patients (Pt_{all}) and HC. Subsequently, we tested for medication effects using the following contrasts: Hi_{que} *vs.* HC, Lo_{que} *vs.* HC and Hi_{que} *vs.* Lo_{que}. TBV change served as a co-variate. Since patients and HC did not differ regarding age, gender and MR-scan interval analyses were initially performed without these covariates. *Post-hoc*, these variables were entered as covariates to assess their possible effects. When contrasting Hi_{que} *vs.* Lo_{que} groups, both TBV change and percentage weight change were entered as covariates, because patients significantly gained weight compared to HC. General linear models were estimated non-parametrically using randomize, part of FSL (http://www.fmrib.ox.ac.uk/fsl/randomise/index.html), using 10 000 per-mutations. Small volume correction, applying ROI masks, was used to test *a priori* hypotheses. A false discovery rate threshold of 0.05 was used to correct for multiple comparisons.

The contrasts tested in volumetric analyses were identical to those tested in the voxel-wise analyses. Effects of TBV changes were regressed out. When contrasting Hi_{que} *vs.* Lo_{que} groups, the ROI volumes were corrected for both TBV change and percentage weight change. Age, gender and MR-scan interval were entered as covariates *post-hoc*. Moreover, TBV and weight-corrected volumetric changes and the corresponding follow-up ROI volumes were used to test for linear effects (using Spearman's rank correlation coefficient) of medication and change in psychopathology. Change in psychopathology (baseline – follow-up) was calculated separately for positive, negative and total PANSS scores. Regional percentage volume change was calculated as ROI volume change divided by total brain change.

To control for any lifetime substance abuse diagnosis ($n = 5$), all analyses were also performed excluding these patients. All tests were two-tailed, and the significance level was set to $p < 0.05$.

Results

Attrition

Sixteen patients were not included at follow-up. Reasons for attrition were: clinically inadequate effect ($n = 2$), intolerable side-effects (sedation, weight gain, rise in liver enzymes) ($n = 4$), pregnancy ($n = 2$) or re-fusal to participate at follow-up ($n = 5$). Three patients had stated that after the baseline examinations they were not willing to undergo treatment with quetia-pine. The 16 excluded patients had significantly smaller baseline ventricles ($Z = -2.10$, $p = 0.044$) com-pared to the patients who participated at follow-up. However, there were no baseline differences in demographic measures (p values > 0.38), PANSS scores (p values > 0.23), or in other volumetric brain measures (p values > 0.36).

Baseline

At baseline Hi_{que} patients had significantly higher lifetime exposure to benzodiazepines than Lo_{que} patients (Fisher's exact test, $p = 0.046$). There were no other significant differences on baseline demographic, clinical and volumetric measures between the patient subgroups (Tables 1 and 3).

Follow-up

Demographics

The interval between baseline and follow-up MR scans did not differ between any of the patient groups and HC ($Z = -0.51$ $p = 0.61$). Patients gained significantly more weight than did HC ($Z = -3.43$ $p = 0.001$). The mean weight gain in patients was 7.8 kg (s.d. = 8.4), corresponding to 11.1% (s.d. = 12.4). There was no as-sociation between quetiapine dosage and percentage weight gain ($\rho = 0.26$, $p = 0.24$). Hi_{que} patients tended to use more benzodiazepines than Lo_{que} patients (Fisher's exact test, $p = 0.055$). None of the patients

6   *B. H. Ebdrup et al.*

Table 2. Results of the voxel-wise analyses

Region	Subregion	Contrast	Side	Z score	p value	MNI coordinates (x, y, z)	Cluster size
Striatum	Cau	$Pt_{all} \times HC$	Left	3.66	0.003	−15, 8, 22	2680
	Cau		Right	3.01	0.004	19, 18, 15	2590
	Put		Left	3.35	0.003	−30, −8, 10	2110
	Put		Right	3.56	0.003	24, 1, 12	2180
	–	$Hi_{que} \times HC$	–	–	n.s.	–	–
	Cau	$Lo_{que} \times HC$	Left	3.51	0.004	−16, 18, 11	5530
	Cau		Right	3.36	0.004	18, 14, 13	3020
	Put		Left	3.20	0.003	−26, −7, 9	2230
	Put		Right	3.67	0.004	26, 2, 10	2610
	–	$Lo_{que} \times Hi_{que}$	–	–	n.s.	–	–
Hippocampus	–	$Pt_{all} \times HC$	Left	3.04	0.006	−22, −34, −4	3140
	–		Right	3.09	0.006	15, −38, −1	2070
	–		Right	2.44	0.02	14, −10, −17	75
	–	$Hi_{que} \times HC$	Left	3.39	0.00	−33, −31, −10	2970
	–		Right	3.73	0.007	23, −33, −5	1500
	–		Right	2.18	0.03	15, −12, −17	47
	–	$Lo_{que} \times HC$	–	–	n.s.	–	–
	–	$Hi_{que} \times Lo_{que}$	–	–	n.s.	–	–
Ventricles	–	$Pt_{all} \times HC$	–	–	n.s.	–	–
	–	$Hi_{que} \times HC$	–	–	n.s.	–	–
	–	$Lo_{que} \times HC$	–	–	n.s.	–	–
	–	$Lo_{que} \times Hi_{que}$	–	–	n.s.	–	–

Results of small volume correction with the study-specific masks applied to the different contrasts.

Lo_{que}, Patients treated with quetiapine <538 mg/d; Hi_{que}, patients treated with quetiapine ≥538 mg/d; Pt_{all}, all patients; HC, healthy control subjects; Cau, caudate nucleus; Put, putamen; MNI, Montreal Neurological Institute coordinates (cluster sizes are in mm³).

The displayed contrasts test for volume loss between the groups; however, in the ventricles, enlargement is tested. The opposite contrasts were also tested, but all were non-significant (data not shown). Contrasts were performed with total brain volume (TBV) change as a covariate. However, the contrast $Hi_{que} \times Lo_{que}$ was performed with both TBV change and percentage weight change as covariates. All significant contrasts are displayed ($p < 0.05$). Non-significant contrasts are assigned n.s.

Entering age, gender and MR scan interval as covariates did not change the results. Exclusion of the five subjects with a lifetime substance abuse diagnosis did not alter the results.

p values are false discovery rate-corrected ($p < 0.05$).

developed EPS. Follow-up PANSS scores were missing for one patient.

Global brain volumes

No significant global brain tissue volume (TBV, GM, WM) changes were observed between $Pt_{all} \times HC$, $Hi_{que} \times Lo_{que}$, $Hi_{que} \times HC$, and $Lo_{que} \times HC$ (p values >0.15).

Striatum

The voxel-wise analyses revealed significant bilateral volume loss in Pt_{all} compared to HC in the caudate nucleus and putamen (Table 2). The volumetric analyses paralleled the voxel-wise results. The striatal volume was significantly reduced over time in Pt_{all}

compared to HC ($Z = -2.21$, $p = 0.027$). In *post-hoc* analyses of striatal subregions separately Pt_{all} compared to HC had significant caudate ($Z = -2.62$, $p = 0.009$), putamen ($Z = -1.99$, $p = 0.046$), but not accumbens ($Z = -1.72$, $p = 0.17$) volume loss over time.

At follow-up Pt_{all} had significantly smaller striatal volumes than did HC ($Z = -2.15$, $p = 0.032$). *Post-hoc* analyses of the striatal structures separately, revealed smaller caudate ($Z = -2.76$, $p = 0.006$) and accumbens ($Z = -2.52$, $p = 0.012$), but not putamen follow-up volumes ($Z = 1.04$, $p = 0.30$).

Striatum, dose-dependent medication effect

In the voxel-wise analyses bilateral striatal volume loss was significant in Lo_{que}, but not in Hi_{que} patients,

compared to HC. Direct comparison between Hi_{que} and Lo_{que} patients was not significant (Table 2).

The volumetric analyses paralleled the voxel-wise results (Table 3). Lo_{que} patients had significant striatal volume loss over time as compared to HC ($Z = -2.22$, $p = 0.027$). Hi_{que} and HC did not differ in total striatal volume change ($p = 0.23$). Comparison between Hi_{que} and Lo_{que} patients was not significant ($Z = -0.50$, $p = 0.62$). In *post-hoc* analyses the volume loss in Lo_{que} patients was accounted for by significant volume loss in caudate ($Z = -2.55$, $p = 0.010$) and putamen ($Z = -1.99$, $p = 0.047$), but not in accumbens ($Z = -1.37$, $p = 0.17$).

At follow-up Lo_{que} ($Z = -2.10$, $p = 0.036$), but not Hi_{que} ($Z = -1.24$, $p = 0.22$) patients had significantly smaller striatal volumes compared to HC. In direct comparison the patient groups did not differ significantly ($Z = -1.30$, $p = 0.19$). In *post-hoc* analyses the follow-up volume reduction in the Lo_{que} group appeared in the caudate ($Z = -2.35$, $p = 0.019$) and in the accumbens ($Z = -2.47$, $p = 0.014$), but not in the putamen ($Z = -1.18$, $p = 0.24$).

The percentage striatal volume loss (corrected for total brain change) in the different groups were: $Pt_{all} = 0.8\%$, $Lo_{que} = 1.0\%$, $Hi_{que} = 0.5\%$, HC $= -0.6\%$ (Fig. 1).

In Pt_{all} no significant linear correlations were observed between quetiapine dose and striatal volume loss or follow-up volume, respectively (p values > 0.46).

Ventricles

Neither the voxel-wise (Table 2) nor the volumetric analyses revealed ventricle differences between any of the groups (p values > 0.27). Exploratory analyses testing for group differences for third and lateral ventricle volumes separately were not significant. In Pt_{all} no linear correlation between mean quetiapine dose and ventricle volumes were observed (p values > 0.19).

Hippocampus

Significant bilateral hippocampal volume loss in Pt_{all} compared to HC was revealed both by the voxel-wise analyses (Table 2) and the volumetric analyses ($Z = -3.23$, $p = 0.002$) (Table 3). At follow-up Pt_{all} had significantly smaller hippocampal volumes than HC ($Z = -2.13$, $p = 0.033$).

Hippocampus, dose-dependent medication effect

In the voxel-wise analyses bilateral hippocampal volume loss was significant in Hi_{que}, but not in Lo_{que}
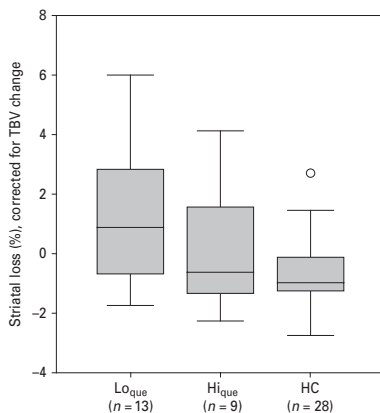
Fig. 1. Boxplot of percentage striatal volume loss in the three subject groups. Volumes are corrected for total brain volume (TBV) change. Positive values indicate more volume loss over time. In the box-and-whisker plot, the central box represents the values from the lower to upper quartile. The transverse line in the box represents the median corrected volume. The vertical line extends from the minimum to the maximum value, excluding outside values. Outside values are defined as values smaller or larger than the lower quartile minus 1.5 times the interquartile range and are displayed as separate points (○). No outliers were identified. See text for the results of the statistical comparisons.

patients compared to HC. Direct comparison between Hi_{que} and Lo_{que} patients was not significant (Table 2).

The volumetric analyses paralleled the voxel-wise results by showing significant hippocampal volume loss in Hi_{que} ($Z = -3.22$, $p = 0.001$), and trend-level volume loss in Lo_{que} ($Z = -1.93$, $p = 0.053$) patients compared to HC. There was no difference between the two patient groups ($Z = -1.37$, $p = 0.17$).

At follow-up Hi_{que} ($Z = -2.90$, $p = 0.004$), but not Lo_{que} ($Z = -0.76$, $p = 0.45$) patients had smaller hippocampal volumes compared to HC; however, this difference was not significant ($Z = -97$, $p = 0.33$) between the patient groups.

The percentage hippocampal volume loss (corrected for total brain change) in the different groups were: $Pt_{all} = 0.6\%$, $Lo_{que} = 0.3\%$, $Hi_{que} = 1.0\%$, HC $= -0.4\%$ (Fig. 2).

In Pt_{all} no linear correlations were observed between quetapine dose and hippocampal volume loss or follow-up volume, respectively (p values > 0.21).

Table 3. Volume estimates for regions of interest (mm³)

Region	Time-point	Lo_{que} ($n = 13$)	Hi_{que} ($n = 9$)	Pt_{all} ($n = 22$)	HC ($n = 28$)
Striatum	B	16203.8 (1859.6)	17055.0 (2225.4)	16552.0 (2011.5)	17155.1 (1240.3)
	F	15868.7 (1992.5)	16801.9 (2328.1)	16250.6 (2134.0)	17117.6 (1318.5)
Caudate nucleus	B	7170.5 (814.8)	7465.8 (1065.2)	7291.3 (913.1)	7691.1 (687.5)
	F	6998.7 (864.3)	7335.9 (1099.8)	7136.6 (957.3)	7688.6 (715.0)
Nucleus accumbens	B	687.9 (79.5)	739.5 (119.7)	709.0 (98.7)	760.0 (74.4)
	F	679.8 (82.3)	734.1 (125.0)	702.0 (102.8)	760.0 (78.7)
Putamen	B	8345.5 (1019.5)	8849.6 (1136.1)	8551.7 (1072.4)	8703.9 (695.7)
	F	8190.2 (1086.1)	8731.9 (1189.1)	8411.8 (1134.7)	8671.0 (724.7)
Hippocampus	B	8845.7 (878.6)	8810.1 (789.1)	8831.1 (823.8)	9077.2 (666.3)
	F	8758.6 (914.1)	8665.2 (859.7)	8720.4 (872.5)	9071.9 (677.1)
Ventricles	B	15584.7 (5629.3)	18773.3 (7821.3)	16889.1 (6882.9)	15350.7 (6034.3)
	F	15606.2 (5696.9)	18353.2 (7821.3)	16730.0 (6615.1)	15305.0 (6034.3)

Lo_{que}, Patients treated with quetiapine < 538 mg/d; Hi_{que}, patients treated with quetiapine ≥ 538 mg/d; Pt_{all}, all patients; HC, healthy control subjects; B, baseline; F, follow-up.
Values are mean (S.D.).

Whole brain

Exploratory voxel-wise whole-brain analyses did not reveal additional regional GM, WM or CSF volume loss between groups.

Psychopathology

From baseline to follow-up patients improved significantly on positive ($t_{20} = 5.74$, $p < 0.001$) and total symptoms ($t_{20} = 2.88$, $p = 0.009$), but not on negative symptoms ($t_{20} = 1.56$, $p = 0.14$). There were no significant correlations between mean quetiapine doses and baseline, follow-up or changes in PANSS positive, negative and total scores (p values > 0.15).

A positive correlation between baseline positive symptoms and striatal volume loss over time ($\rho = 0.44$, $p = 0.042$) was found (Fig. 3a). *Post-hoc* analyses revealed positive correlations with volume loss in all three striatal structures separately (caudate: $\rho = 0.51$, $p = 0.016$; accumbens: $\rho = 0.52$, $p = 0.013$; putamen: $\rho = 0.43$, $p = 0.047$). Further, we found a positive correlation between baseline positive symptoms and hippocampal volume loss over time ($\rho = 0.51$, $p = 0.016$) (Fig. 3b). Finally, ventricle increase over time was associated with less improvement in negative symptoms ($\rho = -0.46$, $p = 0.038$) (Fig. 4). The correlations did not survive a correction for multiple comparisons. No other linear correlations between volumetric changes or follow-up volumes, and positive, negative or total symptoms were observed.

Adding age, gender and MR interval as covariates did not change the above results significantly. Similarly, exclusion of the five subjects with lifetime
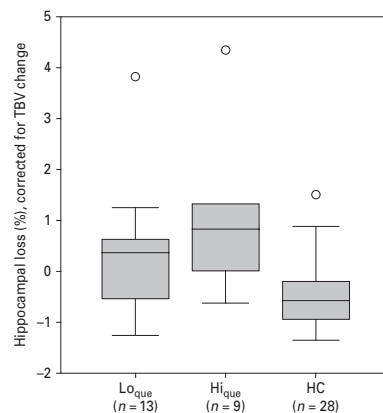
Fig. 2. Boxplot of percentage hippocampal volume loss in the three subject groups. Volumes are corrected total brain volume (TBV) change. Grubbs' test detected one outlier in the high quetiapine group. Exclusion of this outlier did not change the results significantly. See text for the results of the statistical comparisons. (Information about interpretation of the boxplot is provided in Fig. 1.)

substance abuse diagnosis did not significantly alter the results.

Discussion

In this longitudinal TBM study we investigated medication and psychopathological effects on brain
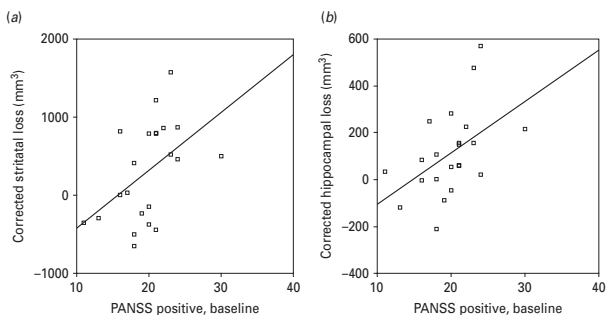
Fig. 3. Positive symptoms and striatal and hippocampal loss. Positive correlations between baseline Positive and Negative Syndrome Scale (PANSS) positive symptoms and (*a*) striatal ($\rho = 0.44$, $p = 0.042$), and (*b*) hippocampal ($\rho = 0.51$, $p = 0.016$) volume loss (in mm³) over time. Volumes were corrected for changes in total brain volume (TBV) and percentage weight change. The correlations did not survive a correction for multiple comparisons. Note, that grey-matter loss is indicated with higher values on the y-axis. See text for details.

structure in 22 initially antipsychotic-naive, first-episode schizophrenia patients after treatment with quetiapine for approximately 6 months. The main finding was that patients had significant bilateral striatal and hippocampal volume loss during the treatment period. The striatal volume loss was most pronounced in patients treated with low quetiapine doses whereas the volume loss was less apparent in patients treated with high doses. Conversely, hippocampal volume loss appeared more pronounced in patients treated with high quetiapine doses than in patients treated with low doses. However, the dose-dependent differences were only apparent in patient subgroups when compared to HC. Clinically, higher baseline positive symptoms were associated with more striatal and hippocampal volume loss over time. Although patients' ventricles did not change significantly over time, ventricular increases were associated with less improvement on negative symptoms. No significant changes in global brain measures (TBV, GM, WM) were observed.

Quetiapine treatment has previously been associated with striatal volume loss in already medicated patients (Stip *et al.* 2008). However, in the present study patients were initially antipsychotic-naive and therefore quetiapine in itself may be associated with striatal volume reduction. One previous study in antipsychotic-naive patients reported no significant caudate volume reduction in 10 patients following 12 wk of quetiapine treatment (mean dose 494 mg/d) (Tauscher-Wisniewski *et al.* 2005). Nevertheless, they observed that the absolute caudate volume decreased
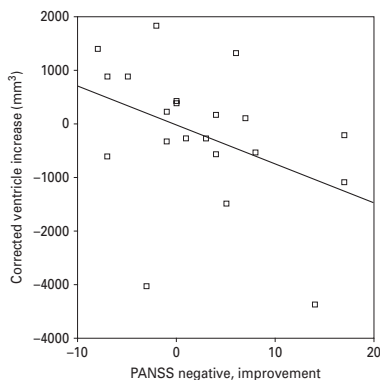
Fig. 4. Negative symptoms and ventricular volume increase. A negative correlation between improvement in negative symptoms [Positive and Negative Syndrome Scale (PANSS) negative baseline – follow-up] and ventricle increase (in mm³) over time ($\rho = -0.46$, $p = 0.038$). Volumes were corrected for changes in TBV and percentage weight change. The correlation did not survive a correction for multiple comparisons. Note that symptom improvement is indicated with higher values on the x-axis and that ventricular increase is indicated with higher values on the y-axis. See text for details.

over time. Their failure to observe significant effects might be related to the small subject sample and the relative short treatment period.

10   *B. H. Ebdrup et al.*

Our data suggest that high quetiapine doses may attenuate the striatal volume loss. Dose-dependent volumetric effects of quetiapine have not previously been described. Interestingly, clinical studies with risperidone have associated striatal volume increases with high doses of risperidone (6.05 mg/d) (Massana *et al.* 2005), whereas moderate (3.64 mg/d) (Glenthoj *et al.* 2007) and low (2.7 mg/d) (Lang *et al.* 2001) risperidone doses caused marginal increases or no striatal volume changes, respectively. According to a hypothesis put forward by Kapur & Seeman (2001), a transiently high striatal D_2 blockade may drive the antipsychotic effect in SGAs. We infer that our observation of relative striatal volume increases with high quetiapine doses could reflect this transiently high D_2 occupancy. Conversely, in low doses the clinical effect may be more related to $5-HT_{2A}$ occupancy as suggested by our previous PET data (Rasmussen *et al.* 2010). From the present study it is not possible to determine whether the observed striatal volume reduction is a consequence of the disease progress *per se* or of the $5-HT_{2A}$ blockade. However, post-mortem studies have indicated that $5-HT_{2A}$ receptor density in striatum is low (Dwivedi & Pandey, 1998) and that the striatal volume and neuron number decrease over the course of the illness regardless of chronic treatment with FGAs (Kreczmanski *et al.* 2007).

Since we did not asses D_2 blockade, inferences from the present data must be made cautiously. Nevertheless, the absence of linear correlations between quetiapine dose and striatal and hippocampal changes, respectively, supports the hypothesis of a threshold of $5-HT_{2A}$- and D_2-mediated clinical effects. Although quetiapine doses of 400–450 mg have resulted in dopamine D_2 occupancies of $\sim 60\%$ 2 h post-dose (Kapur *et al.* 2000; Tauscher-Wisniewski *et al.* 2002) also lower occupancies of 44% and 30% 2 h post-450 mg quetiapine have been reported (Gefvert *et al.* 1998, 2001). Indisputably, a dose of 538 mg/d as applied in our study may not address the 'true' threshold. Larger sample sizes, preferably including PET data are required to confirm this possible dose-dependent effect of quetiapine and to identify a more precise threshold. Finally, the mechanisms behind striatal volume increase after sustained blockade of the D_2 receptors are still elusive, but up-regulation of the D_2 receptors (Burt *et al.* 1977; Seeman, 1987), axonal sprouting (Benes *et al.* 1983) and increased striatal blood flow (Corson *et al.* 2002; Miller *et al.* 1997) have been suggested.

Contrary to findings in preclinical studies, quetiapine did not seem to protect against hippocampal volume loss (Bi *et al.* 2009; Park *et al.* 2006). No linear correlation between mean dose and volume loss was observed and the hippocampal volume loss appeared most pronounced in the high-dose group compared to HC. Interestingly, this inverted dose-dependent association is supported by a preclinical study on rat hippocampi in which low doses of clozapine (0.5 mg/kg) increased markers of DNA synthesis in hippocampus whereas high doses (20 mg/kg) had no effect (Halim *et al.* 2004).

Accumulating evidence suggests that ventricular enlargement occurs during the early course of schizophrenia (Steen *et al.* 2006; Van Haren *et al.* 2008; Vita *et al.* 2006). Although antipsychotic treatment may exert a preserving effect on ventricular volume (Lieberman *et al.* 2001), a recent review has suggested that antipsychotic treatment may on the contrary be associated with ventricular enlargement (Moncrieff & Leo, 2010). Similarly, the long-term effects of antipsychotic compounds on global brain volume are unclear (Moncrieff & Leo, 2010). The present results suggest that quetiapine may protect against ventricular enlargement and global brain loss in the early course of illness.

Treatment with quetiapine improved PANSS positive and total scores although negative symptoms did not improve significantly. The absence of correlations between mean quetiapine dose and any of the PANSS measures, allowed for independent investigations of mediation effects and psychopathology. On the other hand, this absence of an association between medication dose and psychopathology renders it controversial whether regional GM changes induced by antipsychotics are clinically beneficial (Navari & Dazzan, 2009; Smieskova *et al.* 2009). The clinical complexity of schizophrenia combined with the pharmacological complexity of quetiapine may partly explain why a dose–response relationship is not well-established (Kinon *et al.* 2004) and an optimal therapeutic range for quatiapine remains to be identified (Mauri *et al.* 2007).

MRI studies have previously associated striatal volume reductions with positive symptoms (Crespo-Facorro *et al.* 2007; Scheepers *et al.* 2001); however, the present study is the first to show that the severity of positive symptoms in the antipsychotic-naive state may predict progressive striatal volume loss. Interestingly, in subjects at high risk for developing psychosis, progressive hippocampal volume reductions have been associated with later transition to schizophrenia, although also reduced activation in prefrontal cortex, reduced neuronal density, and increased membrane turnover in frontal and cingulate cortex seem implicated in transition (Smieskova *et al.*

2010; Wood *et al.* 2008). Our finding of a positive correlation between baseline positive symptoms and progressive hippocampal loss could therefore suggest that the hippocampus is particularly sensitive to positive symptoms around and right after transition to psychosis. We speculate that this hippocampal sensitivity might reflect a higher level of stress accompanying a psychotic state possibly related to disturbances in the hypothalamic–pituitary–adrenal (HPA) axis (Phillips *et al.* 2006). Although we did not find ventricular enlargement over time a significant correlation between ventricular increase and less negative symptom improvement was observed. As such our data are consistent with the growing body of evidence which has associated negative symptoms and poor prognosis with ventricular enlargement (Hulshoff Pol & Kahn, 2008).

The present study is limited by several factors. First, the attrition was considerable during the 6-month period (42%). Notably, only 6/16 dropouts were directly related to quetiapine. Only ventricular volumes were significantly different (smaller) and no other demographic, clinical or structural differences between the dropouts and re-scanned patients were found. This suggests that our results were not biased by baseline differences. In our analyses of dose-dependent effects the patient subgroups are small and the observed differences appear in comparison with HC, whereas direct comparisons between the subgroups are non-significant. Nevertheless, the direction of the dose-dependent effect on striatum was *a-priori* hypothesized, rather than a result of a *post-hoc* comparison. Hence our failure to detect significant changes in direct comparison between the patient subgroups could be attributable to lack of power (a type II error). Moreover, a potential inaccuracy in our threshold of 538 mg/d would also reduce the differences between the patient groups. Ideally, a study of dose-dependent medication effects should apply a double-blind, randomized design; however, for ethical reasons this was not performed. The absence of correlations between our obtained clinical measures and medication dose indicate that the patient subgroups were not biased by illness severity. Finally, it should be emphasized that although clinically meaningful, our findings regarding structural changes and psychopathology appeared among several correlations and they would not survive a correction for multiple comparisons.

In conclusion we found that 6 months' treatment with quetiapine in antipsychotic-naive, first-episode schizophrenia patients was associated with progressive bilateral volume loss in striatum and hippocampus. The progressive volumetric loss may be dose-dependent and clinically relevant. The mechanisms underlying associations between progressive brain changes and specific antipsychotic compounds and clinical symptoms warrant further clarification.

Acknowledgements

Statement of Interest

None.

References

Andersson C, Hamer RM, Lawler CP, Mailman RB, *et al.* (2002). Striatal volume changes in the rat following long-term administration of typical and atypical antipsychotic drugs. *Neuropsychopharmacology* **27**, 143–151.

Angelucci F, Mathe AA, Aloe L (2000). Brain-derived neurotrophic factor and tyrosine kinase receptor TrkB in rat brain are significantly altered after haloperidol and risperidone administration. *Journal of Neuroscience Research* **60**, 783–794.

Arango C, Moreno C, Martinez S, Parellada M, *et al.* (2008). Longitudinal brain changes in early-onset psychosis. *Schizophrenia Bulletin* **34**, 341–353.

Ashburner J (2007). A fast diffeomorphic image registration algorithm. *Neuroimage* **38**, 95–113.

Ashburner J, Andersson JL, Friston KJ (2000). Image registration using a symmetric prior – in three dimensions. *Human Brain Mapping* **9**, 212–225.

Baare WF, van Oel CJ, Hulshoff Pol HE, Schnack HG, *et al.* (2001). Volumes of brain structures in twins discordant for schizophrenia. *Archives of General Psychiatry* **58**, 33–40.

Bai O, Chlan-Fourney J, Bowen R, Keegan D, *et al.* (2003). Expression of brain-derived neurotrophic factor mRNA in rat hippocampus after treatment with antipsychotic drugs. *Journal of Neuroscience Research* **71**, 127–131.

Benes FM, Paskevich PA, Domesick VB (1983). Haloperidol-induced plasticity of axon terminals in rat substantia nigra. *Science* **221**, 969–971.

Bi X, Yan B, Fang S, Yang Y, *et al.* (2009). Quetiapine regulates neurogenesis in ischemic mice by inhibiting NF-kappaB p65/p50 expression. *Neurological Research* **31**, 159–166.

Borgwardt SJ, Dickey C, Hulshoff PH, Whitford TJ, *et al.* (2009). Workshop on defining the significance of progressive brain change in schizophrenia: 12 December 2008, American College of Neuropsychopharmacology (ACNP) all-day satellite, Scottsdale, Arizona. The Rapporteurs' report. *Schizophrenia Research* **112**, 32–45.

Burt DR, Creese I, Snyder SH (1977). Antischizophrenic drugs: chronic treatment elevates dopamine receptor binding in brain. *Science* **196**, 326–328.

Cahn W, Hulshoff Pol HE, Bongers M, Schnack HG, *et al.* (2002). Brain morphology in antipsychotic-naive schizophrenia: a study of multiple brain structures. *British Journal of Psychiatry* (Suppl.) **43**, 66–72.

Chakos MH, Lieberman JA, Bilder RM, Borenstein M, *et al.* (1994). Increase in caudate nuclei volumes of first-episode schizophrenic patients taking antipsychotic drugs. *American Journal of Psychiatry* **151**, 1430–1436.

Chouinard G, Margolese HC (2005). Manual for the Extrapyramidal Symptom Rating Scale (ESRS). *Schizophrenia Research* **76**, 247–265.

Corson PW, O'Leary DS, Miller DD, Andreasen NC (2002). The effects of neuroleptic medications on basal ganglia blood flow in schizophreniform disorders: a comparison between the neuroleptic-naive and medicated states. *Biological Psychiatry* **52**, 855–862.

Crespo-Facorro B, Roiz-Santianez R, Pelayo-Teran JM, Gonzalez-Blanch C, *et al.* (2007). Caudate nucleus volume and its clinical and cognitive correlations in first episode schizophrenia. *Schizophrenia Research* **91**, 87–96.

Crespo-Facorro B, Roiz-Santianez R, Perez-Iglesias R, Pelayo-Teran JM, *et al.* (2008). Effect of antipsychotic drugs on brain morphometry. A randomized controlled one-year follow-up study of haloperidol, risperidone and olanzapine. *Progress in Neuropsychopharmacology and Biological Psychiatry* **32**, 1936–1943.

Dazzan P, Morgan KD, Orr K, Hutchinson G, *et al.* (2005). Different effects of typical and atypical antipsychotics on grey matter in first episode psychosis: the AESOP study. *Neuropsychopharmacology* **30**, 765–774.

Dwivedi Y, Pandey GN (1998). Quantitation of 5HT2A receptor mRNA in human postmortem brain using competitive RT-PCR. *Neuroreport* **9**, 3761–3765.

Ebdrup BH, Glenthoj B, Rasmussen H, Aggernaes B, *et al.* (2010). Hippocampal and caudate volume reductions in antipsychotic-naive first-episode schizophrenia. *Journal of Psychiatry and Neuroscience* **35**, 95–104.

Gefvert O, Bergstrom M, Langstrom B, Lundberg T, *et al.* (1998). Time course of central nervous dopamine-D2 and 5-HT2 receptor blockade and plasma drug concentrations after discontinuation of quetiapine (Seroquel) in patients with schizophrenia. *Psychopharmacology* (*Berlin*) **135**, 119–126.

Gefvert O, Lundberg T, Wieselgren IM, Bergstrom M, *et al.* (2001). D(2) and 5HT(2A) receptor occupancy of different doses of quetiapine in schizophrenia: a PET study. *European Neuropsychopharmacology* **11**, 105–110.

Geuze E, Vermetten E, Bremner JD (2005). MR-based in vivo hippocampal volumetrics: 2. Findings in neuropsychiatric disorders. *Molecular Psychiatry* **10**, 160–184.

Glenthoj A, Glenthoj BY, Mackeprang T, Pagsberg AK, *et al.* (2007). Basal ganglia volumes in drug-naive first-episode schizophrenia patients before and after short-term treatment with either a typical or an atypical antipsychotic drug. *Psychiatry Research* **154**, 199–208.

Grubbs F (1969). Procedures for detecting outlying observations in samples. *Technometrics* **11**, 1–21.

Halim ND, Weickert CS, McClintock BW, Weinberger DR, *et al.* (2004). Effects of chronic haloperidol and clozapine treatment on neurogenesis in the adult rat hippocampus. *Neuropsychopharmacology* **29**, 1063–1069.

Hulshoff Pol HE, Kahn RS (2008). What happens after the first episode? A review of progressive brain changes in chronically ill patients with schizophrenia. *Schizophrenia Bulletin* **34**, 354–366.

Jovicich J, Czanner S, Greve D, Haley E, *et al.* (2006). Reliability in multi-site structural MRI studies: effects of gradient non-linearity correction on phantom and human data. *Neuroimage* **30**, 436–443.

Kapur S, Seeman P (2001). Does fast dissociation from the dopamine d(2) receptor explain the action of atypical antipsychotics?: a new hypothesis. *American Journal of Psychiatry* **158**, 360–369.

Kapur S, Zipursky R, Jones C, Shammi CS, *et al.* (2000). A positron emission tomography study of quetiapine in schizophrenia: a preliminary finding of an antipsychotic effect with only transiently high dopamine D2 receptor occupancy. *Archives of General Psychiatry* **57**, 553–559.

Kay SR, Fiszbein A, Opler LA (1987). The positive and negative syndrome scale (PANSS) for schizophrenia. *Schizophrenia Bulletin* **13**, 261–276.

Kerwin R (2007). When should clozapine be initiated in schizophrenia?: some arguments for and against earlier use of clozapine. *CNS Drugs* **21**, 267–278.

Keshavan MS, Rosenberg D, Sweeney JA, Pettegrew JW (1998). Decreased caudate volume in neuroleptic-naive psychotic patients. *American Journal of Psychiatry* **155**, 774–778.

Kessler RM, Ansari MS, Riccardi P, Li R, *et al.* (2006). Occupancy of striatal and extrastriatal dopamine D2 receptors by clozapine and quetiapine. *Neuropsychopharmacology* **31**, 1991–2001.

Kinon BJ, Ahl J, Stauffer VL, Hill AL, *et al.* (2004). Dose response and atypical antipsychotics in schizophrenia. *CNS Drugs* **18**, 597–616.

Kreczmanski P, Heinsen H, Mantua V, Woltersdorf F, *et al.* (2007). Volume, neuron density and total neuron number in five subcortical regions in schizophrenia. *Brain* **130**, 678–692.

Lang DJ, Kopala LC, Vandorpe RA, Rui Q, *et al.* (2001). An MRI study of basal ganglia volumes in first-episode schizophrenia patients treated with risperidone. *American Journal of Psychiatry* **158**, 625–631.

Leucht S, Corves C, Arbter D, Engel RR, *et al.* (2009). Second-generation *vs.* first-generation antipsychotic drugs for schizophrenia: a meta-analysis. *Lancet* **373**, 31–41.

Lidow MS, Goldman-Rakic PS (1997). Differential regulation of D2 and D4 dopamine receptor mRNAs in the primate cerebral cortex vs. neostriatum: effects of chronic treatment with typical and atypical antipsychotic drugs. *Journal of Pharmacology and Experimental Therapeutics* **283**, 939–946.

Lieberman J, Chakos M, Wu H, Alvir J, *et al.* (2001). Longitudinal study of brain morphology in first episode schizophrenia. *Biological Psychiatry* **49**, 487–499.

Lieberman JA, Bymaster FP, Meltzer HY, Deutch AY, *et al.* (2008). Antipsychotic drugs: comparison in animal models of efficacy, neurotransmitter regulation, and neuroprotection. *Pharmacological Reviews* **60**, 358–403.

Luo C, Xu H, Li XM (2005). Quetiapine reverses the suppression of hippocampal neurogenesis caused by repeated restraint stress. *Brain Research* **1063**, 32–39.

Markianos M, Hatzimanolis J, Lykouras L (2001). Neuroendocrine responsivity of the pituitary dopamine system in male schizophrenic patients during treatment with clozapine, olanzapine, risperidone, sulpiride, or haloperidol. *European Archives of Psychiatry and Clinical Neuroscience* **251**, 141–146.

Massana G, Salgado-Pineda P, Junque C, Perez M, *et al.* (2005). Volume changes in gray matter in first-episode neuroleptic-naive schizophrenic patients treated with risperidone. *Journal of Clinical Psychopharmacology* **25**, 111–117.

Mauri MC, Volonteri LS, Colasanti A, Fiorentini A, *et al.* (2007). Clinical pharmacokinetics of atypical antipsychotics: a critical review of the relationship between plasma concentrations and clinical response. *Clinical Pharmacokinetics* **46**, 359–388.

Meltzer HY, Huang M (2008). In vivo actions of atypical antipsychotic drug on serotonergic and dopaminergic systems. *Progress in Brain Research* **172**, 177–197.

Meltzer HY, Li Z, Kaneda Y, Ichikawa J (2003). Serotonin receptors: their key role in drugs to treat schizophrenia. *Progress in Neuropsychopharmacology and Biological Psychiatry* **27**, 1159–1172.

Miller DD, Rezai K, Alliger R, Andreasen NC (1997). The effect of antipsychotic medication on relative cerebral blood perfusion in schizophrenia: assessment with technetium-99 m hexamethyl-propyleneamine oxime single photon emission computed tomography. *Biological Psychiatry* **41**, 550–559.

Moncrieff J, Leo J (2010). A systematic review of the effects of antipsychotic drugs on brain volume. *Psychological Medicine* **20**, 1–14.

Navari S, Dazzan P (2009). Do antipsychotic drugs affect brain structure? A systematic and critical review of MRI findings. *Psychological Medicine* **39**, 1763–1777.

Park SW, Lee SK, Kim JM, Yoon JS, *et al.* (2006). Effects of quetiapine on the brain-derived neurotrophic factor expression in the hippocampus and neocortex of rats. *Neuroscience Letters* **402**, 25–29.

Phillips LJ, McGorry PD, Garner B, Thompson KN, *et al.* (2006). Stress, the hippocampus and the hypothalamic-pituitary-adrenal axis: implications for the development of psychotic disorders. *Australian and New Zealand Journal of Psychiatry* **40**, 725–741.

Rasmussen H, Ebdrup BH, Erritzoe D, Aggernaes B, *et al.* (2010). Serotonin 2A receptor blockade and clinical effect in first-episode schizophrenia patients treated with quetiapine. *Psychopharmacology*. Published online: 7 July 2010. doi:10.1007/s00213-010-1941-5.

Scheepers FE, Gispen de Wied CC, Hulshoff Pol HE, Kahn RS (2001). Effect of clozapine on caudate nucleus volume in relation to symptoms of schizophrenia. *American Journal of Psychiatry* **158**, 644–646.

Scherk H, Falkai P (2006). Effects of antipsychotics on brain structure. *Current Opinion in Psychiatry* **19**, 145–150.

Seeman P (1987). Dopamine receptors and the dopamine hypothesis of schizophrenia. *Synapse* **1**, 133–152.

Shenton ME, Dickey CC, Frumin M, McCarley RW (2001). A review of MRI findings in schizophrenia. *Schizophrenia Research* **49**, 1–52.

Smieskova R, Fusar-Poli P, Allen P, Bendfeldt K, *et al.* (2009). The effects of antipsychotics on the brain: what have we learnt from structural imaging of schizophrenia? – a systematic review. *Current Pharmaceutical Design* **15**, 2535–2549.

Smieskova R, Fusar-Poli P, Allen P, Bendfeldt K, *et al.* (2010). Neuroimaging predictors of transition to psychosis – a systematic review and meta-analysis. *Neuroscience & Biobehavioral Reviews* **34**, 1207–1222.

Steen RG, Mull C, McClure R, Hamer RM, *et al.* (2006). Brain volume in first-episode schizophrenia: systematic review and meta-analysis of magnetic resonance imaging studies. *British Journal of Psychiatry* **188**, 510–518.

Stip E, Mancini-Marie A, Fahim C, Bentaleb LA, *et al.* (2008). Decrease in basal ganglia grey matter density associated with atypical antipsychotic treatment in schizophrenia patients. *Schizophrenia Research* **103**, 319–321.

Tarazi FI, Zhang K, Baldessarini RJ (2001). Long-term effects of olanzapine, risperidone, and quetiapine on dopamine receptor types in regions of rat brain: implications for antipsychotic drug treatment. *Journal of Pharmacology and Experimental Therapeutics* **297**, 711–717.

Tauscher-Wisniewski S, Kapur S, Tauscher J, Jones C, *et al.* (2002). Quetiapine: an effective antipsychotic in first-episode schizophrenia despite only transiently high dopamine-2 receptor blockade. *Journal of Clinical Psychiatry* **63**, 992–997.

Tauscher-Wisniewski S, Tauscher J, Christensen BK, Mikulis DJ, *et al.* (2005). Volumetric MRI measurement of caudate nuclei in antipsychotic-naive patients suffering from a first episode of psychosis. *Journal of Psychiatric Research* **39**, 365–370.

Taylor S, Christensen JD, Holcomb JM, Garver DL (2005). Volume increases in striatum associated with positive

14   *B. H. Ebdrup et al.*

symptom reduction in schizophrenia: a preliminary observation. *Psychiatry Research* **140**, 85–89.

Van Haren NE, Pol HE, Schnack HG, Cahn W, et al. (2008). Progressive brain volume loss in schizophrenia over the course of the illness: evidence of maturational abnormalities in early adulthood. *Biological Psychiatry* **63**, 106–113.

Vita A, De Peri L (2007). The effects of antipsychotic treatment on cerebral structure and function in schizophrenia. *International Review of Psychiatry* **19**, 429–436.

Vita A, De Peri L, Silenzi C, Dieci M (2006). Brain morphology in first-episode schizophrenia: a meta-analysis of quantitative magnetic resonance imaging studies. *Schizophrenia Research* **82**, 75–88.

Wing JK, Babor T, Brugha T, Burke J, et al. (1990). SCAN. Schedules for Clinical Assessment in Neuropsychiatry. *Archives of General Psychiatry* **47**, 589–593.

Wood SJ, Pantelis C, Velakoulis D, Yucel M, et al. (2008). Progressive changes in the development toward schizophrenia: studies in subjects at increased symptomatic risk. *Schizophrenia Bulletin* **34**, 322–329.

Xu H, Qing H, Lu W, Keegan D, et al. (2002). Quetiapine attenuates the immobilization stress-induced decrease of brain-derived neurotrophic factor expression in rat hippocampus. *Neuroscience Letters* **321**, 65–68.

Yan B, Bi X, He J, Zhang Y, et al. (2007). Quetiapine attenuates spatial memory impairment and hippocampal neurodegeneration induced by bilateral common carotid artery occlusion in mice. *Life Sciences* **81**, 353–361.

Bibliography

[1] DICOM Homepage, http://medical.nema.org/.

[2] A Alzheimer. Beiträge zur pathologischen Anatomie der Hirnrinde und zur anatomischen Grundlage einiger Psychosen. (Part 2 of 2). *European Neurology*, 2(2):107–120, 1897.

[3] Marti J. Anderson and John Robinson. Permutation Tests for Linear Models. *Australian ¡html_ent glyph="@amp;" ascii="&"/¿ New Zealand Journal of Statistics*, 43(1):75–88, March 2001.

[4] J Ashburner, J L Andersson, and K J Friston. High-dimensional image registration using symmetric priors. *NeuroImage*, 9(6 Pt 1):619–28, June 1999.

[5] J Ashburner and K Friston. Multimodal image coregistration and partitioning–a unified framework. *NeuroImage*, 6(3):209–17, October 1997.

[6] J Ashburner and K J Friston. Nonlinear spatial normalization using basis functions. *Human brain mapping*, 7(4):254–66, January 1999.

[7] J Ashburner and K J Friston. Voxel-based morphometry–the methods. *NeuroImage*, 11(6 Pt 1):805–21, June 2000.

[8] John Ashburner. *Computational Neuroanatomy*. PhD thesis, University College London, 2000.

[9] John Ashburner. A fast diffeomorphic image registration algorithm. *NeuroImage*, 38(1):95–113, October 2007.

[10] John Ashburner. Computational anatomy with the SPM software. *Magnetic resonance imaging*, 27(8):1163–74, October 2009.

[11] John Ashburner, John G Csernansky, Christos Davatzikos, Nick C Fox, Gio-
     vanni B Frisoni, and Paul M Thompson. Computer-assisted imaging to assess
     brain structure in healthy and diseased brains. *Lancet neurology*, 2(2):79–88,
     February 2003.

[12] John Ashburner and Karl J. Friston. Why voxel-based morphometry should be
     used. *NeuroImage*, 14(6):1238–43, December 2001.

[13] John Ashburner and Karl J Friston. Unified segmentation. *NeuroImage*,
     26(3):839–51, July 2005.

[14] Josephine Barnes, Rachael I Scahill, Richard G Boyes, Chris Frost, Emma B
     Lewis, Charlotte L Rossor, Martin N Rossor, and Nick C Fox. Differentiat-
     ing AD from aging using semiautomated measurement of hippocampal atrophy
     rates. *NeuroImage*, 23(2):574–81, October 2004.

[15] Y Benjamini and Y Hochberg. Controlling the false discovery rate: a practi-
     cal and powerful approach to multiple testing. *Journal of the Royal Statistical
     Society. Series B*, 57:289–300, 1995.

[16] Y Benjamini and D Yekutieli. The Control of the false discovery rate in multiple
     testing under dependency. *The Annals of Statistics*, 29(4):1165–1188, 2001.

[17] F L Bookstein. "Voxel-based morphometry" should not be used with imperfectly
     registered images. *NeuroImage*, 14(6):1454–62, December 2001.

[18] Geoffrey M Boynton, S A Engel, Gary H Glover, and D J Heeger. Linear systems
     analysis of functional magnetic resonance imaging in human V1. *The Journal of
     neuroscience : the official journal of the Society for Neuroscience*, 16(13):4207–
     21, July 1996.

[19] Simona M Brambati, Natasha C Renda, Katherine P Rankin, Howard J Rosen,
     William W Seeley, John Ashburner, Michael W Weiner, Bruce L Miller, and
     Maria Luisa Gorno-Tempini. A tensor based morphometry study of longitudinal
     gray matter contraction in FTD. *NeuroImage*, 35(3):998–1003, April 2007.

[20] Caroline C Brun, Natasha Leporé, Xavier Pennec, Agatha D Lee, Marina Bary-
     sheva, Sarah K Madsen, Christina Avedissian, Yi-Yu Chou, Greig I de Zu-
     bicaray, Katie L McMahon, Margaret J Wright, Arthur W Toga, and Paul M
     Thompson. Mapping the regional influence of genetics on brain structure
     variability–a tensor-based morphometry study. *NeuroImage*, 48(1):37–49, Oc-
     tober 2009.

[21] E T Bullmore, J Suckling, S Overmeyer, S Rabe-Hesketh, E Taylor, and M J
     Brammer. Global, voxel, and cluster tests, by theory and permutation, for a

difference between two groups of structural MR images of the brain. *IEEE transactions on medical imaging*, 18(1):32–42, January 1999.

[22] Geraldo F Busatto, Griselda E J Garrido, Osvaldo P Almeida, Claudio C Castro, Cândida H P Camargo, Carla G Cid, Carlos A Buchpiguel, Sergio Furuie, and Cassio M Bottino. A voxel-based morphometry study of temporal lobe gray matter reductions in Alzheimer's disease. *Neurobiology of aging*, 24(2):221–31, 2003.

[23] Ronald Christensen. *Plane Answers to Complex Questions.* Springer, 1996.

[24] J Chumbley, K Worsley, G Flandin, and K Friston. Topological FDR for neuroimaging. *NeuroImage*, 49(4):3057–64, February 2010.

[25] Benedicto Crespo-Facorro, Roberto Roiz-Santiáñez, José María Pelayo-Terán, Cesar González-Blanch, Rocío Pérez-Iglesias, Agustín Gutiérrez, Enrique Marco de Lucas, Diana Tordesillas, and José Luis Vázquez-Barquero. Caudate nucleus volume and its clinical and cognitive correlations in first episode schizophrenia. *Schizophrenia research*, 91(1-3):87–96, March 2007.

[26] Bjørn H. Ebdrup. *Structural Brain Changes in Antipsychotic-Naïve First-Episode Schizophrenia Patients Before and After Six Months of Antipsychotic Monotherapy.* PhD thesis, Copenhagen University, November 2010.

[27] Bjørn H. Ebdrup, Birte Glenthø j, Hans Rasmussen, Bodil Aggernaes, Annika R Langkilde, Olaf B Paulson, Henrik Lublin, Arnold Skimminge, and William Baaré. Hippocampal and caudate volume reductions in antipsychotic-naive first-episode schizophrenia. *Journal of psychiatry & neuroscience : JPN*, 35(2):95–104, March 2010.

[28] Bjørn H. Ebdrup, Arnold Skimminge, Hans Rasmussen, Bodil Aggernaes, Bob Oranje, Henrik Lublin, William F C Baaré, and Birte Glenthø j. Progressive striatal and hippocampal volume loss in initially antipsychotic-naive, first-episode schizophrenia patients treated with quetiapine: relationship to dose and symptoms. *The international journal of neuropsychopharmacology / official scientific journal of the Collegium Internationale Neuropsychopharmacologicum (CINP)*, pages 1–14, August 2010.

[29] Simon B Eickhoff, Tomas Paus, Svenja Caspers, Marie-Helene Grosbras, Alan C Evans, Karl Zilles, and Katrin Amunts. Assignment of functional activations to probabilistic cytoarchitectonic areas revisited. *NeuroImage*, 36(3):511–21, July 2007.

[30] AC Evans, DL Collins, SR Mills, and ED Brown. 3D statistical neuroanatom-
ical models from 305 MRI volumes. *proceedings of Nuclear Science Sympo-
sium and Medical Imaging Conference, 1993., 1993 IEEE Conference Record.*,
3:1813 – 1817, 1993.

[31] Massimo Filippi, Antonia Ceccarelli, Elisabetta Pagani, Roberto Gatti, Alice
Rossi, Laura Stefanelli, Andrea Falini, Giancarlo Comi, and Maria Assunta
Rocca. Motor learning in healthy humans is associated to gray matter changes:
a tensor-based morphometry study. *PloS one*, 5(4):e10198, January 2010.

[32] B Fischl, M I Sereno, R B Tootell, and A M Dale. High-resolution intersub-
ject averaging and a coordinate system for the cortical surface. *Human brain
mapping*, 8(4):272–84, January 1999.

[33] Bruce Fischl, David H Salat, Evelina Busa, Marilyn Albert, Megan Dieterich,
Christian Haselgrove, Andre van Der Kouwe, Ron Killiany, David Kennedy,
Shuna Klaveness, Albert Montillo, Nikos Makris, Bruce Rosen, and Anders M
Dale. Whole brain segmentation: automated labeling of neuroanatomical struc-
tures in the human brain. *Neuron*, 33(3):341–55, January 2002.

[34] R A Fisher. *The Design of Experiments.* Olyver and Boyd Edinburgh, 1935.

[35] K J Friston, J Ashburner, S J Kiebel, T E Nichols, and W D Penny, editors.
Statistical Parametric Mapping: The Analysis of Functional Brain Images. Aca-
demic Press, 2007.

[36] Karl J. Friston, A P Holmes, J B Poline, P J Grasby, S C Williams, R S J Frack-
owiak, and R Turner. Analysis of fMRI time-series revisited. *NeuroImage*,
2(1):45–53, March 1995.

[37] Karl J. Friston, P Jezzard, and R Turner. Analysis of Functional MRI Time-
Series. *Human Brain Mapping*, 1:153–171, 1994.

[38] Karl J. Friston, K. J. Worsley, R. S. J. Frackowiak, J. C. Mazziotta, and A. C.
Evans. Assessing the significance of focal activations using their spatial extent.
Human Brain Mapping, 1(3):210–220, 1993.

[39] Christopher R Genovese, Nicole A Lazar, and Thomas Nichols. Thresholding
of statistical maps in functional neuroimaging using the false discovery rate.
NeuroImage, 15(4):870–8, April 2002.

[40] E Geuze, E Vermetten, and J D Bremner. MR-based in vivo hippocampal volu-
metrics: 1. Review of methodologies currently employed. *Molecular psychiatry*,
10(2):147–59, February 2005.

[41] E Geuze, E Vermetten, and J D Bremner. MR-based in vivo hippocampal volumetrics: 2. Findings in neuropsychiatric disorders. *Molecular psychiatry*, 10(2):160–84, February 2005.

[42] C D Good, I S Johnsrude, J Ashburner, R N Henson, K J Friston, and R S Frackowiak. A voxel-based morphometric study of ageing in 465 normal adult human brains. *NeuroImage*, 14(1 Pt 1):21–36, July 2001.

[43] Catriona D Good, Rachael I Scahill, Nick C Fox, John Ashburner, Karl J Friston, Dennis Chan, William R Crum, Martin N Rossor, and Richard S J Frackowiak. Automatic differentiation of anatomical patterns in the human brain: validation with studies of degenerative dementias. *NeuroImage*, 17(1):29–46, September 2002.

[44] Jessica A Grahn, John A Parkinson, and Adrian M Owen. The cognitive functions of the caudate nucleus. *Progress in neurobiology*, 86(3):141–55, November 2008.

[45] E. Mark Haacke, Robert W. Brown, and Michael R. Thompson. *Magnetic resonance imaging: physical principles and sequence design*. Wiley-Liss, 1999.

[46] M V Hansen, Kathrine Skak Madsen, William F C Baaré, Arnold Skimminge, Lisser Rye Ejersbo, Christian Gerlach, P Å keson, O B Paulson, and Terry L Jernigan. Verbal fluency performance is associated with white matter microstructure in a left hemisphere network in children. In *Proceedings 15th Annual Meeting of the Organization for Human Brain Mapping, San Francisco*, 2009.

[47] L G Hanson, Torben Ellegaard Lund, and C G Hanson. Encoding of electrophysiology and other signals in {MR} images. *J Magn Reson Imaging*, 25(5):1059–1066, May 2007.

[48] Lars G Hanson, Arnold Skimminge, and Christian G Hanson. Strategies for Avoiding Image Artefacts When Scanner is Used for Recording of Non-MR Signals. In *Proceedings 14th Scientific Meeting, International Society for Magnetic Resonance in Medicine, Seattle*, page 2389, 2006.

[49] Lars G Hanson, Arnold Skimminge, and Christian G Hanson. Encoding of EEG in MR Images. In *Proceedings 15th Scientific Meeting, International Society for Magnetic Resonance in Medicine, Berlin*, page 1958, 2007.

[50] Lars G Hanson, Arnold Skimminge, and Christian G Hanson. Minimalist EEG-recording for improving fMRI: Simple encoding of noise variables in MRI data. In *Proceedings 16th Scientific Meeting, International Society for Magnetic Resonance in Medicine, Toronto*, page 2427, 2008.

[51] Lars G Hanson, Arnold Skimminge, Torben Ellegaard Lund, and Christian G Hanson. Encoding of EEG in MR images. In *Proceedings of the 12th Annual Meeting of the Organization for Human Brain Mapping, Florence*, page 185, 2006.

[52] Trevor Hastie, Robert Tibshirani, and Jerome Friedman. *The Elements of Statistical Learning: Data Mining, Inference, and Prediction:The Elements of Statistical Learning: Data Mining, Inference, and Prediction*. Springer, 2. edition edition, June 2004.

[53] Xue Hua, Suh Lee, Igor Yanovsky, Alex D Leow, Yi-Yu Chou, April J Ho, Boris Gutman, Arthur W Toga, Clifford R Jack, Matt A Bernstein, Eric M Reiman, Danielle J Harvey, John Kornak, Norbert Schuff, Gene E Alexander, Michael W Weiner, and Paul M Thompson. Optimizing power to track brain degeneration in Alzheimer's disease and mild cognitive impairment with tensor-based morphometry: an ADNI study of 515 subjects. *NeuroImage*, 48(4):668–81, December 2009.

[54] Xue Hua, Alex D Leow, Jennifer G Levitt, Rochelle Caplan, Paul M Thompson, and Arthur W Toga. Detecting brain growth patterns in normal children using tensor-based morphometry. *Human brain mapping*, 30(1):209–19, January 2009.

[55] Xue Hua, Alex D Leow, Neelroop Parikshak, Suh Lee, Ming-Chang Chiang, Arthur W Toga, Clifford R Jack, Michael W Weiner, and Paul M Thompson. Tensor-based morphometry as a neuroimaging biomarker for Alzheimer's disease: an MRI study of 676 AD, MCI, and normal subjects. *NeuroImage*, 43(3):458–69, November 2008.

[56] Hilleke E Hulshoff Pol and René S Kahn. What happens after the first episode? A review of progressive brain changes in chronically ill patients with schizophrenia. *Schizophrenia bulletin*, 34(2):354–66, March 2008.

[57] Andrew Janke, Huawei Zhao, Gary J Cowin, Graham J Galloway, and David M Doddrell. Use of spherical harmonic deconvolution methods to compensate for nonlinear gradient effects on MRI images. *Magnetic resonance in medicine : official journal of the Society of Magnetic Resonance in Medicine / Society of Magnetic Resonance in Medicine*, 52(1):115–22, July 2004.

[58] M Jenkinson and S Smith. A global optimisation method for robust affine registration of brain images. *Medical image analysis*, 5(2):143–56, June 2001.

[59] Mark Jenkinson, Peter Bannister, Michael Brady, and Stephen Smith. Improved optimization for the robust and accurate linear registration and motion correction of brain images. *NeuroImage*, 17(2):825–41, October 2002.

[60] Dominic E Job, Heather C Whalley, Sarah McConnell, Mike Glabus, Eve C Johnstone, and Stephen M Lawrie. Structural gray matter differences between first-episode schizophrenics and normal controls using voxel-based morphometry. *NeuroImage*, 17(2):880–9, October 2002.

[61] Jorge Jovicich, Silvester Czanner, Douglas Greve, Elizabeth Haley, Andre van Der Kouwe, Randy Gollub, David Kennedy, Franz Schmitt, Gregory Brown, James Macfall, Bruce Fischl, and Anders Dale. Reliability in multi-site structural MRI studies: effects of gradient non-linearity correction on phantom and human data. *NeuroImage*, 30(2):436–43, April 2006.

[62] Matcheri S Keshavan, Rajiv Tandon, Nash N Boutros, and Henry a Nasrallah. Schizophrenia, "just the facts": what we know in 2008 Part 3: neurobiology. *Schizophrenia research*, 106(2-3):89–107, December 2008.

[63] S J Kiebel, J Ashburner, J B Poline, and K J Friston. MRI and PET coregistration–a cross validation of statistical parametric mapping and automated image registration. *NeuroImage*, 5(4 Pt 1):271–9, May 1997.

[64] Junghoon Kim, Brian Avants, Sunil Patel, John Whyte, Branch H Coslett, John Pluta, John A Detre, and James C Gee. Structural consequences of diffuse traumatic brain injury: a large deformation tensor-based morphometry study. *NeuroImage*, 39(3):1014–26, February 2008.

[65] C M Kipps, A J Duggins, N Mahant, L Gomes, J Ashburner, and E A McCusker. Progression of structural neuropathology in preclinical Huntington's disease: a tensor based morphometry study. *Journal of neurology, neurosurgery, and psychiatry*, 76(5):650–5, May 2005.

[66] Arno Klein, Jesper Andersson, Babak A Ardekani, John Ashburner, Brian Avants, Ming-Chang Chiang, Gary E Christensen, D Louis Collins, James Gee, Pierre Hellier, Joo Hyun Song, Mark Jenkinson, Claude Lepage, Daniel Rueckert, Paul Thompson, Tom Vercauteren, Roger P Woods, J John Mann, and Ramin V Parsey. Evaluation of 14 nonlinear deformation algorithms applied to human brain MRI registration. *NeuroImage*, 46(3):786–802, July 2009.

[67] Korbinian Brodmann. *Vergleichende Lokalisationslehre der Grosshirnrinde in ihren Prinzipien dargestellt auf Grund des Zellenbaues.* Johann Ambrosius Barth Verlag, 1909.

[68] Kirsten Korsholm, Kristoffer Hougaard Madsen, Jette Lautrup Frederiksen, Arnold Skimminge, and Torben Ellegaard Lund. Recovery from optic neuritis: an ROI-based analysis of LGN and visual cortical areas. *Brain : a journal of neurology*, 130(Pt 5):1244–53, May 2007.

[69] S Langlois, M Desvignes, J M Constans, and M Revenu. MRI geometric distortion: a simple approach to correcting the effects of non-linear gradient fields. *Journal of magnetic resonance imaging : JMRI*, 9(6):821–31, June 1999.

[70] Alex D Leow, Andrea D Klunder, Clifford R Jack, Arthur W Toga, Anders M Dale, Matt A Bernstein, Paula J Britson, Jeffrey L Gunter, Chadwick P Ward, Jennifer L Whitwell, Bret J Borowski, Adam S Fleisher, Nick C Fox, Danielle Harvey, John Kornak, Norbert Schuff, Colin Studholme, Gene E Alexander, Michael W Weiner, and Paul M Thompson. Longitudinal stability of MRI for mapping brain change using tensor-based morphometry. *NeuroImage*, 31(2):627–40, June 2006.

[71] N Lepore, C Brun, Y Y Chou, M C Chiang, R A Dutton, K M Hayashi, E Luders, O L Lopez, H J Aizenstein, A W Toga, J T Becker, and P M Thompson. Generalized tensor-based morphometry of HIV/AIDS using multivariate statistics on deformation tensors. *IEEE transactions on medical imaging*, 27(1):129–41, January 2008.

[72] Natasha Lepore, Caroline A Brun, Ming-Chang Chiang, Yi-Yu Chou, Rebecca A Dutton, Kiralee M Hayashi, Oscar L Lopez, Howard J Aizenstein, Arthur W Toga, James T Becker, and Paul M Thompson. Multivariate statistics of the Jacobian matrices in tensor based morphometry and their application to HIV/AIDS. *Medical image computing and computer-assisted intervention : MICCAI ... International Conference on Medical Image Computing and Computer-Assisted Intervention*, 9(Pt 1):191–8, January 2006.

[73] Jeffrey A Lieberman, Gary D Tollefson, Cecil Charles, Robert Zipursky, Tonmoy Sharma, Rene S Kahn, Richard S E Keefe, Alan I Green, Raquel E Gur, Joseph McEvoy, Diana Perkins, Robert M Hamer, Hongbin Gu, and Mauricio Tohen. Antipsychotic drug effects on brain morphology in first-episode psychosis. *Archives of general psychiatry*, 62(4):361–70, April 2005.

[74] Torben Ellegaard Lund, Kristoffer Hougaard Madsen, Karam Sidaros, Wen-Lin Luo, and Thomas E Nichols. Non-white noise in fMRI: does modelling have an impact? *NeuroImage*, 29(1):54–66, January 2006.

[75] H Lundell, D Barthelemy, A Skimminge, T B Dyrby, F Biering-Sø rensen, and J B Nielsen. Independent spinal cord atrophy measures correlate to motor and sensory deficits in individuals with spinal cord injury. *Spinal cord : the official journal of the International Medical Society of Paraplegia*, August 2010.

[76] Angus W MacDonald and S Charles Schulz. What we know: findings that every theory of schizophrenia should explain. *Schizophrenia bulletin*, 35(3):493–508, May 2009.

[77] J Macoveanu, J Wegener, Arnold Skimminge, B Hornboll, R Elliott, H Siebner, O Paulson, and James B Rowe. Separate neural systems for evaluating risks and reward in decision making. In *Proceedings 17th Scientific Meeting, International Society for Magnetic Resonance in Medicine, Honolulu*, page 3710, 2009.

[78] Kathrine Skak Madsen, William F C Baaré, Martin Vestergaard, Arnold Skimminge, Lisser Rye Ejersbo, Thomas Z Ramsø y, Christian Gerlach, Per Akeson, Olaf B Paulson, and Terry L Jernigan. Response inhibition is associated with white matter microstructure in children. *Neuropsychologia*, 48(4):854–62, March 2010.

[79] Kathrine Skak Madsen, Terry L Jernigan, Arnold Skimminge, E Mortensen, G M Knudsen, and William F C Baaré. Cingulum bundle asymmetry predicts trait neuroticism: A DTI study. In *Proceedings 17th Scientific Meeting, International Society for Magnetic Resonance in Medicine, Honolulu*, page 1459, 2009.

[80] Kathrine Skak Madsen, Terry L Jernigan, Arnold Skimminge, E L Mortensen, G M Knudsen, and William F C Baaré. Inferior Cingulum Bundle Asymmetry Predicts Extroversion: A DTI study. In *Proceedings 15th Annual Meeting of the Organization for Human Brain Mapping, San Francisco*, 2009.

[81] Kristoffer Hougaard Madsen. *Modelling Strategies for Functional Magnetic Resonance Imaging*. PhD thesis, Technical University of Denmark, 2008.

[82] J C Mazziotta, A W Toga, A Evans, P Fox, and J Lancaster. A probabilistic atlas of the human brain: theory and rationale for its development. The International Consortium for Brain Mapping (ICBM). *NeuroImage*, 2(2):89–101, June 1995.

[83] John McGrath, Sukanta Saha, David Chant, and Joy Welham. Schizophrenia: a concise overview of incidence, prevalence, and mortality. *Epidemiologic reviews*, 30:67–76, January 2008.

[84] Andrea Mechelli, Cathy J. Price, Karl J. Friston, and John Ashburner. Voxel-Based Morphometry of the Human Brain: Methods and Applications. *Current Medical Imaging Reviews*, 1(2):105–113, June 2005.

[85] Daniel Mietchen and Christian Gaser. Computational morphometry for detecting changes in brain structure due to development, aging, learning, disease and evolution. *Frontiers in neuroinformatics*, 3:25, January 2009.

[86] I Mikkelsen, D Ziegelitz, B Kjø lby, G Starck, Arnold Skimminge, M Widmark, M Tullberg, S Holtå s, and C Wikkelsø. DSC-MRI perfusion imaging: which input function? - A comparison to CT perfusion imaging. In *Proceedings 16th Scientific Meeting, International Society for Magnetic Resonance in Medicine, Toronto*, page 1897, 2008.

[87] Michael I Miller. Computational anatomy: shape, growth, and atrophy comparison via diffeomorphisms. *NeuroImage*, 23 Suppl 1:S19–33, January 2004.

[88] Jan Modersitzki. *Numerical Methods for Image Registration*. Oxford University Press, 2004.

[89] K Nielsen, Kristoffer Hougaard Madsen, Jette Lautrup Frederiksen, A Tsakiri, Arnold Skimminge, and Torben Ellegaard Lund. LGN activation in patients recovering from acute optic neuritis. In *Proceedings of the 12th Annual Meeting of the Organization for Human Brain Mapping, Florence*, page 215, 2006.

[90] Kirsten Nielsen, Kristoffer Hougaard Madsen, Jette Lautrup Frederiksen, Anna Tsakiri, Arnold Skimminge, and Torben Ellegaard Lund. Investigations of LGN Activation During Recovery from Acute Optic Neuritis. In *Proceedings 14th Scientific Meeting, International Society for Magnetic Resonance in Medicine, Seattle*, page 320, 2006.

[91] Lisa J Phillips, Patrick D McGorry, Belinda Garner, Katherine N Thompson, Christos Pantelis, Stephen J Wood, and Gregor Berger. Stress, the hippocampus and the hypothalamic-pituitary-adrenal axis: implications for the development of psychotic disorders. *The Australian and New Zealand journal of psychiatry*, 40(9):725–41, September 2006.

[92] Thomas Z Ramsø y, Matthew George Liptrot, Arnold Skimminge, Torben Ellegaard Lund, Karam Sidaros, Mark Schram Christensen, William F C Baaré, Olaf B Paulson, and Terry L Jernigan. Regional activation of the human medial temporal lobe during intentional encoding of objects and positions. *NeuroImage*, 47(4):1863–72, October 2009.

[93] Thomas Z Ramsø y, Kristoffer Hougaard Madsen, J S Wegener, S A V Gelskov, D Erritzø e, G M Knudsen, and Arnold Skimminge. From ecstasy to agony: chronic effects of MDMA use on emotional processing. In *Proceedings 15th Annual Meeting of the Organization for Human Brain Mapping, San Francisco*, 2009.

[94] Anat Reiner, Daniel Yekutieli, and Yoav Benjamini. Identifying differentially expressed genes using false discovery rate controlling procedures. *Bioinformatics (Oxford, England)*, 19(3):368–75, February 2003.

[95] Wulf Rössler, Hans Joachim Salize, Jim van Os, and Anita Riecher-Rössler. Size of burden of schizophrenia and psychotic disorders. *European neuropsychopharmacology : the journal of the European College of Neuropsychopharmacology*, 15(4):399–409, August 2005.

[96] C Salmond. The Precision of Anatomical Normalization in the Medial Temporal Lobe Using Spatial Basis Functions. *NeuroImage*, 17(1):507–512, September 2002.

[97] F E Satterthwaite. An approximate distribution of estimates of variance components. *Biometrics*, 2(6):110–4, December 1946.

[98] F E Scheepers, C C Gispen De Wied, H E Hulshoff Pol, and R S Kahn. Effect of clozapine on caudate nucleus volume in relation to symptoms of schizophrenia. *The American journal of psychiatry*, 158(4):644–6, April 2001.

[99] F Schmitt, A Dewdney, and W Renz. Hardware considerations for MR imaging physics. *Magnetic resonance imaging clinics of North America*, 7(4):733–63, vi, November 1999.

[100] M E Shenton, C C Dickey, M Frumin, and R W McCarley. A review of MRI findings in schizophrenia. *Schizophrenia research*, 49(1-2):1–52, April 2001.

[101] Annette Sidaros. *MRI in Severe Traumatic Brain Injury: Micro-and Macrostructural Changes*. PhD thesis, Copenhagen University, 2009.

[102] Annette Sidaros, Arnold Skimminge, Matthew George Liptrot, Karam Sidaros, Aase W Engberg, Margrethe Herning, Olaf B Paulson, Terry L Jernigan, and Egill Rostrup. Long-term global and regional brain volume changes following severe traumatic brain injury: a longitudinal study with clinical correlates. *NeuroImage*, 44(1):1–8, January 2009.

[103] Arnold Skimminge, William F C Baaré, J Macoveanu, and Mark Schram Christensen. Gradient non-linearity correction relocates normalized group activation hotspot. In *Proceedings 15th Annual Meeting of the Organization for Human Brain Mapping, San Francisco*, 2009.

[104] Arnold Skimminge and Mark Schram Christensen. Gradient non-linearity correction relocates normalised group activation hotspot. In *Proceedings 17th Scientific Meeting, International Society for Magnetic Resonance in Medicine, Honolulu*, page 1734, 2009.

[105] Arnold Skimminge, Christian G Hanson, and Lars G Hanson. A simple approach to electrophysiological recording during fMRI. In *Proceedings of the 12th Annual Meeting of the Organization for Human Brain Mapping, Florence*, page 132, 2006.

[106] Arnold Skimminge, Karam Sidaros, Matthew George Liptrot, Aase W Engberg, Margrethe Herning, O Paulson, Terry L Jernigan, Egill Rostrup, and Annette Sidaros. Long-term regional atrophy and association with clinical outcome following severe traumatic brain injury: A tensor based morphometry study. In

Proceedings 15th Annual Meeting of the Organization for Human Brain Mapping, San Francisco, 2009.

[107] Arnold Skimminge, Karam Sidaros, Matthew George Liptrot, and Annette Sidaros. Partial Volume Effects in DTI. In *Proceedings 15th Scientific Meeting, International Society for Magnetic Resonance in Medicine, Berlin*, page 1958, 2007.

[108] J G Sled, a P Zijdenbos, and a C Evans. A nonparametric method for automatic correction of intensity nonuniformity in MRI data. *IEEE transactions on medical imaging*, 17(1):87–97, March 1998.

[109] R C Smith, M Calderon, G K Ravichandran, J Largen, G Vroulis, A Shvartsburd, J Gordon, and J C Schoolar. Nuclear magnetic resonance in schizophrenia: a preliminary study. *Psychiatry research*, 12(2):137–47, June 1984.

[110] S M Smith, N De Stefano, M Jenkinson, and P M Matthews. Normalized accurate measurement of longitudinal brain change. *Journal of computer assisted tomography*, 25(3):466–75, 2001.

[111] Stephen M Smith, Yongyue Zhang, Mark Jenkinson, Jacqueline Chen, P M Matthews, Antonio Federico, and Nicola De Stefano. Accurate, robust, and automated longitudinal and cross-sectional brain change analysis. *NeuroImage*, 17(1):479–89, September 2002.

[112] R Grant Steen, Courtney Mull, Robert McClure, Robert M Hamer, and Jeffrey A Lieberman. Brain volume in first-episode schizophrenia: systematic review and meta-analysis of magnetic resonance imaging studies. *The British journal of psychiatry : the journal of mental science*, 188:510–8, June 2006.

[113] J Talairach and P Tournoux. *Co-planar Stereotaxic Atlas of the Human Brain: 3-Dimensional Proportional System - an Approach to Cerebral Imaging*. Thieme Medical Publishers, New York, 1988.

[114] Rajiv Tandon, Matcheri S Keshavan, and Henry a Nasrallah. Schizophrenia, "just the facts" what we know in 2008. 2. Epidemiology and etiology. *Schizophrenia research*, 102(1-3):1–18, July 2008.

[115] Rajiv Tandon, Matcheri S Keshavan, and Henry a Nasrallah. Schizophrenia, "Just the Facts": what we know in 2008 part 1: overview. *Schizophrenia research*, 100(1-3):4–19, March 2008.

[116] Guozhi Tao, Sushmita Datta, Renjie He, Flavia Nelson, Jerry S Wolinsky, and Ponnada A Narayana. Deep gray matter atrophy in multiple sclerosis: a tensor based morphometry. *Journal of the neurological sciences*, 282(1-2):39–46, July 2009.

[117] Danielle J Tisserand, Jens C Pruessner, Ernesto J Sanz Arigita, Martin P J van Boxtel, Alan C Evans, Jelle Jolles, and Harry B M Uylings. Regional frontal cortical volumes decrease differentially in aging: an MRI study to compare volumetric approaches and voxel-based morphometry. *NeuroImage*, 17(2):657–69, October 2002.

[118] H B M Uylings, G Rajkowska, E Sanz-Arigita, K Amunts, and K Zilles. Consequences of large interindividual variability for human brain atlases: converging macroscopical imaging and microscopical neuroanatomy. *Anatomy and embryology*, 210(5-6):423–31, December 2005.

[119] Jim van Os and Shitij Kapur. Schizophrenia. *Lancet*, 374(9690):635–45, August 2009.

[120] Martin Vestergaard, Kathrine Skak Madsen, William F.C. Baare, Arnold Skimminge, Lisser Rye Ejersbo, Thomas Z. Ramsø y, Christian Gerlach, Per Å keson, Olaf B. Paulson, and Terry L. Jernigan. White matter microstructure in superior longitudinal fasciculus associated with spatial working memory performance in children. *submitted to Jounal of Cognitive Neuroscience*, 2010.

[121] Deming Wang, Wendy Strugnell, Gary Cowin, David M Doddrell, and Richard Slaughter. Geometric distortion in clinical MRI systems Part I: evaluation using a 3D phantom. *Magnetic resonance imaging*, 22(9):1211–21, November 2004.

[122] Deming Wang, Wendy Strugnell, Gary Cowin, David M Doddrell, and Richard Slaughter. Geometric distortion in clinical MRI systems Part II: correction using a 3D phantom. *Magnetic resonance imaging*, 22(9):1223–32, November 2004.

[123] B L Welch. The Generalization of 'Student's' Problem when Several Different Population Variances are Involved. *Biometrika*, 34(1/2):28–35, 1947.

[124] Heather C Whalley, Viktoria-Eleni Gountouna, Jeremy Hall, Andrew McIntosh, Marie-Claire Whyte, Enrico Simonotto, Dominic E Job, David G C Owens, Eve C Johnstone, and Stephen M Lawrie. Correlations between fMRI activation and individual psychotic symptoms in un-medicated subjects at high genetic risk of schizophrenia. *BMC psychiatry*, 7:61, January 2007.

[125] R P Woods, S T Grafton, C J Holmes, S R Cherry, and J C Mazziotta. Automated image registration: I. General methods and intrasubject, intramodality validation. *Journal of computer assisted tomography*, 22(1):139–52, 1998.

[126] R P Woods, S T Grafton, J D Watson, N L Sicotte, and J C Mazziotta. Automated image registration: II. Intersubject validation of linear and nonlinear models. *Journal of computer assisted tomography*, 22(1):153–65, 1998.

[127] Roger P Woods. Characterizing volume and surface deformations in an atlas framework: theory, applications, and implementation. *NeuroImage*, 18(3):769–88, March 2003.

[128] M W Woolrich, B D Ripley, M Brady, and S M Smith. Temporal autocorrelation in univariate linear modeling of fMRI data. *Neuroimage*, 14(6):1370–1386, December 2001.

[129] K J Worsley, C H Liao, J Aston, V Petre, G H Duncan, F Morales, and A C Evans. A general statistical analysis for fMRI data. *NeuroImage*, 15(1):1–15, January 2002.

[130] K J Worsley, S. Marrett, P. Neelin, A C Vandal, Karl J. Friston, and A C Evans. A unified statistical approach for determining significant signals in images of cerebral activation. *Human brain mapping*, 4(1):58–73, January 1996.

[131] K J Worsley, S Marrett, P Neelin, A C Vandal, Karl J. Friston, and A C Evans. A unified statistical approach for determining significant voxels in images of cerebral activation. *Human Brain Mapping*, 4:58–73, 1996.

[132] I C Wright, Z R Ellison, T Sharma, K J Friston, R M Murray, and P K McGuire. Mapping of grey matter changes in schizophrenia. *Schizophrenia research*, 35(1):1–14, January 1999.

[133] I C Wright, P K McGuire, J B Poline, J M Travere, R M Murray, C D Frith, R S Frackowiak, and K J Friston. A voxel-based method for the statistical analysis of gray and white matter density applied to schizophrenia. *NeuroImage*, 2(4):244–52, December 1995.

[134] Xingchen Wu, Lars G. Hanson, Arnold Skimminge, Per Soelberg Sø rensen, Olaf B. Paulson, Morten Blinkenberg, and Henrik Kahr Mathiesen. Cortical N-acetyl aspartate is a predictor of long-term clinical disability in newly diagnosed relapsing-remitting multiple sclerosis. *submitted to Multiple Sclerosis*, 2010.

[135] Michael A Yassa and Craig E L Stark. A quantitative evaluation of cross-participant registration techniques for MRI studies of the medial temporal lobe. *NeuroImage*, 44(2):319–27, January 2009.